To the Graduate Council:

I am submitting herewith a dissertation written by Jeff Steill entitled "Molecular Anion Spectroscopy and Stability." I have examined the final electronic copy of this dissertation for form and content and recommend that it be accepted in partial fulfillment of the requirements for the degree of Doctor of Philosophy, with a major in Chemistry.

R. N. Compton, Major Professor

We have read this dissertation
and recommend its acceptance:

George Schweitzer

Charles Feigerle

Joseph Macek

Accepted for the Council:

Carolyn R. Hodges, Vice Provost
and Dean of the Graduate School

(Original signature are on file with official student records.)

Molecular Anion Spectroscopy and Stability

A Dissertation
Presented for the
Doctor of Philosophy
Degree
The University of Tennessee, Knoxville

Jeffrey Daniel Steill
August 2007

Dedication

This work is dedicated to my muse and my rock, Amy.

Acknowledgments

There have been many who have helped me in my scientific efforts. First and foremost, the guidance, critical thinking and profound curiosity of my advisor Dr. Robert Compton has deeply shaped the way I perceive and practice science. I will carry the benefits of his tutelage throughout my life. In addition, many of the faculty of the University of Tennessee chemistry department have been extremely helpful to me, including Dr. Schell, Dr. Schweitzer, Dr. Hinde, and Dr. Feigerle. I thank with the physics department faculty members Dr. Blass and Dr. Macek for their time and rescources.

External collaborations have been very useful for my scientific development. Collaborations with Dr. Eph Klots, Dr. F.B. Dunning, Dr. Steen Nielsen, and Dr. Jos Oomens have been very productive and I thank these scientists for their time and guidance. The research efforts here were produced in close collaboration with my laboratory coworkers, including Dr. Stewart Hager, Nasrin Mirsaleh-Kohan, Maria Oliveros, Shaun Ard, Watheq Al-Basheer and Andy Fisher. I would like to thank them for their lively discussions about science and everything else, especially politics. Fellow graduate students within the chemistry graduate department have been a source of great scientific and social collaboration. In particular, Tim Lillestollen, Peter Yaron, Sami Chanaa, Michelle Dolgos, and Rick Cook will be fondly remembered.

My family is of immeasurable importance to me, especially my wife, Amy, who's emotional support made this possible, my daughter Aislin, who's fascination with her world is inspiring, and my son Dylan who won't let me stop smiling. I also am grateful for my mother Barbara, who's unabashed love for life I inherited, my father Dan, who was never afraid to get his hands dirty in order to see his plans come to life, my brother John, who shares and shaped my enthusiasm for nature revealed through experiment, my sister Jessica, who thinks just like me and can read my mind, and my sister Jennifer, who's self-discipline I could only hope to approximate.

Generous financial support has been provided that I am very thankful for. The UT Chemistry department provided Teaching Assistantships and Dr. Compton provided Research Assistantships funded through NSF. The UT Center for Envioronmental Biotechnology provided a two-year additional stipend, and thanks are due to Gary Sayler for this. Finally, due to the generous support of Ed McDaniels, the Hilton Smith Fellowship was made available to me for the entire duration of my graduate studies.

I took advantage of the extensive travel funding opportunities from the UT Chemical Physics Program to give presentations at world-class scientific conferences. I strongly suggest future and current graduate students pursue both the Chemical Physics curriculum and funding opportunities, and I urge the administration to make them a priority.

Abstract

A detailed and thorough computational investigation of the SF_6^- anion is undertaken, with additional calculations of other stable SF_n^- anions. The calculations are used to interpret recent infrared multi-photon dissociation (IRMPD) experiments of SF_6^- and SF_5^- anions done with the FELIX free electron tunable infrared laser in the spectral range of 450-850 cm^{-1}. The vibrational spectroscopy of negative molecular ions is crucial towards understanding the dynamics of electron transfer processes, as well as providing experimental validation for computational models of molecular bonding in anions. Many molecular negative ions have been shown to exhibit long (i.e. $> 1\mu s$) lifetimes with respect to electron autodetachment, and a recent reformulation of QET, or quasi-equilibrium theory, has shown success in reproducing these experimental lifetimes for a variety of molecules. In particular, the SF_6^- anion has an interesting history of disparate results for autodetachment lifetime measurements, largely dependent upon the type of experimental method employed. Analysis of the experimental data in reference to the theoretical predictions of QET suggests this disparity may be related to the degree of IVR, or inter-vibrational coupling occurring in the anion. Calculation of the electron autodetachment lifetime according to QET requires accurate values for the electron affinity as well as the vibrational frequencies for both the neutral and the anion. Ab-initio and DFT computations are extremely useful for providing reasonable estimates of the anion vibrational frequencies, however, experimental constraints upon these values are essential. An additional benefit of anion vibrational spectroscopy is the elucidation of molecular structure and symmetry. This is particularly relevant for the case of SF_6^-, as certain computational methods show interesting results in regard to the distortion to lowered C_{4v} symmetry. This is in contradiction to the expected O_h symmetry of the SF_6^- anion, and the potential energy surface along this multi-dimensional vector of S-F bond dissociation is further computationally explored, as are the theoretical implications of a multiple-well potential surface.

Contents

List of Tables

List of Figures

Chapter 1

Introduction

Exploration of molecular anion stability is important for both thermodynamic and kinetic concerns. This information may be of relevance for atmospheric chemistry, such as in freon processing in the upper atmosphere, or it may be of fundamental physical concern, as in the case of the unanswered questions regarding the sulfur hexafluoride anion.

Negative ions may either be of higher or lower energy than their neutral counterparts. For the case of lower energy anions these are considered bound states, and are thermodynamically stable if made under proper conditions. Anions of a higher energy than the associated neutral may also be formed in a temporary metastable state. If the lifetime of the state is short, such as on the order of nanoseconds or less, such as for N_2^-, it may be experimentally probed by electron scattering techniques. If the lifetime is long enough, such as on the order of microseconds or more, the metastable anion may persist long enough for detection by mass spectrometry, as is the case for CO_2^-. Thermodynamically stable anions may also exist in a metastable state as well, if no relaxation process occurs subsequent to electron attachment. The lifetime of these metastable anions with respect to autodetachment has been demonstrated to be directly related to the vibrational characteristics of the molecule [1].

The thermodynamic stability of the anion can be explored with modern computational chemistry techniques. The advent of modern computing methods and power has made accurate numerical solution of the Schrodinger equation feasible for even large polyatomic molecules. Computational investigation of anion thermodynamic stability requires careful exploration of the possible changes in structure and symmetry, and full account of vibrational frequencies. The successful application of this approach provides insight into the vibrational dynamics and the details of the potential energy surfaces of the neutral and negative ion. Limitations in computing power require approximations which introduce errors that must be carefully assessed, but the application of modern methods of chemical computing can produce many meaningful results. The use of molecular orbital computations for exploration of multi-dimensional potential energy surfaces has become an indispensable tool for study of molecules and ions. In fact, molecular orbital calculations for determination of anion properties often provide the only available data on the vibrational characteristics of gas-phase molecular anions since the vibrational spectroscopy of these species is a relatively undeveloped field. For the vibrational spectroscopy of novel species, electronic structure theory is used to aid in the interpretation

of experimental spectra.

The use of vibrational spectroscopy for investigations of molecular structure and bonding is a well-established methodology. It is also an invaluable tool for identification and quantification of chemical compounds, and is therefore highly effective as an in-situ analysis technique. The vibrational characteristics of molecules and ions are also related to dynamic behavior such as electron transfer processes and molecular dissociation. This work examines the usefulness of computational and spectroscopic methods for establishing vibrational properties of molecular anions, which are then used for modeling dynamic behavior. In particular, a re-formulation of the quasi-equilibrium theory, or QET, of metastable anion electron autodetachment rates is undertaken. The vibrational frequencies of the molecule and molecular anion play a crucial role in the application of this approach. The well-studied but often experimentally infuriating SF_6^- anion is studied in detail.

The partnership of computation and spectroscopy leads to a critique of existing theories and towards the development of new theoretical approaches. The interplay between computation and spectroscopy is evident in the use of computational spectral predictions, and subsequent refinement of computed potential surfaces with spectral data. This process follows the established pattern of the scientific method; the predictions of a model are subjected to experimental verification, and the subsequent refinement of the model by acquired data leads to further insight into the underlying physics represented as parameters in the model.

1.1 Atmospheric Chemistry and Spectroscopy

In the Earth's atmospheric system, the spectroscopic characteristics of the component gases provide the foundation for understanding radiative transfer through the atmosphere. The energy input into the Earth's climate system from solar radiation is essentially the engine for the entire climate system, and thus optical spectroscopy of the Earth's atmosphere is a well-studied field of crucial importance for concerns of global climate change. The vibrational spectroscopy of the Earth's atmosphere provides a foundation for discussion of the vibrational spectroscopy of many types of molecules, and in particular the spectroscopy of molecular anions and models of their dynamic behavior.

Many molecules with positive electron affinities and significant electron capture cross-sections are of interest for atmospheric chemistry, as well as of fundamental physical interest. The climate-forcing potential of atmospheric gases is related to both the infrared absorption characteristics of the molecule and it's chemical stability in the atmospheric environment. For molecules with a high degree of chemical inertness and low photoionization or photodissociation cross-sections, such as SF_6 and many freons, electron capture processes in the upper atmosphere may provide the primary destruction pathway. Thus, for these molecules, the behavior of the molecule towards electron capture and the characteristics of the resulting molecular anion are of crucial importance for modeling the Earth's climate system and understanding the results of anthropogenic influences.

1.2 SF_6^- Anions

Often, the detailed and thorough analysis of certain molecules leads to advances in general approaches. In this spirit, a significant focus is devoted to electron attachment to the SF_6 molecule. Sulfur hexafluoride negative ions are well-studied stable molecular anions that are of practical and fundamental physical interest. SF_6 is a relatively inert, nontoxic, and volatile molecule which attaches low-energy electrons with a cross section approaching the maximum allowable for s-wave capture [2]. Among many applications, SF_6 is widely employed to increase the dielectric strength of gases (electrical transmission and distribution systems, circuit breakers, etc.), as a plasma etching gas, in charged-particle accelerators and as an atmospheric pollutant tracer gas. Inadvertent release of SF_6 gas to the environment is of great concern since SF_6 exhibits a global warming potential much greater than that of CO_2 due to its atmospheric stability and very strong infrared absorption band in a region of the spectrum where there are fewer overlapping atmospheric absorptions. The lifetime of SF_6 in the atmosphere is also determined primarily by the reactions of SF_6^- [3]. These characteristics make SF_6 electron transfer chemistry a question of industrial, theoretical and environmental interest. many molecules are similar to SF_6 in this respect, including a wive variety of halogenated hydrocarbons.

The fundamental properties of the SF_6^- anion have been under some debate for many years. Properties such as electron affinity and electron auto-detachment lifetimes have a history of disparate experimental and computational reports. Development of a theoretical model for prediction of these properties can be applied to other anionic systems. Successfully modeling these properties in general leads to greater ability to interpret experimental spectra, and allows further corrections of the models employed. A method for prediction of the temperature-dependent autodetachment lifetimes of metastable anions is developed, and for the case of SF_6, vibrational spectroscopy of the gas-phase SF_6^- anion complements computational investigation.

1.3 Molecular Orbital Calculations

The use of electronic structure theory to aid in the assessment of molecular spectra is a modern revolution in applied quantum chemistry. Limitations in computing power require approximations which introduce errors that must be carefully assessed, but the application of modern methods of chemical computing can produce many meaningful results. These theoretical predictions are used as guides for future experiments and development and refinement of physical models. The success of this approach is a testament to the predictive power of a model refined by experimental data.

The molecular system is modeled by the time-independent Schrödinger equation

$$\hat{H}(\Psi) = E\Psi \tag{1.1}$$

where $\hat{H}()$ is the non-relativistic Hamiltonian operator acting upon the molecular wavefunction, Ψ, with energy E. Numerical solution of this equation using a basis set of molecular orbitals constructed from atomic orbitals provides a solution to the molecular wavefunction which contains all of the information about the molecule. Analysis of the dependance of the energy of this wavefunction as a function of molecular geometry

provides the basis for computational geometry optimizations and vibrational frequency calculations. With the ability to calculate the vibrational frequencies of negative ions with a wide range of methods, experimental verification is required to guide the application of various quantum chemical methods to the system. This critique can provide confidence in the calculated frequencies and other computed properties, allowing these quantities to be used for spectral prediction and models of dynamic behavior.

A central approximation in the solution of equation (1.1) involves assuming the seperability of the nuclear and electronic wavefunctions of the molecule, known as the Born-Oppenheimer approximation [4]. The mass differences of the electrons and nuclei suggest the electron distribution responds "instantaneously" to the changes in nuclear positions, and thus the electronic wavefunction, ψ_e, is a parametric function of the nuclear positions. The molecular wavefunction Ψ is then represented by the product

$$\Psi = \psi_N \psi_e. \tag{1.2}$$

The Hamiltonian operator of equation (1.1) can be assumed to be a linear combination of a nuclear Hamiltonian, $\hat{H}_N()$, and an electronic Hamiltonian, $\hat{H}_e()$, and thus for each possible nuclear configuration the relationship

$$\hat{H}_e(\psi_e) = E_e \psi_e \tag{1.3}$$

holds. This assumption is what allows for the computational description of a molecular potential energy surface.

The spin of an electron is an intrinsic property that must be accounted for in a proper description of the electronic wavefunction, and thus the electronic wavefunction for an N-electron molecule is a function of 4N coordinates. The electronic wavefunction, ψ_e, for a multi-electron system is built from N 4-D one-electron spin orbitals, $\chi_{e_N}(x_i, y_i, z_i, s_i)$. To ensure that the electronic wavefunction follows the Pauli exclusion principle and the anti-symmetry exchange principle for fermions, the necessary form of the electronic wavefunction for a two-electron molecule is

$$\psi_{e_1 e_2} = \frac{1}{\sqrt{2}}(\chi_{e_1}(x_1, y_1, z_1, s_1)\chi_{e_2}(x_2, y_2, z_2, s_2) - \chi_{e_2}(x_1, y_1, z_1, s_1)\chi_{e_1}(x_2, y_2, z_2, s_2)).$$

This form is reproduced correctly for the N-electron wavefunction when represented as a Slater determinant [4]. This is the determinant of a matrix of the N x N exchange possibilities of electrons.

The analytical solution of the Schrödinger equation is not possible for all but the one-electron system, so an important approximation is made for numerical solution. The Hartree-Fock approximation assumes that the Hamiltonian operator can be reduced to a sum of one and two-electron interaction potentials. However, each two-electron potential depends upon the others, so the problem becomes a non-linear eigenvalue problem. The typical method for solving this problem is to employ the self-consistent field, SCF, method. This is done by making an initial guess at the initial spin-orbitals, and then the average field for each electron is calculated. This defines the properties of the Hartree-Fock Hamiltonian operator, and the eigenvalue problem is solved to produce a new set of spin orbitals. These new orbital solutions are used as a new guess, and the

procedure is repeated until the spin orbital guess and solution are identical. This is the method upon which most modern computational chemistry algorithms are based.

For open-shell systems, a method called unrestricted Hartree-Fock, UHF, is used that relaxes the requirement of spin-paired electrons in each spatial orbital. Thus, every electron is free to occupy a unique spatial orbital, and a system of equations results that treats the spin up and spin down electrons separately. This method is required for description of radicals, triplet states, and also for bond dissociation calculations. However, since the electronic UHF wavefunction is no longer an eigenfunction of the squared spin angular momentum operator, errors may result from "contamination" from states with higher order spin multiplicities.

The SCF-HF method shows general reliability and sometimes even remarkable agreement with experimental results. Considering the approximations this method employs, though, this agreement can be demonstrated to be a cancelation of errors. Errors are introduced by finite size of the basis set used. The quality of a SCF-HF calculation is also limited because the SCF Hartree-Fock method uses a single Slater-determinant to describe ψ_e and thus neglects correlation between electrons with different spin [4]. This can often lead to a "restricted" description of the electronic wavefunction, and hence an incorrectly computed lowest energy molecular structure. Many methods exist for addressing this shortfall, some employ empirical adjustments to the Hamiltonian operator itself, such as Density Functional Methods (DFT), and some employ adjustments to the basis set used to form the electronic wavefunction, such as the use of multiple Slater-determinants in the coupled-cluster (CC) and configuration-interaction (CI) methods. These methods all attempt to account for the ability of the electrons to respond to each other individually and instantaneously, instead of through an average over electron pairs. Incorporating this into the model lowers the energy of the system relative to the HF-SCF solution by an amount known as the recovered correlation energy. Use of these higher-order methods often dramatically improves the quality of the calculated molecular properties, but often at the expense of much higher computational cost. The highly accurate CCSD(T) method requires the use of much smaller basis sets than are possible for SCF, DFT and even MP2 methods. This issue of basis set size is critical, as is the case with any representation of a wave in terms of expanded orthogonal component waves; the larger the basis set, the more "overtones" are accessible to allow the model system to better respond to the operators, producing a more accurate eigenvalue. The detailed description of the basis sets considered within is available in many sources [4]. A series of calculations using the same method but with increasing basis set size can show how quickly the computed energy converges. This basis set convergence is often very slow, especially for radicals or unusual bonding moieties, requiring a very large basis sets for adequate agreement with experiment.

In each case, careful consideration must be given to the suitability of each method for the molecular system under consideration. With the ability to calculate the electron affinities, molecular structure, and vibrational frequencies of negative ions with a wide range of methods, experimental verification is required to guide the application of various quantum chemical methods to the system. The application of the various methods to atoms and molecules with experimentally verified properties can guide the selection of the suitable level of computational theory. Two issues must be weighed: the issue of

basis set size, and how to include the correlation energy. The density functional theory methods are almost as fast as the Hartree-Fock method, but have been tailored to hydrocarbons, so for other types of systems may not be reliable. MP2 is often the practical limit for large molecules on current personal computers. Unfortunately, although MP2 makes a large improvement in many calculated properties, it been shown to sometimes be insufficient for a satisfactory description of negative ions [5], with significant error in calculated electron affinities. When not limited by very small basis sets, the CCD and CCSD(T) methods produce good agreement with experimentally measured electron affinities. However, these methods are much more expensive computationally, and thus limited to small molecules and moderate basis sets. Restriction from large basis set calculations means basis set convergence is not verified. Nonetheless, the application of these methods with reasonably large basis sets gives useful qualitative description and in many cases reliable numerical prediction.

For simple molecules or molecules of high symmetry, the potential energy surface can be examined directly by calculation of the energy at various different structures. Provided all internal degrees of freedom have been examined, the minimum energy configuration is close to the one of lowest calculated energy. A functional fit of a thorough set of energy-position points produces a calculated potential energy function of the molecule, from which the optimal structure and vibrational frequencies can be determined. This is the preferable method when possible, since the information about vibrational mode coupling and anharmonicities is available. This method is very labor-intensive, and prohibitively so for most molecules. Using a lower level of theory allows for calculations that employ computationally expensive internal algorithms for determination of optimal structure and vibrational frequencies.

Optimal structures are computationally determined by examining the curvature of the potential surface to ensure there is essentially zero slope. The slope of a potential surface at a given point is proportional to the force, so the derivative of the electronic energy with respect to molecular position will be zero at the minimum structure. However, since there are not only valleys in the potential surfaces of molecules, but ridges as well, there are structures where despite there being zero force on the atoms, the energy is lowered by a change in structure. This kind of structure, such as a linear H_2O molecule with optimum O-H bond length, represents a saddle point on the potential surface and is not the minimum energy configuration. Thus a molecular geometry optimization calculation using only first derivatives must be verified by a frequency calculation. The degree of curvature of molecules potential surface is given by the second derivative of the energy with respect to position. This degree of curvature is analogous to the tension in a spring, and dictates the frequency and direction at which the atoms vibrate relative to each other. The sign of the second derivative will be negative for the case of curvature to a lower energy structure, and thus a vibrational frequency calculation with a negative eigenvalue shows the direction to a lower energy structure. In addition to verifiying the structure, these calculated vibrational frequencies and symmetries are useful for many purposes. For spectral interpretation, it is been demonstrated that frequency calculations often slightly overestimate the observed values. Thus, a scaling factor is used. For consistency within the current work, DFT calculations are scaled by 0.98 and *ab-initio* calculations are scaled by 0.95. These values are empirical and are taken from standard

practice [4].

There are ample opportunities for relevant computational investigations to complement experiential and theoretical chemistry. A powerful application of quantum chemical calculations is the calculation of minimum energy optimal molecular structures. The change in molecular structure upon electron transfer plays a significant role in the considerations of anion stability. Pairs of neutral and anion optimization and frequency calculations make an efficient and powerful start for a treatment of the electron autodetachment rate. The theoretical treatment requires the anion and neutral molecule vibrational frequencies and the electron affinity, all available computationally if not experimentally.

The process of establishing a set of reliable calculations for determination of molecular structures, vibrational frequencies and electron affinities is followed in detail for the SF_6 molecule. These values are then used to aid in the interpretation of multiple photon infrared dissociation spectra and in the development of a theoretical treatment for anion electron detachment. A concurrent exploration of SF_5^- spectroscopy and SF_4-^* autodetachment lifetimes allows for further experimental critique of the computational methods employed for the SF_n^- molecules. The detailed computational investigation of the SF_n^- molecules provides a context for the use of computations in a general theoretical approach to the calculation of anion autodetachment lifetimes.

Chapter 2

Sulfur Fluoride Series Molecular Orbital Calculations

2.1 Introduction

Sulfur hexafluoride is a well-studied molecular anion but significant ambiguities remain regarding crucial properties such as the electron affinity, anion structure, vibrational frequencies, and autodetachment lifetime. Recent measurements have begun to resolve some of these discrepancies, but many remain, especially as regards the electron autodetachment rate from the metastable anion.

Many experimental and computational electron affinity determinations have been done for this molecule, including reported values that have ranged from 0.5 eV to 3.0 eV. The adiabatic electron affinity, $EA_{ad.}$, is presently believed to be equal to 1.05 eV, according to the experimental determinations of Streit [6], and Grimsrud *et al.* [7]. These values are supported by high level ab-initio computations by Gutsev and Bartlett [8].

Due to the A_{1g} symmetry of the SF_6 LUMO, the symmetry of the anion would not be expected to change upon electron attachment due to a Jahn-Teller interaction. The LUMO is an antibonding orbital, however, so elongation in the S-F bond length would be expected. The structure of the anion has been calculated to be of octahedral symmetry like the parent molecule, as would be expected [8]. However, detailed studies of the potential energy surface of the SF_6 molecule suggest the possibility of a lower symmetry ground state geometry. Certain ab-initio methods have reproduced an interesting feature of certain DFT methods originally explored by Brinkmann and Schaefer [9] that determined the O_h symmetry of the anion not to be at a global minimum. Rather, these computations predict a minimum energy structure of C_{4v} symmetry. These reduced-symmetry global minima have interesting implications.

There are practical applications of these computational studies as well as opportunities for experimental validation. The SF_6 and SF_6^- system is studied in detail, but significant attention is given to SF_5^- as well. The vibrational frequency calculations of SF_5^- and SF_6^- are compared to recent results from IR-MPD experiments. The SF_6^- calculations are also used in a study of the lifetimes of these anions as formed in their initial metastable states upon free-electron attachment.

The accurate calculation of energies and properties of negative ions is a notoriously difficult problem. It is necessary to account for the large change in the polarizabilities of electron-attached molecules, and electron correlation becomes essential for even a qualitative description. Recent publications provide a thorough computational exploration of the entire sulfur fluoride series. The DFT studies of King *et al.* [10] are complemented by GAUSSIAN03 [11] methods employed by Miller *et al.* [12]. The current study is not intended to be as comprhensive in the analysis of this entire series. Calculations of the F, F^-, S, S^-, S^+, SF, SF^- components of the SF_6^- molecule are used for calibration and comparison of the methods used, and to explore the effects of basis set truncation. These caluclations are used to help gauge the reliability of the larger SF_n and SF_n^- molecule calculations.

2.2 Computational Methods

Calculations are performed with both Gaussian Inc.'s G03 program [11] and the NWChem Version 5.0 computational package [13]. All calculations employed are capable of being performed on current standard mid-grade technology single-processer PC's. Geometry optimizations and frequency calculations are done with DFT, and MP2 methods as well as coupled-cluster (CCD) methods. The CCSD(T) method is used to study the SF_6 and SF_6^- potential energy surfaces.

Unfortunately, each of these methods has some limitation. It has been demonstrated that the MP2 level of theory often provides an insufficient description of molecular anions, despite large basis sets. DFT methods are of much more reasonable computational expense, and often provide an excellent description, but their behavior towards fluorine-containing molecules and anions in general is not completely characterized. Coupled-cluster methods have shown to provide very reliable descriptions of anions provided a basis set of sufficient size is used, but this is very quickly limited by computational expense. With the SCF method basis set sizes of up to aug-cc-pVQZ (564 functions) for SF_6^- are feasible, on the same system, CCSD(T) methods require a basis set no larger than 6-311+G(S:3df,F:2d) (209 functions). The effects of basis set truncation are explored for SF_6 and for the atomic and molecular components of SF_6^- with the CCSD(T) method.

2.2.1 SF_6^- Basis Set Truncation

The Sulfur Hexafluoride molecule is "hypervalent", and thus a minimum basis set that includes additional polarization functions is required to correctly describe the bonding. In addition to this, as is typical of negative ion calculations, diffuse functions are also required. The effects of the basis set truncation is examined with SCF-HF calculations. An octahedral symmetry is assumed for both the neutral and the anion. Since the minimum energy bond length will differ from one basis set to the next, a large "low-resolution" scan of 11 different bond lengths was employed to ensure bracketing of the minimum energy. These scans are shown in Figure 2.1. A least squares fit is done to estimate the global minimum for each basis set. Table 2.1 summarizes the results of the Hartree-Fock (HF) SCF calculations for SF_6 and the unrestricted Hartree-Fock (UHF)

for SF_6^-. Upon comparison of these minima, it is clear that convergence is slow, and quite large basis set sizes are required to account for even the un-correlated electronic energy. Thus, we must expect a measure of inaccuracy in all ab-initio calculations done with reasonable cost.

As seen in Table 2.1, even with extremely large basis sets, the SCF method incorrectly predicts the electron affinity, greatly overestimating it. Extension of the basis set to very large sizes barely improves the issue, even for the largest basis set used. The aug-cc-pVQZ basis with SCF-HF methods brings the calculated electron affinity out of the absurd range of 15 eV, but predicts a negative electron affinity for SF_6.

The fact that the electron affinity is of the wrong sign with the uncorrelated SCF Hartree-Fock calculation despite the extremely large basis set underscores the importance of the correlation method employed. MP2 calculations may be suitable as a first approximation for negative ion properties, and when used with care they may serve as a guidepost for higher-order theory calculations, but often are insufficient for accurate description. Coupled-cluster theory has demonstrated success in modeling anion energetics [8]. Provided that a sufficiently large basis set is used, these methods would be expected to yield accurate information about SF_6 and SF_6^- properties. However, computational expense for these methods is large, and places restriction on feasible basis set size. The determination to concentrate on CCD and CCSD(T) methods despite this limitation was made based upon suitability for dissociation energies as well as the demonstrated ability of the method to approximate experimentally established electron affinities with basis sets of moderate size.

2.2.2 Atomic and Diatomic Components: Basis Set Truncation

To determine the influence of the basis set size on capturing the correlation energy with CCSD(T) methods, an approximation was employed. Energies of fragments of SF_6^-, namely, F, F^-, S, S^-, S^+, SF and SF^-, were calculated with CCSD(T) methods. Electron affinities calculated using the CCSD(T) method have consistently demonstrated success provided a sufficient basis set is employed [8]. A comparison of calculated and experimental electron affinities for the atomic and diatomic components of SF_6 can provide some measure of the importance of basis set size for describing sulfur-fluorine bonding using computational models that include electron-electron correlation. Examination of the relationship of basis set and energy for the fragments reveals the importance of the basis set size in accounting for the correlation energy. It is not unreasonable to infer a similar relationship between these smaller fragments and the parent molecule.

Fluorine

Table 2.2 summarizes the results for CCSD(T) calculations of the Fluorine atom and Fluoride ion. The experimental reference is from Blondel *et al.* [14]. The neutral molecule is calculated as a doublet state and the ion as a singlet. It is apparent that multiple additional polarization functions are required for even a 10% agreement of electron affinity values.

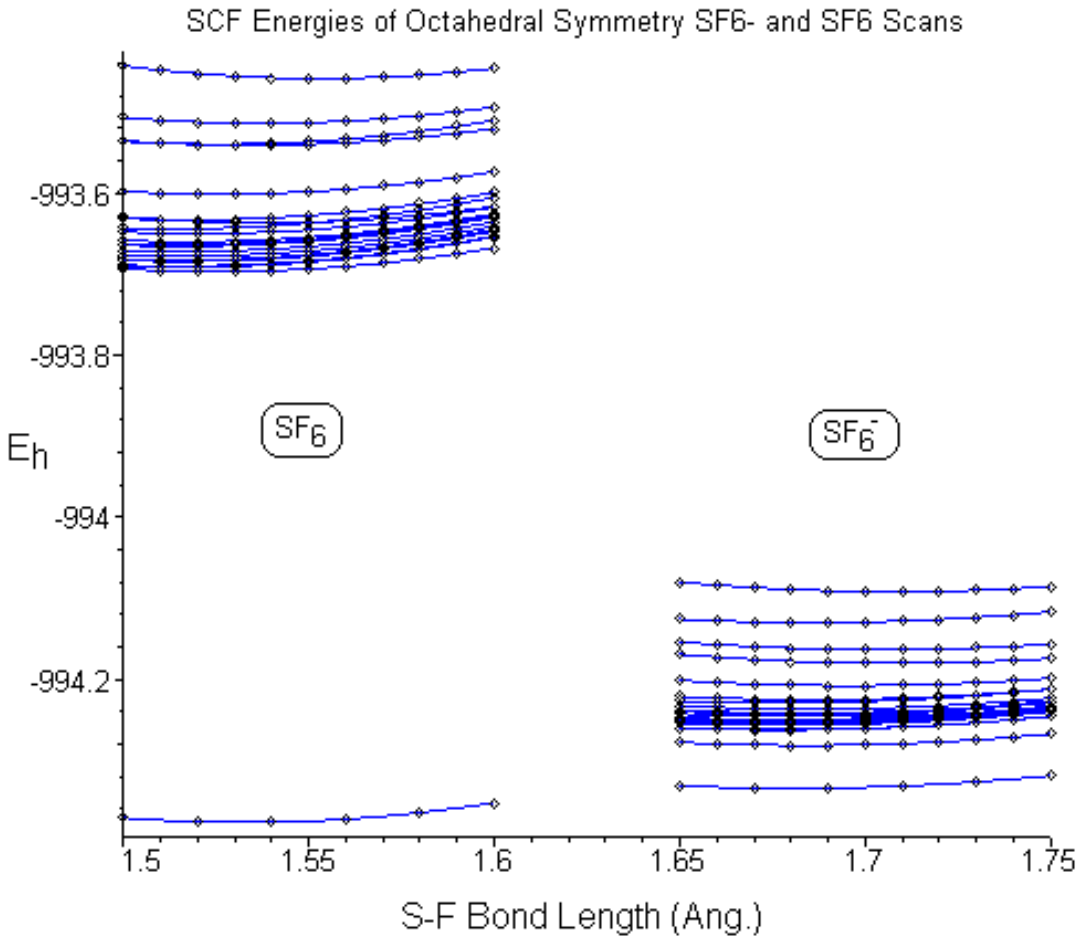

Figure 2.1: SF_6 and SF_6^- SCF O_h scans with various basis sets.

Table 2.1: SF_6 and SF_6^- SCF O_h scan minima from fits to scans from various basis sets, shown in Figure 2.1. Also shown are non-zero-point energy corrected electron affinity values. Values are in very poor agreement, accentuating the need for higher order calculations for accurate prediction of molecular anion properties.

S basis	F basis	# fxns.	SF_6^- R_{eq}	SF_6^- E_{min}	SF_6 R_{eq}	SF_6 E_{min}	EA(eV)
6-311+G*	6-311+G*	162	1.704	-994.164	1.537	-993.514	17.7
aug-cc-pVDZ	aug-cc-pVDZ	165	1.708	-994.092	1.553	-993.459	17.2
6-311+G(2d)	6-311+G*	167	1.708	-994.180	1.534	-993.541	17.4
6-311+G(2df)	6-311+G*	174	1.685	-994.225	1.517	-993.633	16.1
6-311+G(3df)	6-311+G*	179	1.676	-994.229	1.512	-993.645	15.9
6-311+G(2d)	6-311+G(2d)	197	1.696	-994.208	1.526	-993.602	16.5
aug-cc-pVTZ	aug-cc-pVDZ	188	1.686	-994.130	1.526	-993.540	16.1
6-311+G(2df)	6-311+G(2d)	204	1.685	-994.237	1.520	-993.650	16.0
6-311+G(3df)	6-311+G(2d)	209	1.678	-994.245	1.516	-993.666	15.8
6-311+G(3d2f)	6-311+G(2d)	216	1.679	-994.243	1.514	-993.664	15.7
6-311+G(3df)	6-311+G(3d)	239	1.678	-994.252	1.515	-993.678	15.6
6-311+G(2df)	6-311+G(2df)	246	1.683	-994.242	1.517	-993.660	15.8
6-311+G(3df)	6-311+G(2df)	251	1.677	-994.250	1.515	-993.673	15.7
6-311+G(3df)	6-311+G(3df)	281	1.677	-994.257	1.515	-993.685	15.6
6-311+G(3d2f)	6-311+G(3df)	288	1.677	-994.254	1.512	-993.684	15.5
aug-cc-pVDZ	aug-cc-pVTZ	303	1.696	-994.245	1.538	-993.637	16.5
6-311+G(3df)	6-311+G(3d2f)	323	1.677	-994.262	1.515	-993.690	15.6
aug-cc-pVTZ	aug-cc-pVTZ	326	1.684	-994.282	1.525	-993.697	15.9
6-311+G(3d2f)	6-311+G(3d2f)	330	1.676	-994.263	1.514	-993.692	15.5
aug-cc-pVQZ	aug-cc-pVQZ	564	1.680	-994.335	1.533	-994.377	-1.1

Table 2.2: Fluorine Atom Electron Affinities Calculated With the CCSD(T) Method Using Various Basis Sets and Comparison to Experimental Reference.

Basis Set	# fxns	$^2F^-$ E_h	^1F E_h	EA (eV)	% error
experimental [14]				*3.401*	
6-311+G(d)	22	-99.680	-99.572	2.948	13.3
aug-cc-pVDZ	23	-99.669	-99.550	3.226	5.1
6-311+G(2d)	27	-99.705	-99.592	3.074	9.6
6-311+G(df)	29	-99.703	-99.594	2.964	12.8
6-311+G(3d)	32	-99.713	-99.595	3.193	6.1
6-311+G(2df)	34	-99.728	-99.614	3.098	8.9
6-311+G(3df)	39	-99.736	-99.618	3.216	5.4
6-311+G(3d2f)	46	-99.742	-99.622	3.248	4.5
aug-cc-pVTZ	46	-99.750	-99.628	3.312	2.6
aug-cc-pVQZ	80	-99.777	-99.653	3.379	0.7
aug-cc-pV5Z	127	-99.787	-99.662	3.399	0.1

Sulfur

The following table compares calculated Sulfur atom IP and EA values with the experimental. The electron affinity is from the work of Hotop *et al.* [15], and the IP is well characterized [16]. The convergence to the correct value is much more rapid for the cation-neutral pair. This emphasizes the difficulty inherent in obtaining accurate computational values for electron affinities.

Sulfur Fluoride

SF^- exists as a stable gas phase anion with an EA of 2.285 eV, as determined by Polak *et al.* [17]. The calculations of the electron affinity demonstrate the effect of basis set size on accuracy. The minimum energy bond length was determined by loose (0.04 Angstroms) bracketing, not functional fits.

A comparison of the calculated fragment EA values suggests that using the 6-311+G(3df) basis for Sulfur and 6-311+G(2d) for Fluorine might be expected to provide reasonable calculated electron affinities for SF_6 and SF_5. The basis set is hoped to provide sufficient accuracy without excessive computational expense.

2.3 Optimization and Frequency Calculations

Optimization and frequency calculations ensure the structure chosen for adiabatic electron affinity calculations is at a true minimum. These calculations are done for both SF_5^- and SF_6^-. In the case of SF_6^- they also suggest some interesting features of the SF_6^- potential energy surface that are explored further.

2.3.1 SF_6^- Structure and Vibrational Frequencies

Geometry optimizations and frequency calculations of SF_6^- are done with DFT and MP2 methods as well as coupled-cluster (CCD) methods. MP2 and DFT methods have previously been employed, the current study extends the basis set for the MP2 calculations, and also includes MP4(DQ) methods and coupled-cluster theory calculations. The results for harmonic vibrational frequency calculations done for SF_6^- constrained to O_h symmetry are shown in Table 2.5.

Examination of the methods show that there is overall agreement, but there is a very interesting discrepancy among the methods for the result of the T_{1u} mode. For MP4(DQ) and CCD methods with all basis sets but aug-cc-pVDZ this mode is calculated to be the coordinate along which a distortion produces a lower energy structure. Even among calculations producing real frequencies, the CCD/aug-cc-pVDZ, MP4(DQ)/aug-cc-pVDZ, and DFT results show a dramatic decrease of the frequency of the low-energy T_{1u} mode compared to the MP2 results.

The methods that show an unstable O_h structure all optimize to a structure with an elongated S-F bond of overall C_{4v} symmetry. The vibrational frequencies arising from this C_{4v} symmetry structure predicted from these methods are shown in Table 2.6.

The disagreement within the CCD methods is surprising considering the usual reliability of CCD methods. This suggests that basis set truncation may play a role in the

Table 2.3: Sulfur Atom Electron Affinity and Ionization Potential Calculated With the CCSD(T) Method Using Various Basis Sets and Comparison to Experimental References.

Basis Set	# basis fxns	^{3}S E_h	^{2}S$^-$ E_h	^{4}S$^+$ E_h	EA(eV)	% error	IP(eV)	% error
experimental					*2.0771* [15]		*10.36* [16]	
aug-cc-pVDZ	27	-397.611	-397.676	-397.249	1.784	14.1	9.827	5.1
6-311+G(d)	30	-397.601	-397.654	-397.252	1.440	30.7	9.512	8.2
6-311+G(2d)	35	-397.620	-397.680	-397.261	1.636	21.2	9.754	5.9
6-311+G(df)	37	-397.624	-397.680	-397.264	1.533	26.2	9.800	5.4
6-311+G(3d)	40	-397.622	-397.686	-397.262	1.761	15.2	9.777	5.6
6-311+G(2df)	42	-397.643	-397.708	-397.273	1.759	15.3	10.061	2.9
6-311+G(3df)	47	-397.645	-397.714	-397.275	1.878	9.6	10.081	2.7
aug-cc-pVTZ	50	-397.656	-397.728	-397.283	1.948	6.2	10.150	2.0
6-311+G(3d2f)	54	-397.647	-397.718	-397.275	1.924	7.4	10.111	2.4
aug-cc-pVQZ	84	-397.668	-397.743	-397.291	2.036	2.0	10.254	1.0

Table 2.4: Sulfur Fluoride Molecule Electron Affinity Calculated With the CCSD(T) Method Using Various Basis Sets and Comparison to Experimental Reference.

Basis Set	# fxns	EA(eV)	% error
experimental		*2.285* [17]	
6-311+G(d)	52	1.997	12.6
aug-cc-pVDZ	50	2.230	2.4
6-311+G (S:d,F:2d)	57	2.084	8.8
6-311+G (2d)	62	2.152	5.8
aug-cc-pV(S:DZ,F:TZ)	73	2.191	4.1
aug-cc-pV(S:TZ,F:DZ)	73	2.254	1.3
6-311+G(S:3df,F:2d)	74	2.152	5.8
6-311+G(2df)	76	2.096	8.3
aug-cc-pVTZ	96	2.244	1.8
6-311+G(3d2f)	100	2.188	4.2
aug-cc-pVQZ	164	2.290	-0.2

Table 2.5: SF_6^- frequency calculations. Frequencies left unscaled. These calculations are constrained to O_h symmetry. The methods that produced imaginary frequencies for the ν_4 mode show a negative value, in boldface. These methods show a minimum energy structure of C_{4v} symmetry.

Method	$v_4(T_{1u})$	$\nu_6(T_{2u})$	$v_5(T_{2g})$	$v_2(E_g)$	$v_1(A_{1g})$	$v_3(T_{1u})$
MP2						
MP2/6-311+G(S:2df, F:2d) [8]	291	225	319	425	595	686
MP2/6-311+G*	251	211	305	414	574	664
MP2/aug-cc-pVDZ	308	220	314	457	602	718
MP2/aug-cc-pVDZ	305	223	317	459	606	709
MP2/aug-cc-pVDZ	302	221	314	456	605	711
MP2/6-311+G(S:3df, F:d)	272	239	329	422	605	678
MP2/6-311+G(S:3df, F:2d)	272	232	323	424	606	679
MP2/6-311+G(3df)	265	229	323	422	602	673
Average of MP2 calculations	*283*	*225*	*318*	*435*	*600*	*690*
% relative standard deviation	*7*	*4*	*2*	*4*	*2*	*3*
DFT						
B3LYP/DZP++ [10]	111	216	313	423	568	627
B3LYP/DZP++ [9]	115	217	314	424	568	628
B3P86/DZP++ [9]	115	222	319	438	589	647
B3LYP/aug-cc-pVDZ	174	213	306	440	564	645
B3LYP/aug-cc-pV(S:TZ, F:DZ)	42	218	314	408	564	614
B3LYP/aug-cc-pVTZ	73	221	316	419	571	618
B3P86/aug-cc-pVDZ	176	218	311	456	585	666
B3P86/aug-cc-pV(S:TZ, F:DZ)	29	222	319	425	587	635
B3P86/aug-cc-pVTZ	65	225	321	434	593	637
Average of DFT calculations	*100*	*219*	*315*	*430*	*577*	*635*
% relative standard deviation	*53*	*2*	*2*	*3*	*2*	*3*
Higher Order Methods						
MP4(DQ)/aug-cc-pVDZ	*129*	*227*	*319*	*474*	*606*	*677*
MP4(DQ)/6-311+G*	**-181**	219	313	431	578	627
MP4(DQ)/6-311+G(S:2d, F:d)	**-90**	224	313	429	572	636
MP4(DQ)/aug-cc-pV(S:TZ, F:DZ)	**-168**	238	329	444	606	643
CCD/aug-cc-pVDZ	*135*	*227*	*319*	*474*	*607*	*678*
CCD/6-311+G*	**-180**	220	312	431	578	628
CCD/6-311+G(S:2d, F:d)	**-87**	224	314	429	572	636

Table 2.6: SF_6^- frequency calculations for methods resulting in C_{4v} structure. Frequencies left unscaled. Modes of symmetry E and A_1 are IR-active for molecules of C_{4v} point group symmetry.

Mode	ν_8	ν_7	ν_{10}	ν_4	ν_{11}	ν_6	ν_9	ν_3	ν_2	ν_5	ν_1
Symmetry	**E**	**E**	$\mathbf{B}_2$	$\mathbf{A}_1$	$\mathbf{B}_1$	**E**	$\mathbf{B}_2$	$\mathbf{A}_1$	$\mathbf{A}_1$	**E**	$\mathbf{A}_1$
CCD/											
6-311+G*	98	248	263	283	365	446	482	507	614	686	751
6-311+G(S:2d,F:d)	98	248	263	283	365	446	482	507	614	686	751

discrepancies. The basis sets that are used for the frequency calculations are relatively small for this molecule, and this is because optimization and frequency calculations require exponentially larger computing resources than do energy calculations. Since energy calculations can be done with larger basis sets and the more reliable CCSD(T) method, further study of the potential energy surface is undertaken along this coordinate.

2.4 O_h Symmetry SF_6^- Potential Energy Surface

Computational investigation of the anion potential energy surface is useful because it allows for more complete treatment of the molecular vibrations. If it is assumed that the SF_6^- ion maintains a global minimum of octahedral symmetry like the parent molecule, than the lowest energy configuration for both is along their mutual symmetric stretch coordinate. The potential energy of the neutral molecule and anion with regard to the totally symmetric stretch is investigated in Figure 2.2.

The calculation method chosen is CCSD(T)/6-311+G(S:3df,F:2d) for reasons discussed previously. Overall the method gives reasonable results, in line with previous studies.

2.4.1 Adiabatic Electron Affinity

The vibrational frequencies calculated allow for an estimation of the zero-point energy corrected adiabatic electron affinity, assuming an O_h symmetry minimum energy SF_6^- structure. The energy difference between the minima of the O_h surfaces is 0.78 eV. Using a zero-point energy of 0.58 eV for SF_6 and 0.35 eV for SF_6^-, the adiabatic electron affinity is 1.01 eV, in excellent agreement with previous calculations [8] and experimental measurement [6].

2.4.2 Vertical Detachment Energy

The vertical detachment energy, or VDE, is defined as the energy required to remove an electron from the anion without any relaxation of the molecular structure. The predicted VDE of 2.9 eV is in line with recent photoelectron spectra of SF_6^- [18], and other calculated values [8]. The agreement with experimental values of the EA and VDE suggests the CCSD(T) method with the 6-311+G(S:3df,F;2d) basis set may provide a sufficiently robust model chemistry for exploration of the SF_6^- potential energy surface.

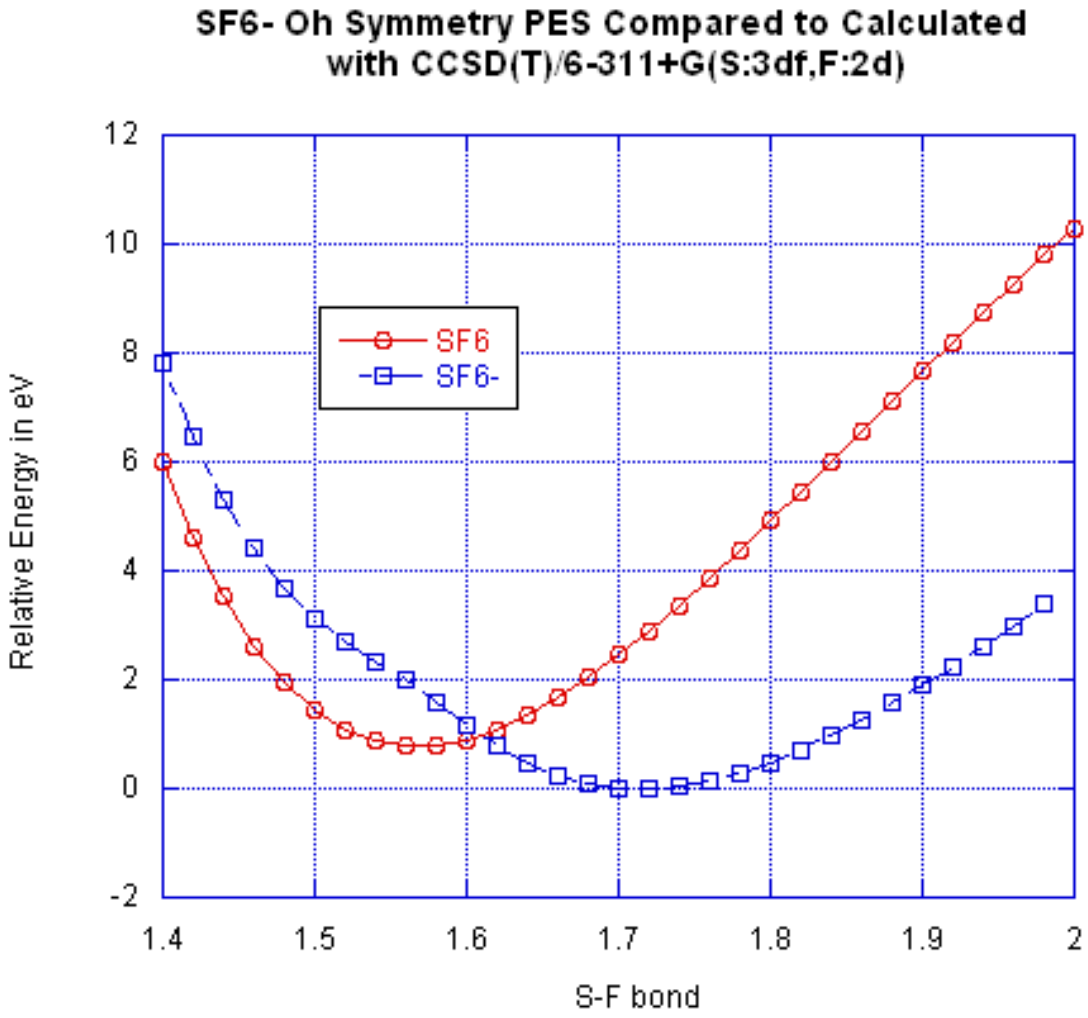

Figure 2.2: SF_6 and SF_6^- O_h symmetry potential energy curves are shown.

2.4.3 Potential Fits and Spectroscopic Constants

Least-squares fitting of functions to the potential energy *ab-initio* data can be useful as surfaces for molecular dynamics studies. These functions also be used to define the internuclear portion Hamiltonian operator is used to generate vibrational spectroscopic parameters. This process is easy to execute for one-dimensional potential energy surfaces, such as for diatomic molecules, or modes of high symmetry in polyatomic molecules, such as the CO_2 symmetric stretch. The SF^- anion will be used as a test and benchmark for the SF_6^- investigation, as the same methods will be used for both anions, establishing a measure of expected reliability.

SF^-

The potential energy surface is calculated at finite intervals along the stretch coordinate of S-F bond length, covering the potential minima in that dimension. The energy along this curve is first fit to a quadratic function with a subset of points near the minimum energy, as shown in Figure 2.3. The energy is then normalized to the function minimum, and the stretch coordinate to the S-F bond length at that minimum. The data thus transformed is only vibrational energy in displacement coordinates, and is fit to a quartic and sixth-order polynomial, as shown in Figure 2.4 It is fit as well with the classic Morse [19] potential, as shown in Figure 2.5.

The spectroscopic parameters derived from the Morse potential are 631.2 cm^{-1} for ω_e and 4.1 cm^{-1} for $\omega_e x_e$, with 0.6% and 5.2% respective error from the experimental values of [17]. The same methods used for the SF neutral radical give 825.1 cm^{-1} for ω_e and 4.4 cm^{-1} for $\omega_e x_e$, with 0.6% and 0.3% respective error from the experimental values of [17]. This excellent agreement with the small SF molecule and SF^- anion suggests some degree of reliability for the larger molecule calculations using the same method and basis.

SF_6^- ν_1, the Symmetric Stretch Mode

For the case SF_6^-, the extension of the S-F bonds retaining O_h symmetry is equivalent to the A_{1g} ν_1 mode of SF_6 and SF_6^-. This provides a simple method for determination of potential energy surface in the direction coordinates of the ν_1 mode. As was demonstrated with SF^-,the energy along this curve is first fit to a quadratic function with a subset of ∼10 points near the minimum energy. The vibrational energy along the SF_6^- ν_1 mode is fit to a quartic and sixth-order polynomial, as shown in Figure 2.6. It is fit as well a Morse potential, as shown in Figure 2.7.

Using the parameters of the Morse fit gives a value of 506.8 cm^{-1} for ω_e and 0.2cm^{-1} for $\omega_e x_e$. The harmonic portion (the q^2 term) of the sixth-order potential function gives a value of 541.0 cm^{-1} for ω_e. There is no experimental standard to gauge these against, but the values are in agreement with the calculated values of Table 2.5. Scaling the DFT frequency results by 0.98 and the *ab-initio* results by 0.95 gives ∼ 550 cm^{-1} for this mode, in rough agreement with the constants from the potential energy surface. The same Morse potential fit procedure applied to the SF_6 neutral molecule ν_1 mode gives a value of 766.0 cm^{-1} for ω_e, which compared to the experimental value of 782.0

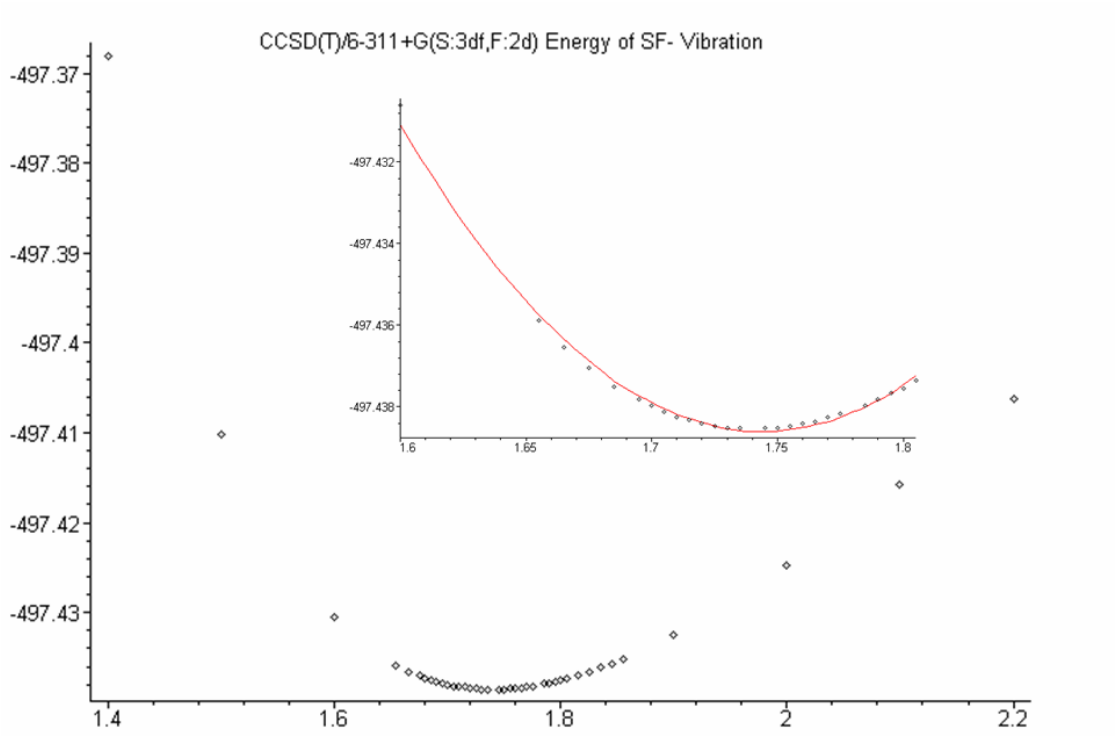

Figure 2.3: SF^- S-F bond stretch potential energy calculations and harmonic fit function.

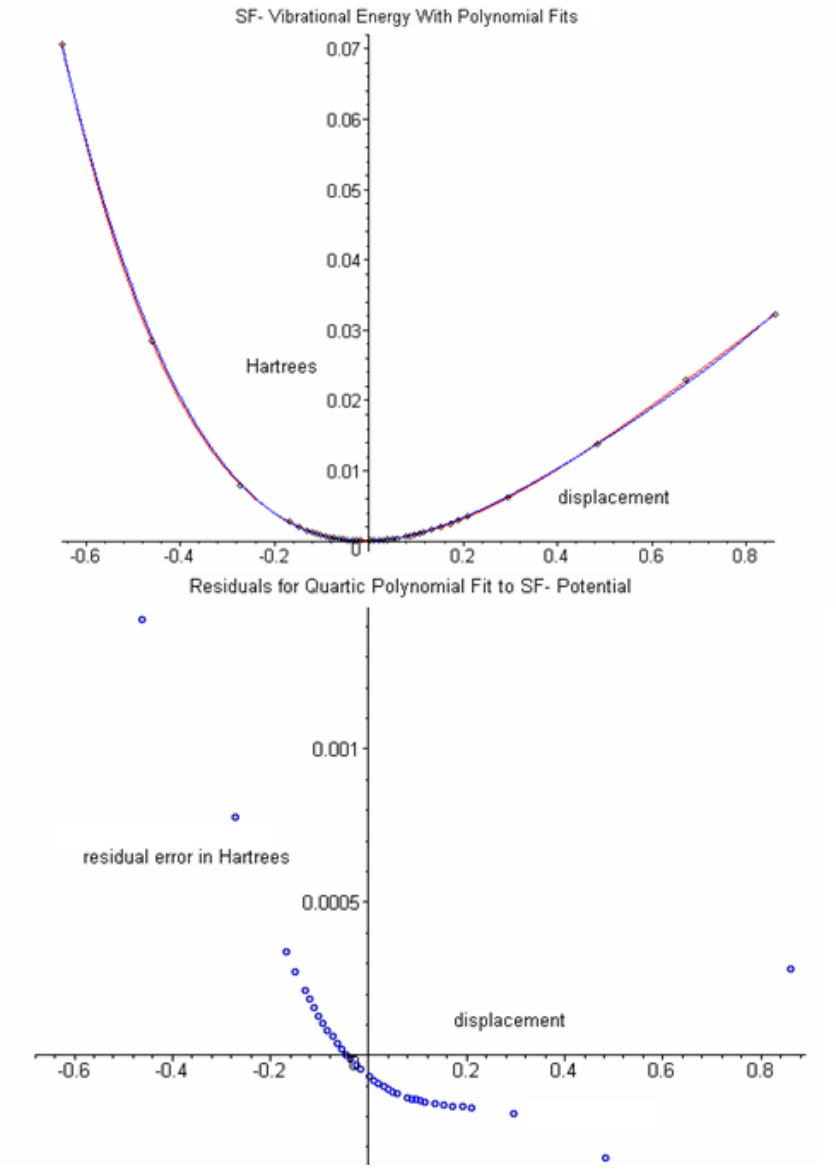

Figure 2.4: The top graph is the SF^- S-F bond stretch potential energy calculations and quartic and sixth-order polynomial fit functions. The bottom graph is the error of the quartic potential function.

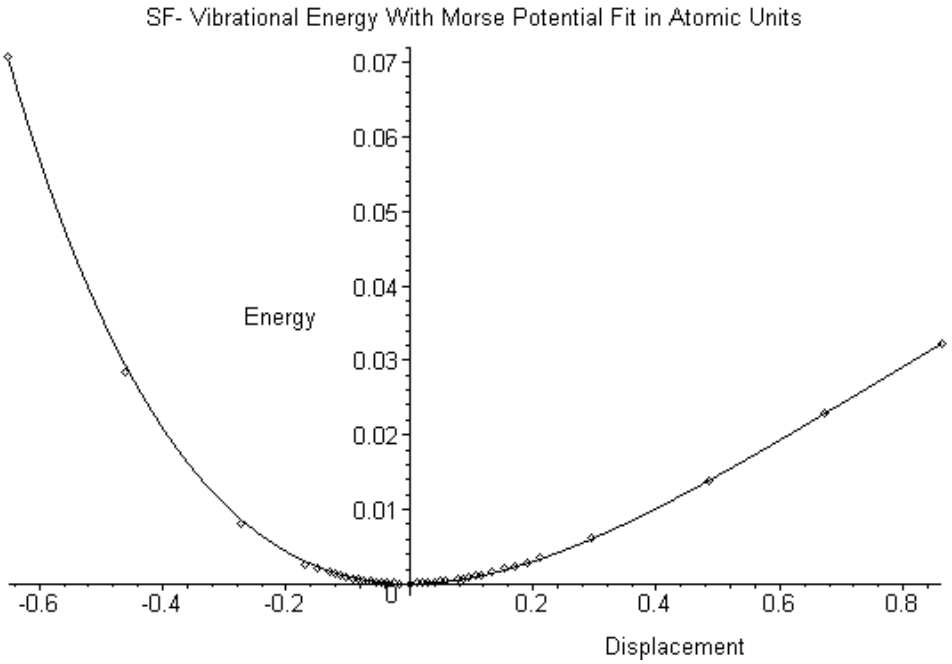

Figure 2.5: SF^- S-F bond stretch potential energy calculations and Morse potential fit function.

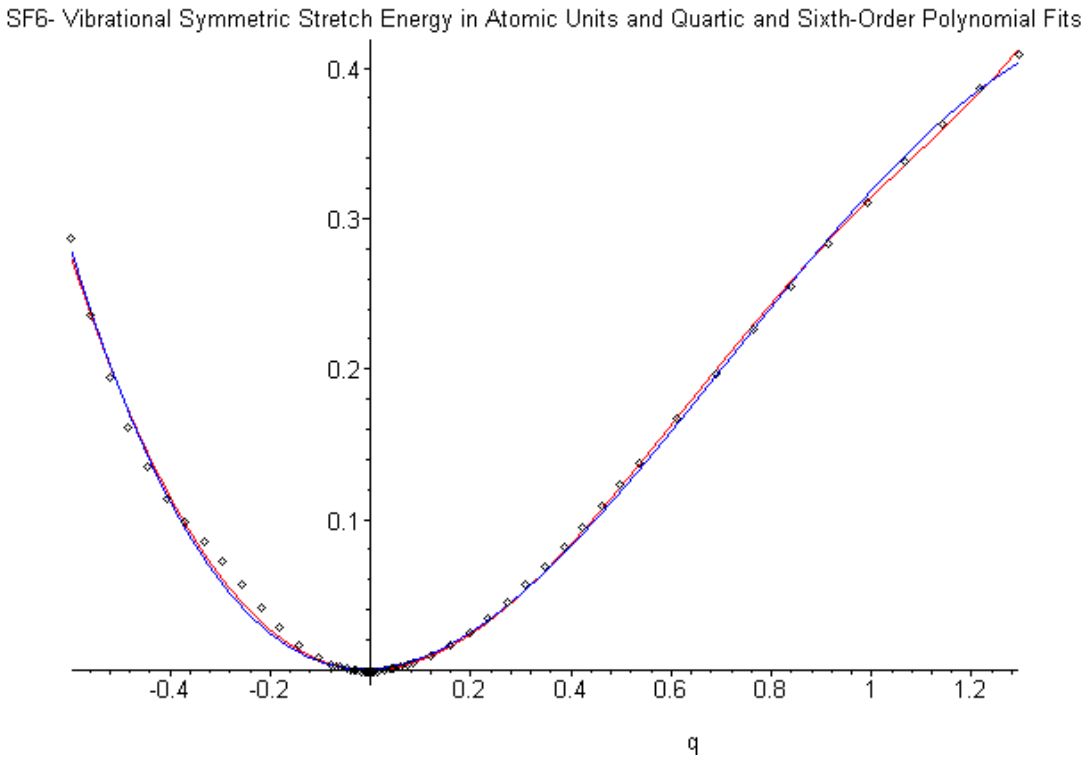

Figure 2.6: SF_6^- O_h symmetric stretch potential energy calculations and higher-order polynomial fit functions

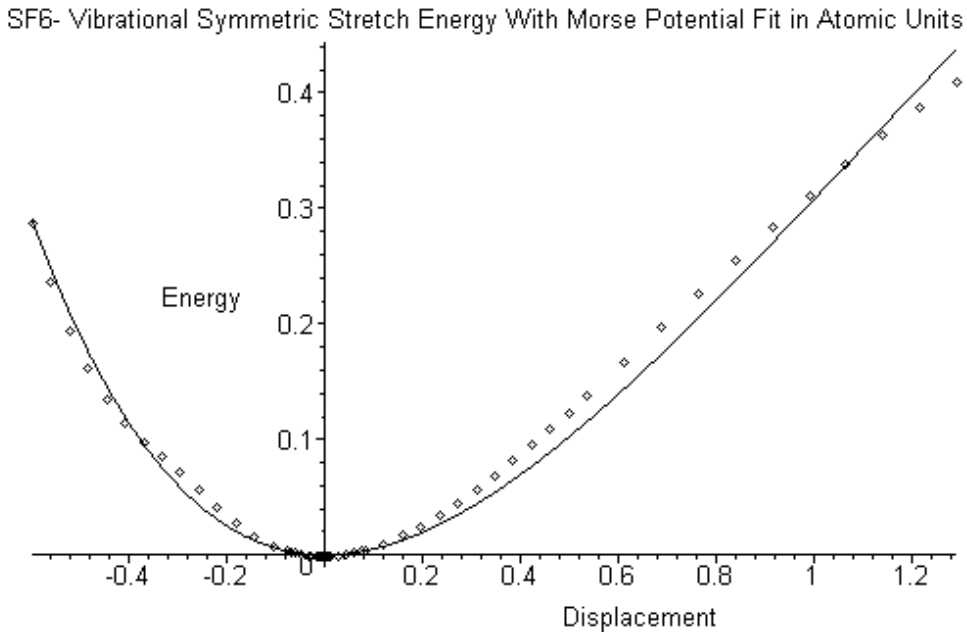

Figure 2.7: SF_6^- O_h symmetric stretch potential energy calculations and Morse potential fit function.

cm^{-1} [20], is only in error by 1.8%. Again, as with the agreement with electron affinities and vertical detachment energies, the agreement of the spectroscopic constants implies the potential surface is possibly adequately represented with the high-order CCSD(T) using the moderate 6-311+G(S:3df,F:2d) basis.

2.5 C_{4v} Symmetry Minima on SF_6^- Potential Surface

Since overall the CCSD(T)/6-311+G(S:3df,F:2d) method gives reasonable results in line with previous studies, it is interesting that upon further investigation the method predicts a minimum energy structure of reduced symmetry. Recalling that certain CCD and DFT vibrational frequency calculations in Table 2.5 suggest of an anion with lowered symmetry, this possibility is explored.

The direction of instability in certain CCD frequency calculations is along the S-F bond dissociation coordinate. A calculation along this dissociation coordinate can be done by doing a "partial optimization." A partial optimization allows the freedom for optimization of other molecular coordinates but the single S-F bond. This gives the lowest calculated possible configuration of the molecule of C_{4v} symmetry for each possible extension of a single S-F bond. As shown in Figure 2.8, a partial optimization with the MP2/6-311+G(S:3df,F:2d) method shows an energy that rises smoothly with bond length. This explains why the MP2 methods do not show any imaginary frequencies. However, the energies of the exact same configurations calculated with a different method reveal a feature that explains why some of the CCD methods produce imaginary frequencies at O_h symmetry.

The other curves shown are CCSD(T)/6-311+G(S:3df,F:2d) energies for SF_6 and SF_6^- calculated along the coordinates determined by the MP2/6-311+G(S:3df,F:2d) partial optimization. These curves are all normalized to reveal only the differences in shape.

Note that dissociation seems to be much easier for SF_6^-, as compared to that of SF_6. The interesting feature in the SF_6^- CCSD(T) energy compared to the MP2 energy at the same geometry is the dip in the potential well at the high S-F bond length. As is the case for the discrepancy in the CCD vibrational frequency calculations, the MP2 results do not show this unexpected behavior that is revealed in the CCSD(T) calculations.

The CCSD(T)/6-311+G(S:3df,F:2d) energy shows a minimum at a non-O_h symmetry structure. Figure 2.9 shows a 1-D overlay of two separate SF_6^- potential energy curves of the same calculation type. The single common dimension is the stretch of one unique S-F bond. The higher energy curve is constrained to O_h symmetry. The lower curve is the CCSD(T)/6-311+G(S:3df,F:2d) energy calculated along the coordinates of a MP2/6-311+G(S:3df,F:2d) partial optimization, as shown in Figure 2.8, and is of C_{4v} symmetry.

It is clear that according to this method, there is no O_h symmetry structure lower in energy than the C_{4v} minimum. There are many interesting implications of this distorted minimum energy if it does have physical significance. Consideration must be given to the moderate size of the basis set employed, here, however. It is possible this feature is an artifact of basis set truncation. Nonetheless, this basis set paired with the CCSD(T) method has demonstrated success in prediction of other molecular properties, so the results are of sufficient quality to merit further study. The theoretical and experimental implications of this type of potential energy surface are discussed. Calculations with

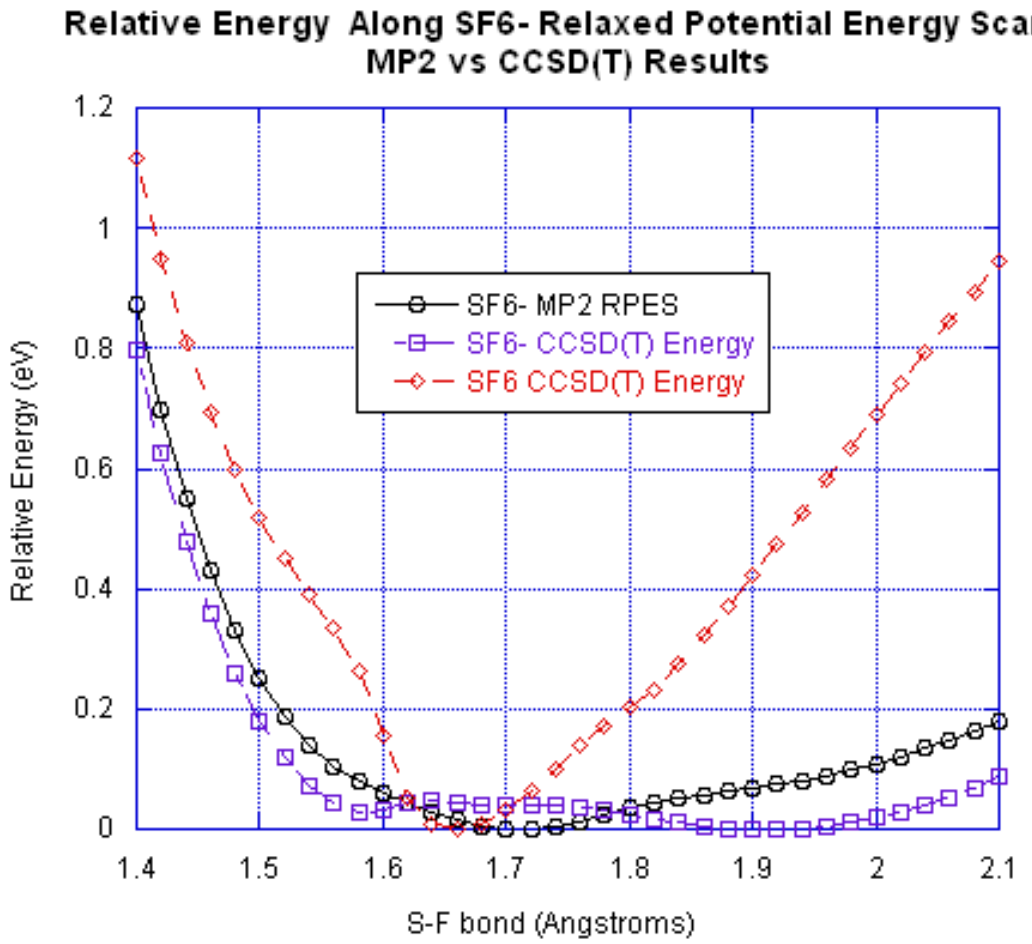

Figure 2.8: Normalized MP2 energy of of SF_6^- and CCSD(T) energies of SF_6^- and SF_6 along S-F bond dissociation of C_{4v} symmetry. Molecular geometry for all three curves is from MP2 optimization of all SF_6^- coordinates but the fixed S-F bond.

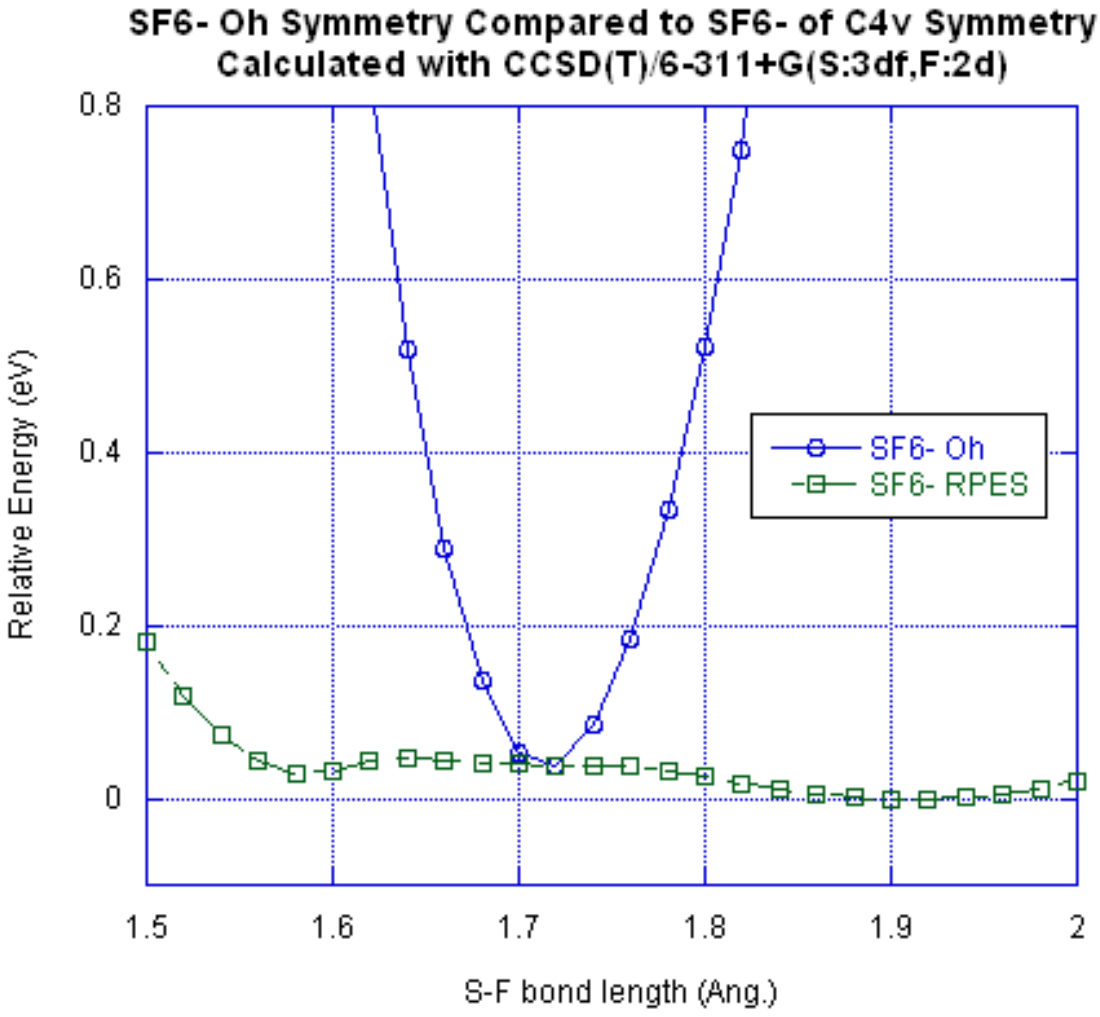

Figure 2.9: CCSD(T) energy of O_h and C_{4v} SF_6^- along single common dimension of dissociating S-F bond.

improved basis sets that are beyond the means of the current computational power available must be undertaken to positively resolve the issue, and future experiments are suggested.

2.6 Implications of SF_6^- C_{4v} Symmetry Minima

2.6.1 C_{4v} Minimum Well Depth and Zero-Point Energy

The potential well observed at large S-F bond distance is about 0.05 eV or ~ 400 cm^{-1} lower in energy than the lowest energy O_h structure. However, even at zero degrees Kelvin, the anion would only be expected to be able to exist in this distorted geometry described by this well if it is deep enough to hold a zero-point energy level. This zero-point energy level is comprised of

$$zpe_S = \sum_{i=1}^{S} p_i \frac{h\nu_i}{2} \tag{2.1}$$

where S is the number of vibrational modes that have some component in the direction of the coordinate change shown in figure 2.8. The projection of the geometry change upon the normal modes of the O_h anion gives p_i with limits of zero and unity, and represents the "degree of involvement" of a given mode. If this summation is greater than the C_{4v} well depth, the SF_6^- anion can be considered to be definitively of O_h symmetry, albeit with a very anharmonic potential well. If this fractional component of the zero-point energy is less than the well depth, this may permit a bound state within the C_{4v} minima. To determine the degree to which this is likely, the C_{4v} geometry "distortion" must be mapped out in normal modes of the O_h form. This is shown in Figure 2.10. The active modes are the two T_{1u} modes, the E_g mode and the A_{1g} mode. The frequencies for these modes and the projection coeficient determines the zero-point energy active in the dimensions of interest. As given in Figure 2.10, mode 15 is 670 cm^{-1} (T_{1u}), mode 12 is 550 cm^{-1} (A_{1g}), modes 10 and 11 are 420 cm^{-1} (E_g), and a value of 130 cm^{-1} (T_{1u}) is used for mode 8. The resulting active portion of the zero-point energy is approximately

$$\frac{1}{2}(0.1(670cm^{-1}) + 0.5(550cm^{-1}) + 2 \times 0.03(420cm^{-1}) + 0.34(130cm^{-1})) = 180cm^{-1}.$$

Thus the portion of the molecule's zero-point energy that is active is approximately 200 cm^{-1}. This is less than the energy difference between the lowest energy O_h and C_{4v} forms so it is possible that the well is of sufficient depth to hold a bound state. In the following section we consider the behavior of this type of system.

2.6.2 Multiple Minima: Splitting and Net O_h Symmetry

Assuming the C_{4v} well is deep enough to hold a bound vibrational state, it is important to recognize that the well depicted at distorted geometry is not unique, but rather one of six degenerate wells corresponding to stretching each of the six S-F bonds. It is instructive to consider the symmetry of the system in this circumstance, as the quantum mechanical description of the molecule will be determined by this property. For systems

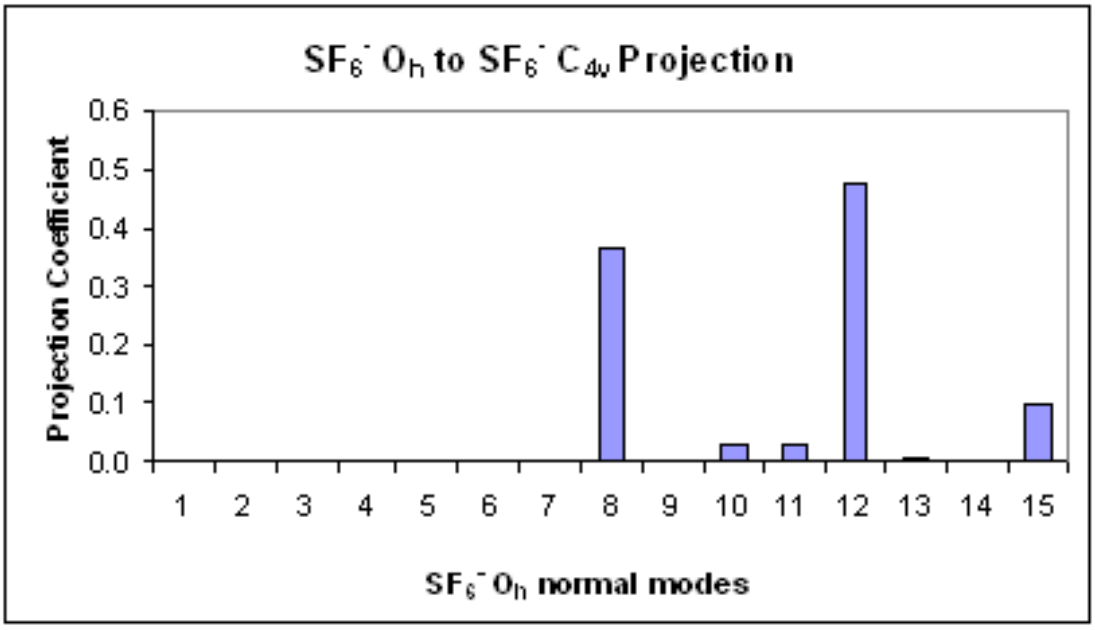

Figure 2.10: Representation in orthogonal vibrational modes of O_h SF_6^- what geometry change is involved in path to C_{4v} SF_6^- minimum.

with multiple potential minima, such as the iversion behavior in the ammonia molecule, the vibrational levels show a distinct spliting due to the two possible linear combinations of the component wavefunctions. For ammonia at low temperatures, the molecular symmetry is C_{3v}, and there are two unique minima with this symmetry. As more energy is input into the "umbrella" bending vibration along the inversion coordiante, eventually the inversion barrier is surmounted and the molecule changes from C_{3v} to net D_{3h} symmetry. This system is exactly analogous to the SF_6^- system with six minima of C_{4v} symmetry. If the C_{4v} state is bound, at low energies splitting in the vibrational levels would be observed as in the case of ammonia. However, either due to tunnelling or sufficient internal energy to surmount the barrier, the SF_6^- molecule will freely interconvert between C_{4v} minima, and the molecule will show a net O_h symmetry. Thus, considering the slight energy barrier seperating the multiple C_{4v} minima, it is unlikely that C_{4v} SF_6^- would be directly observed in any condition. Nonetheless, this theoretical possibility is interesting, and experimental evidence for it's existence could be sought in observation of the characteristic splitting of vibrational levels for these systems.

The vibration levels of ammonia are split due to the quantum mechanical nature of the system. The nuclear wavefunction Ψ_N is composed of the linear combinations of the component minima wavefunctions, $\psi^1_{C_{3v}}$ and $\psi^2_{C_{3v}}$, such that

$$\Psi_N^+ = \psi^1_{C_{3v}} + \psi^2_{C_{3v}} \tag{2.2}$$

and

$$\Psi_N^- = \psi^1_{C_{3v}} - \psi^2_{C_{3v}} \tag{2.3}$$

The extension of this formulation to the N-minima molecular system gives N possible nuclear wavefunctions.

$$\Psi_N = \sum_{i=2}^{N} \psi^1 \pm \psi^i \tag{2.4}$$

Each possible nuclear wavefunction has a degeneracy given by the binomial theorem

$$\frac{N!}{k!(N-k)!}(0.5)^k(0.5)^{(n-k)}. \tag{2.5}$$

An interesting possibility is that this degeneracy would be diminished if the tunnelling is more or less effective from axially related minima relative to the equatorially related minima.

For N=6, there are six possible Ψ_N, formed in the following manner:

$$\Psi_N^{++++++} = \psi^1_{C_{4v}} + \psi^2_{C_{4v}} + \psi^3_{C_{4v}} + \psi^4_{C_{4v}} + \psi^5_{C_{4v}} + \psi^6_{C_{4v}}$$

with degeneracy=1,

$$\Psi_N^{+++++-} = \psi^1_{C_{4v}} + \psi^2_{C_{4v}} + \psi^3_{C_{4v}} + \psi^4_{C_{4v}} + \psi^5_{C_{4v}} - \psi^6_{C_{4v}}$$

AND

$$\Psi_N^{++++-+} = \psi^1_{C_{4v}} + \psi^2_{C_{4v}} + \psi^3_{C_{4v}} + \psi^4_{C_{4v}} - \psi^5_{C_{4v}} + \psi^6_{C_{4v}}$$

etc... with degeneracy=6. The wavefunctions Ψ_N^{++++--}, and Ψ_N^{+++---} have degeneracies of 15 and 20, respectively.

Since the energy difference between all of these possible combinations of lower symmetry wavefunctions is related to the barrier height seperating the lower symmetry forms, the energy splitting may be exceedingly small in SF_6^-, but observation of this unique spectral signature would confirm the existence of a low-symmetry form of SF_6^-.

2.6.3 Vibrational Spectroscopy

Vibrational frequency calculation using CCD/aug-cc-pVDZ method determines a structure of O_h symmetry, but the same method using the 6-311+G(d) and 6-311+G(S:2d,F:d) basis sets results in a structure of C_{4v} symmetry, as shown in Table 2.6. These calculations can be used to examine the different vibrational spectra that would be expected from each possible form. The O_h symmetry SF_6^- molecule has only 2 IR-active vibrational modes, whereas a C_{4v} structure would have many more symmetry-allowed modes, as shown in Figure 2.11.

Direct observation of the vibrational spectrum of SF_6^- would allow for a direct resolution of this ambiguity in structure. If sufficient population of a C_{4v} isomer exists, the vibrational spectra of the anion should show the characteristic absorptions. As discussed in the previous section, however, failure to observe spectral evidence of a C_{4v} structure would be likely due to the shallowness of the C_{4v} minima well, and the quantum mechanical symmetry of the wavefunction. Because of this, observation of a SF_6^- spectrum consistent with a O_h symmetry structure does not guarantee that the calculated minima shown in Figure 2.9 is an artifact without physical significance.

2.7 SF_5 and SF_5^-: Structure, Vibrational Frequencies and Electron Affinity

Since SF_5^- is the primary product of dissociative low energy electron attachment to SF_6^-, it is useful to study for practical concerns, as well as for further assessment of computational chemistry methods employed. Optimization and vibrational frequency calculations for SF_5^- were performed with similar methods to SF_6^-. Unlike SF_6^-, the *ab initio* predictions of the SF_5^- anion frequencies are in relative agreement and unanimously predict an ion of C_{4v} symmetry. Unlike SF_6^-, there are no extreme differences between calculations of SF_5^-, as can be seen in Table 2.7 which summarizes the results of the frequency calculations.

The predicted absorption intensities of the IR-active fundamentals can be used to generate a simulated infrared absorption spectrum, as shown for various methods in Figure 2.12.

The opportunity for experimental validation of the calculated vibrational properties is discussed in the following chapter. Using the optimum structure from CCD/aug-cc-pVDZ vibrational frequency calculations, the SF_5^- and SF_5 CCSD(T)/6-311+G(S:3df,F:2d) energies are calculated. Comparison of these energies allows for a determination of the SF_5 adiabatic electron affinity.

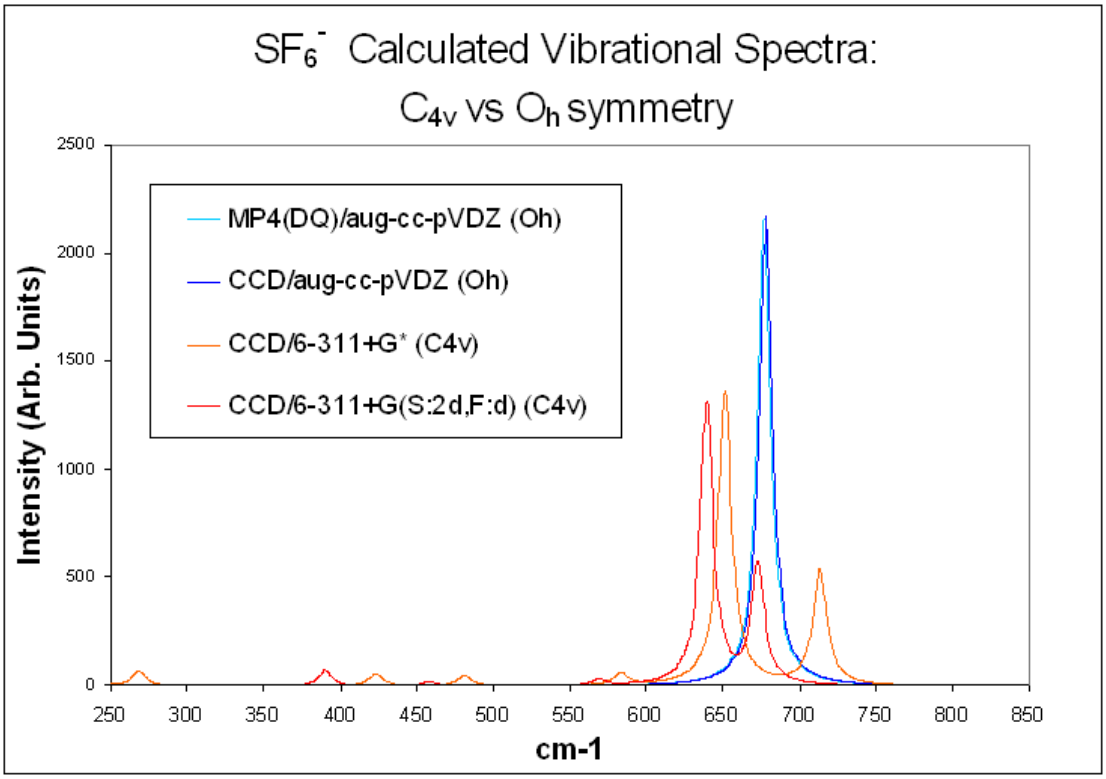

Figure 2.11: Calculated IR spectra for SF_6^-, for various c alculations. The results show O_h symmetry or C_{4v} symmetry, depending upon basis set. Due to the broken symmetry, there are more active IR fundamentals in the C_{4v} form.

Table 2.7: SF_5^- frequency calculations. Frequencies in units of cm^{-1} are left unscaled. These calculations are constrained to C_{4v} symmetry.

Symmetry	E	B_2	B_1	A_1	E	B_2	A_1	E	A_1
Method									
CCD/aug-cc-pVDZ	239	249	323	448	455	471	536	656	814
CCD/6-311+G*	235	260	329	449	465	433	522	617	786
mp2/aug-cc-pVDZ	231	231	307	413	427	443	510	642	774
mp2/aug-cc-PV(S:TZ, F:DZ)	239	253	326	433	454	420	511	614	784

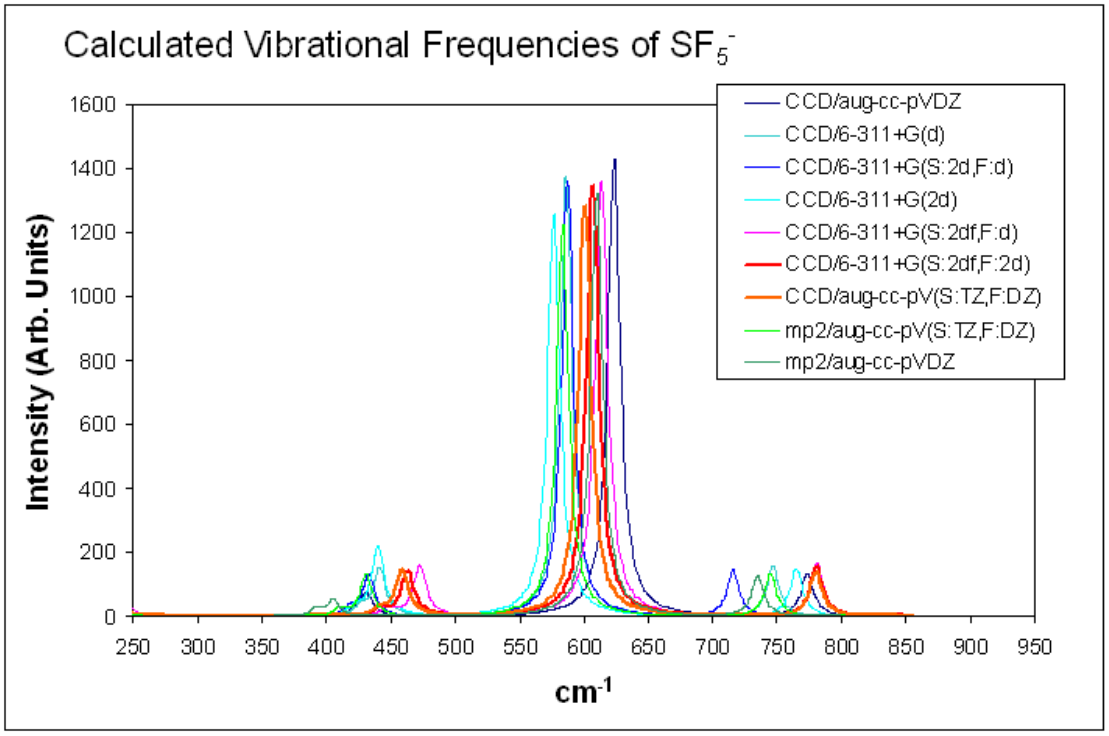

Figure 2.12: Simulated SF_5^- spectra for various calculation methods. Frequency values are scaled by 0.95 for IR simulation.

Table 2.8: SF_5^- and SF_5 energies and C_{4v} symmetry structures. The CCD energies are corrected with CCSD(T) calculations to give an adiabatic electron affinity uncorrected for zero-point energies.

Optimization	CCD/aug-cc-pVDZ (E_h)	R_{axial}	R_{equat}	Θ	CCSD(T)/6-311G(S:3df,F:2d)(E_h)	EA(eV)
SF_5	-895.799	1.586	1.640	91.51	-896.144	
SF_5^-	-895.963	1.635	1.760	85.02	-896.286	3.86

Table 2.9: Results of SF_4 C_{2v} and SF_4^- C_{4v} symmetry vibrational frequency calculations. Frequencies in units of cm^{-1} are left unscaled.

Mode Symmetry	A_1	B_1	A_2	B_2	A_1	A_1	B_2	B_1	A_1
SF_4	213	336	433	498	500	585	782	876	889
Mode Symmetry	B_2	E	E	B_1	A_1	B_2	A_1	E	E
SF_4^-	140	241	241	315	429	459	593	597	597

Table 2.10: CCD optimization energies are improved by higher order CCSD(T) calculations for adiabatic electron affinity. Frequencies from CCD calculations are used to define the zero-point energy.

	CCD/aug-cc-pVDZ(E_h)	zpe (eV)	CCSD(T)/6-311+G(S:3df,F:2d)(E_h)
SF_4	-796.212	0.32	-796.493
SF_4^-	-796.285	0.22	-796.547
EA (eV)	2.07		1.56

The calculated EA is in good agreement with the results of other studies [10, 12]. Extension of this methodology to SF_4 and SF_4^- allows for a more thorough analysis of the thermochemistry and the computational methods.

2.8 SF_4 and SF_4^-: Structure, Vibrational Frequencies and Electron Affinity

SF_4^- is a product of higher-energy of dissociative electron attachment to SF_6^-, and the neutral SF_4 is reactive but less so than the radical SF_5. In addition, SF_4^{-*} has been shown to be one of the interesting class of metastable anions that show long lifetimes for autodetachment [21]. The vibrational frequencies of these anions are used for incorporation in models of electron capture dynamics, as discussed in Chapter 4.

Optimization and vibrational frequency calculations for SF_4^- were performed with similar methods to SF_6^- and SF_5^-. Structures and frequencies are all in relative agreement and unanimously predict an ion of C_{4v} symmetry and a neutral molecule with C_{2v} symmetry. The vibrational frequency calculations are summarized in Table 2.9. Using the optimum structure from CCD/aug-cc-pVDZ calculation the SF_4^- and SF_4 CCSD(T)/6-311+G(S:3df,F:2d) energies are calculated. Comparison of these energies allows for a determination of the SF_4 adiabatic electron affinity.

The CCSD(T) calculated EA is in good agreement with the results of other studies [10,12,22]. This set of calculations for the SF_n^- series using a consistent method provides a foundation for discussion of electron capture reaction thermodynamics, and subsequently, dynamics.

Table 2.11: Enthalpies of reactions of SF_6^- and SF_5^- ions, using experimental data and calculated energies.

Enthalpies of Reaction.	Ref. [16] kJ/mol	Ref. [16] eV	Calculated eV
$SF_6^- \longrightarrow SF_6 + e^-$	99.53	1.03	1.05
$SF_6^- \longrightarrow SF_5^- + F$	149.38	1.55	1.53
$SF_6^- \longrightarrow SF_5 + F^-$	162.79	1.69	2.28
$SF_5^- \longrightarrow SF_5 + e^-$	341.55	3.54	3.82
$SF_5^- \longrightarrow SF_4^- + F$	424.38	4.40	3.88
$SF_5^- \longrightarrow SF_4 + F^-$	238.08	2.47	2.37

2.9 SFn^- Thermochemistry: Detachment and Dissociation Energies

Using the same method and basis set for all fragments allows for a thermodynamic analysis of the simplest detachment and dissociation channels of SF_6^- and SF_5^-, as shown in table 2.11. The enthalpies of reaction are determined by using the heats of formation from the CRC Handbook [16]. The experimental values in units of eV are compared to those calculated with the CCSD(T)/6-311+G(S:3df,F:2d) method in the final column.

Examination of the experimental reaction enthalpies with the calculated values shows that overall, the chosen calculation method reproduces the SF_n^- thermochemistry reasonably well.

Chapter 3

Anion Infrared Multiple Photon Dissociation and Detachment Spectroscopy

3.1 Introduction.

Vibrational spectroscopy of negative ions is a relatively unexplored field compared to their cationic counterparts. Nonetheless, information obtained from spectroscopic studies is essential for developing models of the dynamics of electron transfer processes in molecules, as well as providing experimental validation of computational models of molecular bonding in anions. Results of various computations of the vibrational frequencies of SF_6^- have recently been published [23], and these calculated frequencies are used to successfully predict auto-ionization lifetimes. These ab-initio and DFT computations are extremely useful for providing reasonable estimates of anion vibrational frequencies, however, experimental constraints upon these values are less common. Recently, Bopp et al. [18] have reported a value for the ν_3 frequency of SF_6^- from the IR-photodissociation of the SF_6^- $(Ar)_n$ van der Waals complex for n = 1 and 2. This peak shown a doublet structure that is not explained, and may be related to symmetry-breaking effects due to the Ar atom(s). The ν_3 frequency was reported to be 683(5) cm^{-1} as compared to a previous value of 620 cm^{-1} obtained by Jacox et al. [24] for SF_6^- embedded in a neon matrix.

Electron attachment to SF_6^- is well known to produce an abundance of fragment anions [25]. SF_5^- is the primary product from low-energy electron attachment to SF_6^-. As opposed to SF_6^-, SF_5^- has a closed-shell structure, and a very large vertical detachment energy, at least 2 eV higher than the SF_6^- vertical detachment energy of 3 eV [8]. The vibrational spectrum of SF_5^- has been reported as a Cs^+ salt [26] and also studied more recently. Jacox et al. [24] reported observations of SF_5^- vibrational frequencies from SF_5^- embedded in neon matrix, assigned upon the basis of DFT frequency calculations.

Harmonic vibrational frequency calculations are useful for interpretation of the SF_6^- and SF_5^- IR-MPD spectra, and are presented in Tables 2.5 and 2.7, respectively. The minimum energy configuration of the SF_5^- anion is unambiguously calculated to be of

C_{4v} symmetry, and SF_6^- is expected to retain the O_h symmetry of the neutral. However, certain *ab-initio* and DFT [9] calculations have suggested some interesting features of the SF_6^- potential energy surface with respect to a T_{1u} distortion of the octahedral symmetry, suggesting even a global minimum on the potential energy surface of a C_{4v} symmetry. Due to the strong difference in the predicted spectra of a C_{4v} symmetry molecule (8 IR active fundamental bands) compared to one of O_h symmetry (only 2 IR active fundamental bands), measurement of the infrared absorption spectrum of the anion provides direct insight into the molecular structure. Comparison of the observed IR spectra to that predicted allows not just for investigation into the structural symmetry of the anion, but also for assessment of the quality of the various calculation methods employed. This is important as even among the calculations that agree on the O_h symmetry there are differences.

3.2 Experimental

The experiments are performed by irradiation of ions trapped in an FTICR mass spectrometer, which is described in detail elsewhere [27]. This instrument has now been modified to permit injection of ions from external sources and an external electron ionization source was used for these experiments. SF_6^- ions were generated by unimolecular electron attachment to SF_6 followed by collisional and radiative stabilization. SF_5^- was formed by low energy dissociative electron attachment to SF_6. The free electrons were generated with a filament heated by passing a 4.5A current and held at a bias of -90V relative to ground. The SF_6 source housing was held at a less negative bias of -79V, thus electrons impact the SF_6 gas target with approximately 11 eV of energy. However, electron attachment occurs from an energy distribution centered at lower energy due to collisional cooling. The negative ion current was very sensitive to electron energy (filament vs. housing bias) and filament current, and the maximum anion signal was observed within a narrow range of voltage.

The background pressure of 2 x 10^{-6} torr in the electron ionization source chamber increased with addition of the SF_6 sample to 5 x 10^{-5} torr. The background pressure was 10^{-7} torr in the ICR cell and ion optics region. The ion optics consists of a source region followed by a quadrupole bender and octopole guide into the ICR cell. As is typical for FTICR mass spectrometers, ions can be stored in the analyzer cell for many seconds and are thus thermally stabilized before irradiation. As ions are introduced into the cell, they are given a delay for trapping, followed by a series up RF pulses ∼1s in duration for mass selection, and finally ∼1s delay before IR excitation and fragment ion detection. For the SF_6^- experiments, the parent SF_6^- ion was mass-selected from the other ions produced (SF_5^-, SF_4^-, F^-, etc.) before irradiation. For SF_5^-, the initial SF_5^- signal was enhanced by off-resonance RF excitation of SF_6^- promoting fragmentation to SF_5^-, and then subsequent isolation of the SF_5^- anion prior to IR irradiation.

Dissociation of molecular ions from IR laser radiation from the FELIX free electron laser has been described in detail elsewhere [28]. The resolution of the FELIX laser beam is transform limited at 0.05 μm. The stored ions were subjected to a 450 ms irradiation time, resulting in 3 FELIX macropulses. Each macropulse was ∼ 2ms in length and consisted of 1000 micropulses of 50 psec duration. Power as a function of wavelength is

measured, and the spectra normalized and wavelength calibrated. Four mass spectra are averaged for each wavelength setting to produce a spectral point. Multiple spectra are averaged to improve signal to noise. The power dependence of the IR-MPD process for SF_6 was investigated by attenuation of FELIX IR radiation with a neutral density filter.

The vibrational frequencies and infrared absorption activities calculated by *ab-initio* methods allow for assignment of the observed vibrational bands for SF_6^- and SF^-. Calculations are performed with both Gaussian Inc.'s G03 program [11] and the NWChem Version 5.0 computational package [13]. Various methods are used for calculation of the predicted vibrational spectra and anion molecular structure. Geometry optimizations and frequency calculations are done with DFT, MP2, and MP4(DQ) methods as well as with CCD methods using relatively small basis sets. Potential energy surface calculations are done with CCSD(T) methods and basis sets of moderate size, 6-311+G(3df) for Sulfur and 6-311+G(2d) for Fluorine atoms.

3.3 SF_6^- and SF_5^- Production, Detachment and Dissociation.

In these studies, a wide range of negative ions are produced from electron impact collisions with SF_6: F^-, SF^-, SF_2^-, SF_3^-, SF_4^-, SF_5^- as well as the dominant SF_6^- ion. This wide range of ions is a result of the broad energy distribution of the electron beam. Multiple photon dissociation of SF_6^- resulted primarily in SF_5^-, and MPD of SF_5^- resulted in F^- formation. However, under certain source conditions, F^- and SF_4^- were also detected from SF_6^- and SF_5^-. The SF_4^- (and the F^-) production observed from SF_6^- was due to sequential dissociation of SF_6^- through further dissociation of SF_5^- because the SF_4^- appearance from MPD of SF_6^- requires absorption intensity from both SF_6^- and SF_5^-. The observed products of IR-MPD are in agreement with what would be expected from thermodynamics, as can be seen in Table 2.11. In both cases, depletion of the parent ion signal was beyond that of the fragments observed by photodissociation, implying that photodetachment of electrons from the parent ions may be playing a significant role. Both SF_6^- and SF_5^- have electron affinities in the same range as the dissociation energy, so this is not surprising. This aspect of anion photodetachment is discussed in detail.

3.4 Interpretation of Spectra.

3.4.1 SF_6^-

Symmetry Determination

A subset of the results shown in Table 2.5 are summarized in Table 3.1. There is rough agreement among methods for the calculated frequency values for all vibrational modes but ν_4, the lowest energy T_{1u} symmetry mode.

The moderately sized basis set of the CCD/aug-cc-pVDZ calculation gives reasonable results for a vibrational frequency calculation of SF_6^- but it is certainly not providing a fully sufficient description of the molecular bonding. This method determines a structure of O_h symmetry, but the same method using the 6-311+G(d) and 6-311+G(S:2d,F:d)

Table 3.1: Selected SF_6^- frequency calculations. Frequencies (in units of cm^{-1}) are scaled by 0.95 for ab-initio methods and 0.98 for DFT methods. These calculations are constrained to O_h symmetry.

Method	$\nu_6(T_{2u})$	$v_5(T_{2g})$	$v_4(T_{1u})$	$v_2(E_g)$	$v_1(A_{1g})$	$v_3(T_{1u})$
MP2/6-311G+(S:2df,F:2d) [8]	225	319	291	425	595	686
MP2/aug-cc-pVDZ	223	317	305	459	606	709
MP2/6-311+G(S:3df, F:2d)	232	323	272	424	606	679
MP2/6-311+G(3df)	229	323	265	422	602	673
B3LYP/aug-cc-pVDZ [9]	217	314	115	424	568	628
B3P86/aug-cc-pVDZ [9]	222	319	115	438	589	647
MP4(DQ)/aug-cc-pVDZ	227	319	129	474	606	677
CCD/aug-cc-pVDZ	227	319	135	474	607	678

basis sets results in a structure of C_{4v} symmetry. These results are shown in Table 2.6. The different symmetry structures produce very different predicted vibrational spectra as shown in Figure 2.11. The vibrational spectra are expected to distinguish between the forms.

Shown in Figure 3.1 is the SF_5^- signal resulting from multiphoton dissociation of SF_6^- which peaks at 660 cm^{-1}. To allow for a visual comparison, the predicted and observed spectra are stacked to scale.

There is only one strong band observed in the region above 500 cm^{-1} but the extreme width and asymmetry of the band makes it possible it is composed of multiple bands. However, no distinct bands are observed in the higher energy region where activity is predicted for the C_{4v} spectra. With the resolution of this spectra, this issue may not be resolvable. Comparison of the predicted SF_6^- vibrational spectra to the data Figure 3.1 suggests the possibility that perhaps even both the O_h symmetry and the C_{4v} symmetry isomers make a contribution to the spectrum. This is possible given the nature of the distorted minimum as considered in the previous chapter. The vibrational frequency calculations of both O_h symmetry and C_{4v} symmetry are considered for spectral interpretation and assignment of resonances.

Peak Assignments

The calculations and the IR-MPD data are shown in Figure 3.1. Based upon comparison with Table 2.5, the large peak in the dissociation cross section is interpreted as due to the ν_3 mode of SF_6^-. This gas phase value compares favorably with the value of 683(5) cm^{-1} reported recently by Bopp *et al.* [18] using the Ar tagging method. It is considerably higher than the value of 620 cm^{-1} obtained by Jacox *et al.* [24] for SF_6^- embedded in a neon matrix. The calculated frequencies for this mode agree with the data and between the methods, so this low-resolution assignment is relatively unambiguous. However, it is not possible yet to rule out a contribution from a C_{4v} isomer in the region. The ν_1, ν_5, and ν_2 modes of this form lie in the the range of 600-750 cm^{-1} and are IR-active.

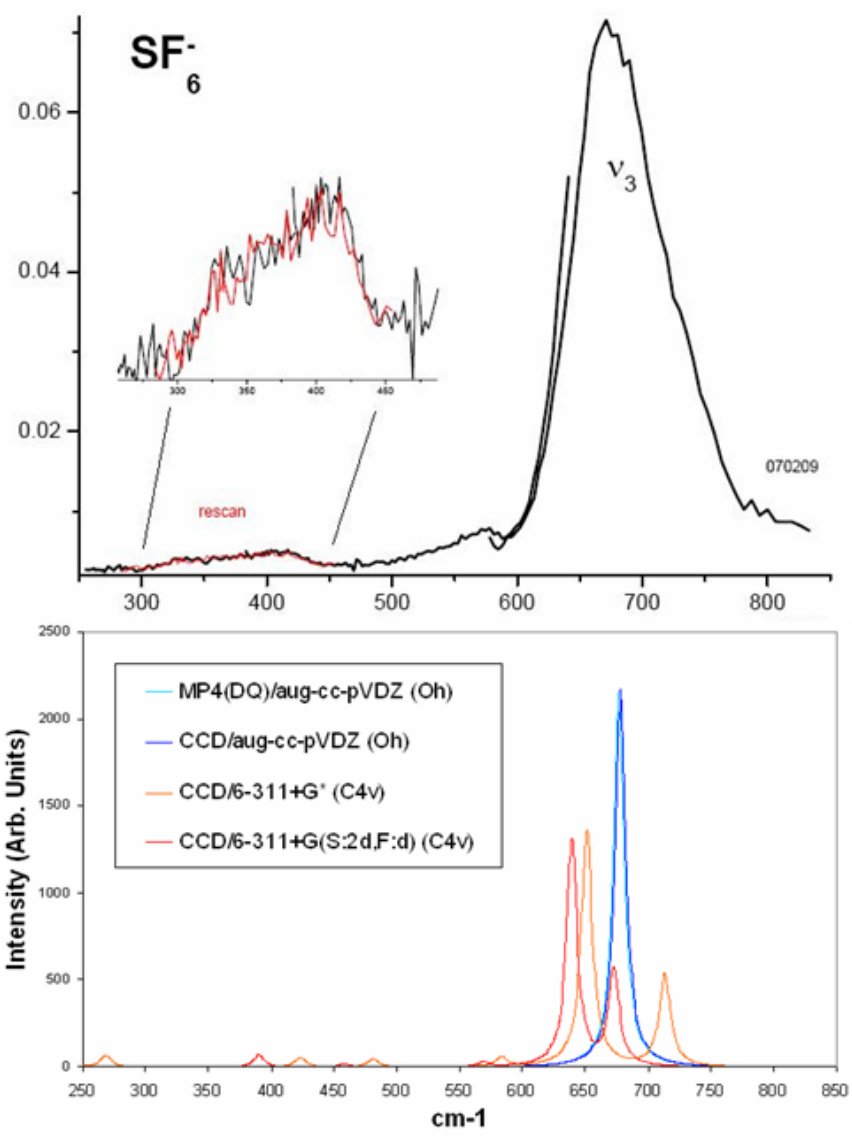

Figure 3.1: Observed and predicted SF_6^- IR spectra.

Observation and positive identification of the other IR-active fundamental of SF_6^-, the ν_4 band, is particularly important for critique of the different computational methods since this is the main point of difference between them. MP2 methods unanimously suggest a frequency in the range of 250 - 300 cm^{-1} , and MP4, CCD, and DFT all suggest a vibrational frequency of approximately half this value, or less. Unfortunately, the spectra do not go to low enough energy to give certainty in this regard. An additional feature is apparent at 350-450 cm^{-1}, but none of the calculations predict any IR active fundamentals within 100 cm^{-1} of that range. The possibility exists that this activity is due to absorption from a C_{4v} symmetry SF_6^- molecule. The ν_6 fundamental at ~420 cm^{-1}, for example, is symmetry allowed. Since the calculations and spectra are ambiguous on this point the the possibility of a IR combination band from the O_h symmetry SF_6^- is considered.

Since the symmetry of the SF_6^- molecule is determined to have the same high O_h symmetry of SF_6, the symmetry-allowed binary combination bands are surprisingly few. IR-active combination bands must contain the T_{1u} representation within the symmetry product. From the symmetry direct product table of the O_h point group [29] it is determined that the binary combinations that contain this representation are A_{1g} x T_{1u}, E_g x T_{1u}, E_g x T_{2u}, T_{2g} x T_{1u}, and T_{2g} x T_{2u}. Table 3.2 lists the possible combination bands and their symmetries and energies. The energy is calculated by using the method-averaged frequency results for the fundamentals.

Upon examination of the table above, the low-energy resonance at 400 cm^{-1} is tentatively assigned as the symmetry-allowed $\nu_1 - \nu_4$ difference band. Other possible candidates exist, such as the $\nu_5 + \nu_4$ band, but the SF_6 neutral shows a significant activity for this combination band, and thus the anion of same symmetry might be expected to as well. Although it is likely this feature is too high in energy to be the ν_4 fundamental, it cannot be ruled out without a positive identification of the ν_4 band. Thus, the limited range of the spectra unfortunately does not allow us to directly assess the value of the vibrational frequency calculation methods as regards this crucial discrepancy. Overall, the MP2, MP4(DQ) and CCD results are reasonable, so it is unfortunate that the inability to definitively assign the ν_4 fundamental prohibits a direct critique of the different methods.

Spectral Broadening

The extreme width of the ν_3 SF_6^- band is interesting, and the effect of laser power is examined. As shown in Figure 3.2, measurements at lower laser power gave somewhat narrower peaks in the cross section but the position of the peak did not change. It is possible that there is a large degree of anharmonicity contributing to the broadening, and there are also potential interfering combination bands such as the symmetry-allowed $\nu_1 + \nu_4$ in the region.

The anharmonicities of the upper vibrational levels typically add to the overall multiple photon detachment on the low energy side of the absorption peak. For this reason it could be argued that the value of 660 cm^{-1} ascribed to the ν_3 mode of SF_6^- may be slightly lower than the true value. The fact that the peak does not shift to lower energies with increasing laser power argues against this possibility.

Table 3.2: Symmetry-allowed SF_6^- binary combination bands. The energy is calculated by using the method-averaged frequency results for the fundamentals. The values in boldface are possible candidates for assignment to the feature at ∼400 cm^{-1} considering only binary combination bands.

Band	Symmetry	MP2 avg.	DFT avg.	MP4 avg.	CCD avg.	method avg.
$\nu3+\nu1$	A_{1g} x T_{1u}	1289	1212	1283	1285	1267
$\nu3-\nu1$	A_{1g} x T_{1u}	90	59	71	71	73
$\nu1+\nu4$	A_{1g} x T_{1u}	883	677	735	742	759
$\nu1-\nu4$	A_{1g} x T_{1u}	316	477	477	472	**436**
$\nu3+\nu2$	E_g x T_{1u}	1124	1065	1151	1152	1123
$\nu3-\nu2$	E_g x T_{1u}	255	206	203	204	217
$\nu2+\nu4$	E_g x T_{1u}	718	530	603	609	615
$\nu2-\nu4$	E_g x T_{1u}	152	330	345	339	291
$\nu2+\nu6$	E_g x T_{2u}	660	649	701	701	678
$\nu2-\nu6$	E_g x T_{2u}	210	211	247	247	229
$\nu3+\nu5$	T_{2g} x T_{1u}	1008	950	997	998	988
$\nu3-\nu5$	T_{2g} x T_{1u}	372	321	358	359	**352**
$\nu5+\nu4$	T_{2g} x T_{1u}	601	415	448	454	**480**
$\nu5-\nu4$	T_{2g} x T_{1u}	35	215	190	184	156
$\nu5+\nu6$	T_{2g} x T_{2u}	543	534	546	546	542
$\nu5-\nu6$	T_{2g} x T_{2u}	93	96	92	92	93

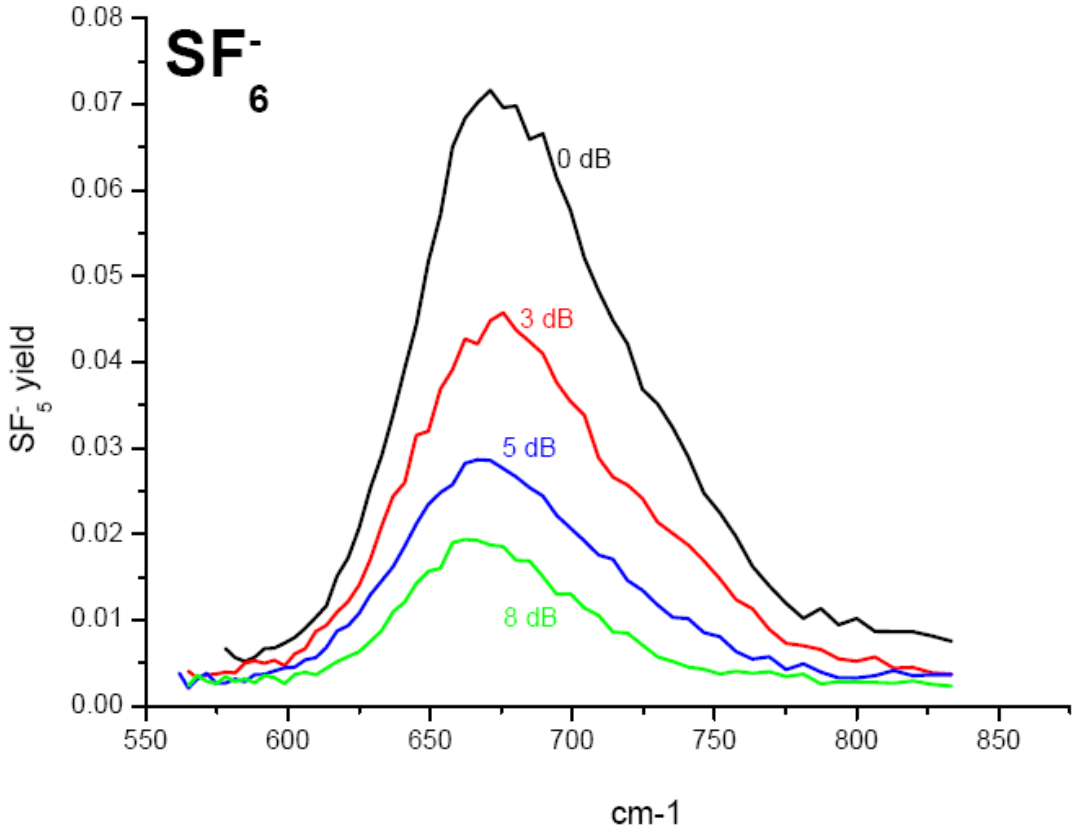

Figure 3.2: Dependence of the dissociation of SF_6^- upon IR laser power.

Table 3.3: SF_5^- frequency calculations. Frequencies (in units of cm^{-1}) are scaled by 0.95 for ab-initio methods and 0.98 for DFT methods. These calculations are constrained to C_{4v} symmetry.

Symmetry	E	B_2	B_1	A_1	E	B_2	A_1	E	A_1
Method									
CCD/aug-cc-pVDZ	239	249	323	448	455	471	536	656	814
CCD/6-311+G*	235	260	329	449	465	433	522	617	786
mp2/aug-cc-pVDZ	231	231	307	413	427	443	510	642	774
mp2/aug-cc-PV(S:TZ, F:DZ)	239	253	326	433	454	420	511	614	784

The intensity of the SF_5^- ions produced as a function of laser power gives insight into the degree of saturation, and the extent of multi-photon processes. The log-log plot of Figure 3.3 is constructed using the relative peak areas vs. the log of power in Figure 3.2. The slope is calculated and displayed for the first and last two points. The slope of this line is related to the number of multiple-photon absorptions. It is clear that in the 8 dB attenuated spectrum is not saturated while the 0 db, full-power spectrum is showing signs of saturation. At this FEL frequency, at least 12 photons are required to dissociate SF_6^-, so it would be expected that with more laser attenuation, the slope of the curve would increase from ∼3 to 12.

3.4.2 SF_5^-

There is no ambiguity in the general symmetry of the calculated structure and for the vibrational frequencies of the SF_5^- anion. All calculated methods give rough agreement, as shown in Table 3.3. The vibrational frequencies of SF_5^- are calculated by methods similar to SF_6^-. The MP2 and CCD predictions of the SF_5^- anion frequencies are in relative agreement, and unanimously predict an ion of C_{4v} symmetry. Unlike SF_6^-, there are no extreme differences between calculations for any modes of SF_5^-, as can be seen in Table 3.3 which summarizes the results of the frequency calculations.

The predicted vibrational spectra of SF_5^- calculated by various methods are shown in Figure 2.12. As is the case for SF_6^-, comparison of the predicted spectra with that observed allows for an assessment of the quality of the various calculation methods employed. For visual comparison the predicted and observed SF_5^- IR spectra are stacked in Figure 3.4.

The IR wavelength dependence of the dissociation of SF_5^- into F^- shown in Figure 3.4 reveals multiple bands that are not subject to the extreme broadening of the SF_6^- feature. The resonances in the IR-MPD spectrum of the SF_5^- anion at 780 cm^{-1} , 620 cm^{-1} , and 450 cm^{-1} are consistent with the predicted positions for the fundamentals. This agreement lends confidence in the interpretation of the spectrum of SF_5^-.

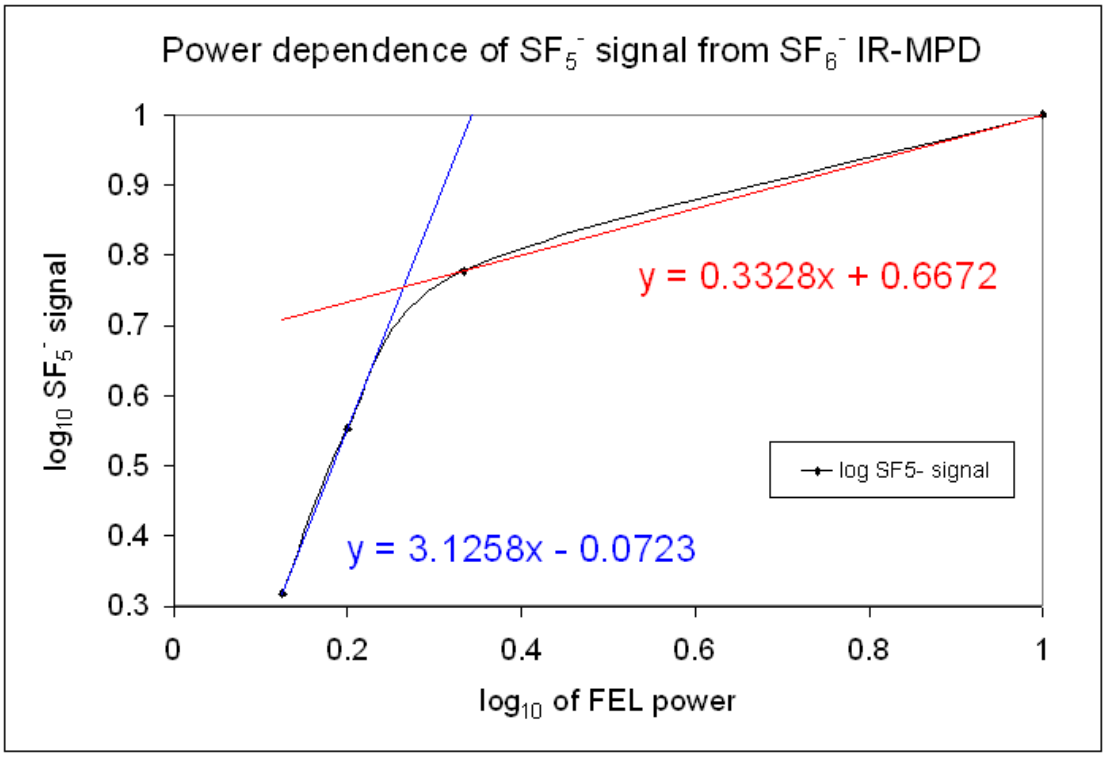

Figure 3.3: Log-log plot of laser power vs SF_5^- signal. Note that unattenuated spectrum is showing signs of saturation.

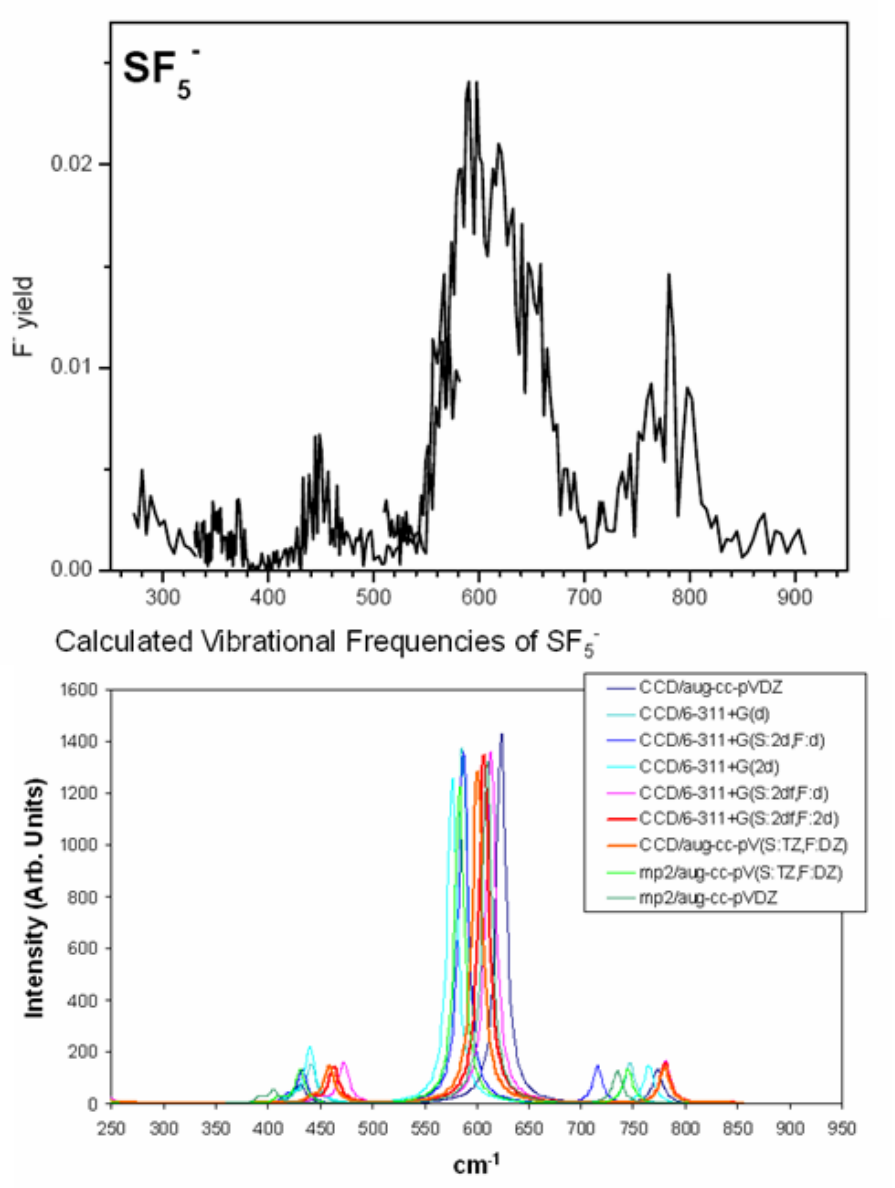

Figure 3.4: Predicted and observed IR absorption spectra of SF_5^-. Calculated frequencies are scaled by 0.95.

3.5 Anion Photodetachment vs. Photodissociation Rates.

The IR-MPD process is typically described as a "multiple-photon" process to be distinguished from the connotation of "multi-photon" absorption. This is because experiments suggest that IVR plays a large role in the dissociation event [30], and that the energy is redistributed through the molecule faster than the individual photon absorption events. For these molecules considered the electron affinities are in the same range as the dissociation energies so the process of electron detachment can compete with molecular dissociation.

This type of competition in an excited molecular system has been experimentally studied and modelled for C_{60} thermionic emission [31], where FEL absorption essentially "boiled off" an electron from C_{60}. Infrared photodetachment of SF_6^- has been studied previously by Dzzaic and Brauman [32], but only at a single wavelength. Strong evidence of photodetachment from SF_6^- and SF_5^- was observed in the current study.

Figure 3.5 shows the F^- production from dissociation of SF_5^- and the total loss of SF_5^- signal. The large difference in magnitudes show that photodetachment is occurring. Further evidence of this is in the observation of weak SF_6^- signal appearing from SF_5^- photodeatchment as background SF_6 in the analyzer cell "scavenges" the detaching eletrons. Use of this process could be manipulated to provide an all-purpose photodetachment detection scheme for extension of the current methods of molecular anion vibrational spectroscopy.

If the energy is assumed to be thoroughly randomized within the molecular degrees of freedom, statistical mechanics can be employed to provide a model for the rates of the photodetachment and dissociation processes. On this basis, Klots [33–35] introduced a method for calculating the relative rates of dissociation vs detachment according to quasi-equilibrium theory. That approach is applied to autoionization rates of metastable anions formed by free-electron capture, but it may be possible to extend the treatment to the multiple photon IR absorption process.

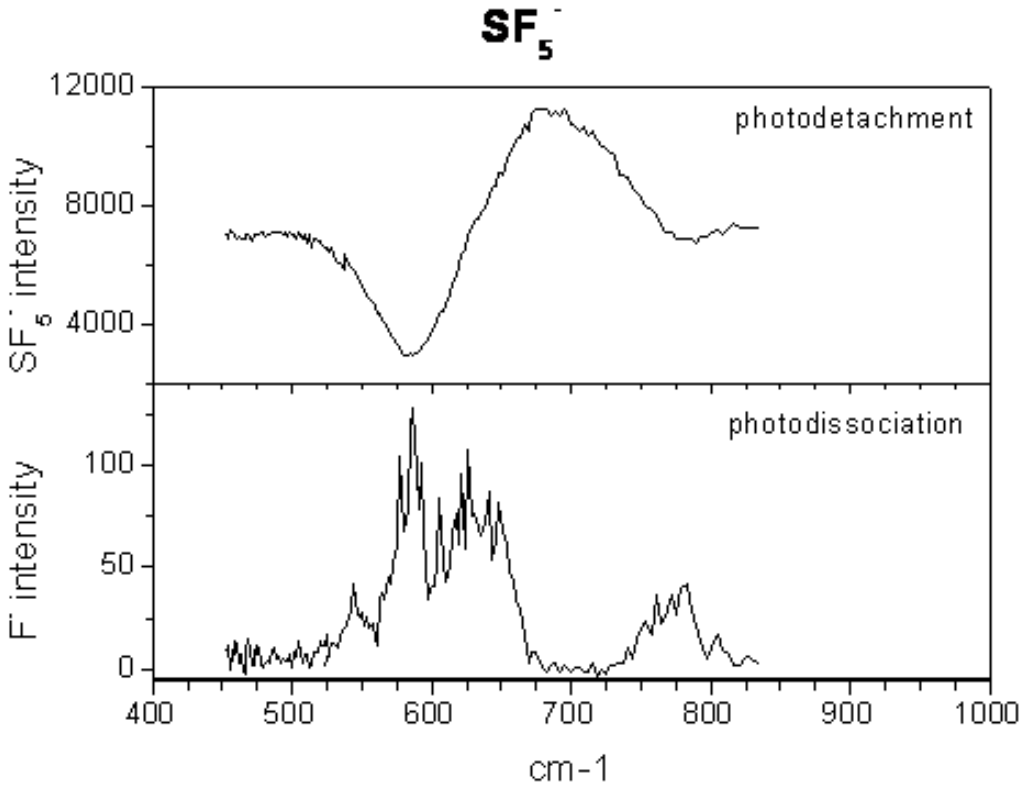

Figure 3.5: F^- production and SF_5^- loss as a function of IR laser frequency.

Chapter 4

Quasiequilibrium Theory Formulation of Electron Autodetachment Lifetimes of Metastable Polyatomic Anions

4.1 Introduction to Autodetachment

Associative electron capture by molecules with a positive electron affinity produces a molecular anion in an energetically excited state, requiring some type of cooling process, such as collisional stabilization or radiative stabilization to produce a stable parent anion. The stabilization process competes with the rate at which the anion autoionizes, reverting to the free electron and neutral molecule. The formation process for a molecule, M, can be represented as

$$M + e^- \longrightarrow M^{-*}$$

and the collisional stabilization process as

$$M^{-*} + M \longrightarrow M^- + M^*$$

and the radiative stabilzation process as

$$M^{-*} \longrightarrow M^- + h\nu.$$

The competing autodetachment process is

$$M^{-*} \longrightarrow M + e^-.$$

Many molecular anions formed by attachment of free low-energy electrons exhibit significant lifetimes with respect to electron autodetachment. For small molecular anions such as O_2^{-*}, this process occurs on a scale of nanoseconds or less. For many polyatomic molecules with sufficient electron affinities the lifetimes are on the order of microseconds and for large polyatomic molecules, such as $C_7F_{14}^{-*}$ the decay process can be on the

order of milliseconds or longer. This dependence upon molecular size has been interpreted as indicative of the strong role the internal vibrational degrees of freedom play in determining the autodetachment lifetime [36–38].

The long lifetimes against autodetachment have been attributed to the sharing of the excess electron kinetic energy and electron affinity energy into the various vibrational degrees of freedom of the anion [36, 39]. Upon electron attachment, excitation in certain vibrational modes of the anion is expected based upon the extent and symmetry of the change in equilibrium geometry compared to the neutral. The energy in these "active" modes is then expected to be rapidly redistributed over other vibrational modes in the molecule, a process termed intramolecular vibrational energy redistribution (IVR), on a timescale that is typically short compared to that for direct autodetachment of the captured electron. Once IVR has occurred, the probability that the energy will be reconcentrated in a mode from which autodetachment can occur is lessened, leading to creation of long-lived "metastable" ions.

The sharing of the excess energy of reaction among internal vibrational degrees of freedom in the anion is analogous to the Bohr compound nucleus theory of neutron capture by nuclei. In this context, Compton *et al.* [36] and Klots [33] introduced a simple theoretical description of negative ion lifetimes based upon the principle of detailed balance and quasi-equilibrium theory (QET) to relate the attachment rate and autodetachment rate. The following treatment is guided greatly by these author's approach, but reinvigorated by the opportunities of computational chemistry and novel experimental data. In addition to refinement of the necessary parameters of the calculation, a rigorous derivation of the density of states for the two-component neutral molecule - free electron system is presented. The approximations employed in the previous approach are examined and justified.

There are recent improvements in the values and methods for investigations of all of the important parameters required for the QET autodetachment lifetime calculation. These include experimental determinations of the electron attachment cross-sections, the vibrational frequencies of the neutrals, and the adiabatic electron affinities. For parameters that have not been experimentally determined, such as the anion vibrational frequencies and electron affinities, modern molecular orbital computations can provide reasonable estimates. Computation of vibrational frequencies for negative ions is essential, but assessment by experiment provides the final test. Application of novel experimental techniques described within allow for critique and validation of the computational approaches.

The previous QET approach is further improved by an explicit inclusion of the initial internal vibrational energy as energy available for autodetachment. Inclusion of this excess internal energy allows for the possibility of autodetachment into excited vibrational states of the neutral even at near-zero electron energies. This provides the dominating factor at high temperatures, since it results in a reduction of the autodetachment lifetime due to the increased availability of possible final product channels accessible with this excess internal energy. The resulting autodetachment lifetime thus has the temperature dependence successfully accounted for in each of the required parameters. These refinements of the QET method allow for a calculation of a predicted temperature and electron energy-dependent autoionization lifetime that is in the same energy and

temperature range as typical experiments. As is demonstrated in detail for a series of examples, the primary effect of the inclusion of the initial internal energy in the neutral is to provide access to many more degenerate channels to final product states, thus lowering the anion lifetime as the target temperature increases.

Because the QET model of electron detachment assumes complete IVR within the anion, the method of formation of the anion should not be important as long as the total energy is accounted for. Thus, both common experimental methods of producing metastable molecular anions, free-electron attachment and Rydberg Electron Transfer, or RET, should be suitable for the QET model. Application of this method to a series of molecules allows for investigation of the strengths and weaknesses of the approach, and thus leads to new insight in the dynamics of molecular anions. In particular, the QET model provides a theoretical interpretation for the interesting experimental discrepancies between free-electron-formed anion autodetachment rates and RET-formed anion autodetachment rates.

4.2 Formulation of QET Autodetachment Lifetime

The basic assumption of quasiequilibrium theory is an assumed statistical sharing of energy between states within a microcanonical ensemble. The internal degrees of freedom within the product and reactant systems determine the statistical likelihood of localization of energy in a reaction coordinate. There is assumed to be no activation barrier to reaction. Therefore an equilibrium equation can be formulated using the principle of microscopic reversibility. Essentially, this in analogy to bulk kinetics, where the ratio of the rates for the forward and reverse processes equals the ratio of the equilibrium concentrations. For a microcanonical ensemble the "concentration" is in energy space instead of physical space, thus the ratio of rates equals the ratio of the densities of states for the product and reactant systems. So for systems with energy-dependent rate constants $k(E)$ and densities of states $\rho(E)$,

$$k_{forward}(E^*)\rho_{reactant}(E^*) = k_{reverse}(E_e)\rho_{product}(E_{int} + E_e).$$

The process of electron autodetachment from meta-stable anions can be formulated in this theoretical framework. We define the reactant system as the metastable anion, and the product system as the neutral molecule plus free electron. Thus, $k_{forward}(E^*)$ is equal to the electron autodetachment rate, $k_d(E^*)$, where E^* is the total energy in the anion. $k_{reverse}(E_e)$ is given by the neutral molecule's free-electron attachment rate, $k_a(E_e)$, where E_e is the energy of the autoionizing electron and E_{int} is the internal energy in the neutral. The total energy in the product system is $E_{int} + E_e$, and thus the energy in the metastable anion is given by

$$E^* = E_{int} + E_e + EA \tag{4.1}$$

where EA is the zero-point-energy-corrected adiabatic electron affinity.

The energy-dependent free-electron attachment rate is experimentally available as an electron-capture cross-section $\sigma(v_e)$ according to the relation

$$k_{reverse}(E_e) = \sigma(v_e)v_e$$

where v_e is the electron velocity. The anion's energy-dependent autodetachment rate is then given as

$$k_d(E^*)\rho_{anion}(E^*) = \sigma(v_e)v_e\rho_{[neutral+e^-]}(E_{int}+E_e).$$

Since the anion autodetachment lifetime, $\tau_{anion}(E^*)$, is given by

$$\tau_{anion}(E^*) \equiv \frac{1}{k_d(E^*)}$$

then

$$\tau_{anion}(E^*) = \frac{\rho_{anion}(E^*)}{\sigma(v_e)v_e\rho_{[neutral+e^-]}(E_{int}+E_e)}. \tag{4.2}$$

From the above equation, we can see that the QET autodetachment rate will be a function of the total energy in the anion as well as a function of the autodetaching electron velocity. Thus we expect a distribution of autodetachment lifetimes to be observed, mirroring the distribution of the autodetaching electron energies. However, for many molecules such as SF_6, the attachment cross-section $\sigma(v_e)$ shows a $1/v_e$ dependence, and thus the attachment rate, $\sigma(v_e)v_e$ shows only a weak energy dependence. We can also use another available experimental value, the energy-integrated thermal electron attachment rate, k_a, to give a representative value of the energy-dependent auto-ionization rate.

$$\tau_{anion}(E^*) \approx \frac{\rho_{anion}(E^*)}{k_a\rho_{[neutral+e^-]}(E_{int}+E_e)}. \tag{4.3}$$

Both $\sigma(v_e)$ and k_a are experimentally available for a wide range of molecules. In addition, the upper and lower limits for these values can often be estimated by comparison to other molecules. Thus, the difficulty in applying the QET formulation to autodetachment lifetimes lies in the accurate calculation of the densities of states for the metastable anion and the product system, the neutral molecule plus free electron.

4.3 Vibrational Density of States for Molecular Anion

The density of states, $\rho(E)$, is defined as the derivative with respect to energy of the sum of states, G(E).

$$\rho(E) = \frac{d}{dE}G(E)$$

The sum of states is the number of available configurations of internal excitations possible at a given energy. This quantity can be computed if details of the energy of the internal degrees of freedom are known. For polyatomic molecules, the active internal degrees of freedom that determine the autoionization lifetime are vibrational [37]. Vibrational densities of states can be calculated either by direct count, or according to the semi-classical formulation of Marcus and Rice [40], revised by Whitten and Rabinovitch [41]. In this method, the sum of states is given as a function of the vibrational frequencies of the molecule and the energy within the molecule. For a molecule with s vibrational modes,

$$G(E) = \frac{(E+a(E)E_z)^s}{s!\prod_{i=1}^{s} h\nu_i} \tag{4.4}$$

The quantity E_z is the zero-point energy of the molecule,

$$E_z = \frac{\sum_{i=1}^{s} h\nu_i}{2}$$

and the factor a(E) mitigates the amount of the zero-point energy that is included according to an empirical fit of a wide variety of molecules. The factor a(E) has limits of 0 and 1 for $E \to 0$ and $E \to \infty$, and is given by

$$a(E) = 1 - \beta\omega(\frac{E}{E_z}).$$

For simplicity the parameter $a(E)$ can be given as a function of E' such that

$$E' \equiv \frac{E}{E_z}.$$

The parameter β is related to the dispersion of the vibrational frequencies,

$$\beta = \frac{s-1}{s}\frac{\langle h\nu_i^2\rangle}{\langle h\nu_i\rangle^2}.$$

The function $\omega(E')$ is determined by an empirical fit, and is given by two distinct functions depending upon whether the energy in the molecule is greater or less than the zero-point energy of the molecule. For $E < E_z$

$$\omega(E') = \frac{1}{5.00(E') + 2.73(E')^{\frac{1}{2}} + 3.51} \tag{4.5}$$

and for $E > E_z$

$$\omega(E') = e^{-2.4191(E')^{\frac{1}{4}}}. \tag{4.6}$$

The vibrational density of states for a molecule is thus given by

$$\rho(E) = \frac{d}{dE}G(E) = \left[1 - \beta\frac{d\omega(E')}{dE'}\right]\frac{(E + aE')E_z)^{s-1}}{\Gamma(s)\prod_{i=1}^{s} h\nu_i} \tag{4.7}$$

and has units of energy^{-1}.

Numerical calculations of this quantity require all the vibrational frequencies of the molecule or ion. This method is therefore greatly facilitated by the availability of modern molecular orbital calculation programs, as even for simple molecules of high symmetry there are often dark modes experimentally inaccessible by IR or Raman spectroscopy. For negative ions, there are few examples of direct experimental observation of vibrational frequencies, so a computational approach to determining the anion vibrational frequencies is essential.

The anion density of states expression in the numerator of equation (4.2) is given directly by substitution of the energy and anion vibrational frequencies into equation (4.7). The density of states expression for the product system, the neutral and free electron, is more complicated.

4.4 Density of States for Product System

To determine the density of states expression for a compound system, we first define the sum of states for the compound system. Since the sum of states is the number of possible configurations available at a given energy, it is important to realize that for this quantity to be defined the energy within the product system must be partitioned between the neutral molecule and the free electron. Since the product system is defined as the separated neutral molecule and electron, the requirement is reasonable. However, this will give an expression for the sum of states that is a function of not only the total energy in the molecule and electron, but also a function of how that energy is partitioned between the two. To begin, we consider

$$E^* - EA = E_{product} = E_{int} + E_e \tag{4.8}$$

such that E_{int} is the excess energy left in the neutral, and E_e is the outgoing electron velocity. Given a particular value of E_{int} and E_e, the sum of the possible states of the system is given by the possible ways of distributing E_{int} within the internal degrees of freedom of the neutral and E_e within the translational motion of the electron. Since the energy is partitioned between the neutral and the electron, we can consider these two sum of states expressions independently. The sum of states for the product system is thus simply the product of the sum of states for the components.

$$G_{[neutral+e^-]}(E_p) = G_{neutral}(E_{int})G_{e^-}(E_e) \tag{4.9}$$

This expression is correlate to the concept of the probability of two independent events as equal to the product of the individual probabilities, but simply the inverse. Given a formulation of the sum of states for the product system, we derive the expression for the density of states for the product system, $\rho_{[neutral+e^-]}(E_p)$, by differentiating equation (4.9) with respect to energy.

$$\rho_{[neutral+e^-]}(E_p) = \frac{d}{dE} G_{neutral}(E_{int})G_{e^-}(E_e)$$

Using the product rule,

$$\rho_{[neutral+e^-]}(E_p) = \rho_{neutral}(E_{int})G_{e^-}(E_e) + G_{neutral}(E_{int})\rho_{e^-}(E_e) \tag{4.10}$$

it is clear that both the sum of states and the density of states must be calculated for each the neutral and the free electron to determine the numerator in the lifetime expression of equation (4.2), and that $\rho_{[neutral+e^-]}(E_p)$ will depend upon the values of E_{int} and E_e, where these energies are constrained by equation (4.8).

The expression for the sum of states for a free electron is derived from the three-dimensional particle-in-a-box eigenvalue expression and the DeBroglie wavelength of a free particle, and is given by

$$G_{\mathrm{e}^-}(E_e) = \frac{m_e^3 v_e^3}{3\pi^2\hbar^3}. \tag{4.11}$$

This expression has units of energy per unit volume, since that is how the states are defined. The density of states for a free electron is given by the derivative with respect

to energy of this expression,

$$\rho_{\mathrm{e}^-}(E_e) = \frac{m_e^2 v_e}{\pi^2 \hbar^3} \tag{4.12}$$

where m_e is the mass of an electron and v_e is the electron velocity given by

$$v_e = \sqrt{\frac{2E_e}{m_e}}.$$

Comparison of equations (4.11) and (4.12) reveals that the ratio of the free electron sum of states to the density of states is equal to a factor of $\frac{m_e v_e^2}{3}$.

$$\frac{\rho_{e^-}(E_e)}{G_{e^-}(E_e)} = \frac{m_e v_e^2}{3}$$

Considering the relative magnitude of the two terms, m_e and v_e, it is clear that the magnitude of the free electron density of states term is always much larger than the sum of states term. As will be discussed in detail in the following chapter, for the energy range under consideration the relative magnitudes of the correlate terms for the neutral molecule show the same ordering. However, as will be demonstrated for a wide variety of molecules and energies, the magnitude of this difference between the neutral terms is always much smaller than the difference between the free electron terms. This allows for a simplification in the expression of the density of states for the product system. Considering the relationships above and comparing the two terms in the summation of equation (4.10), it is clear that the term including the density of states of the electron will be much larger than the term including the sum of states of the free electron. Thus, since

$$G_{neutral}(E_{int})\rho_{e^-}(E_e) \gg \rho_{neutral}(E_{int})G_{e^-}(E_e) \tag{4.13}$$

then

$$\rho_{[neutral+e^-]}(E_p) \approx G_{neutral}(E_{int})\rho_{e^-}(E_e). \tag{4.14}$$

This simplification is examined in detail for the $SF_6 + e^-$ system in the following chapter. It is shown that the terms are seperated by many orders of magnitude at all considered energies.

Using this simplification, the product density of states is given as

$$\rho_{[neutral+e^-]}(E_p) = G_{neutral}(E_{int})\frac{m_e^2 v_e}{\pi^2 \hbar^3} \tag{4.15}$$

where $G_{neutral}(E_{int})$ is given by equation (4.4). The expression for the product system density of states and anion density of states are substituted into equation (4.2) to produce a working expression for the anion autodetachment lifetime. Here a factor of two is introduced to account for the electronic degeneracy of a doublet state. This is the case for the majority of molecular anions, for singlet state anions the inverse operation is required.

$$\tau_{anion}(E^*) = \frac{2\rho_{anion}(E^*)}{\rho_{\mathrm{e}^-}(E_e)\sigma(v_e)v_e G_{neutral}(E_{int})} \tag{4.16}$$

Upon substitution of equations (4.4), (4.7), and (4.12) into equation (4.16) the expression for the autodetachment lifetime becomes

$$\tau_{anion}(E^*) =$$

$$\left[2(1-\beta\frac{d\omega(\frac{E^*}{E_z})}{dE'})\frac{(E^*+a(\frac{E^*}{E_z})E_z)^{s-1}}{\Gamma(s)\prod_{i=1}^{s}h\nu_i}\right]_{anion}\frac{\pi^2\hbar^3}{\sigma(v_e)m_e^2v_e^2}\left[\frac{s!\prod_{i=1}^{s}h\nu_i}{(E_{int}+a(\frac{E_{int}}{E_z})E_z)^s}\right]_{neutral} \quad (4.17)$$

As represented in equation 4.3, the term $\sigma(v_e)v_e$ can be replaced with k_a, the thermal attachment rate.

$$\tau_{anion}(E^*) =$$

$$\left[2(1-\beta\frac{d\omega(\frac{E^*}{E_z})}{dE'})\frac{(E^*+a(\frac{E^*}{E_z})E_z)^{s-1}}{\Gamma(s)\prod_{i=1}^{s}h\nu_i}\right]_{anion}\frac{\pi^2\hbar^3}{k_am_e^2v_e}\left[\frac{s!\prod_{i=1}^{s}h\nu_i}{(E_{int}+a(\frac{E_{int}}{E_z})E_z)^s}\right]_{neutral} \quad (4.18)$$

4.5 A Note On Rotational Degrees of Freedom

The influence of the rotational degrees of freedom in the anion and neutral densities of states has been neglected in the current treatment. The justifiability of this approach is based upon the typical lack of extensive coupling between molecular rotational motion and s-wave electron capture, since the angular momentum of the electron is zero. It is thus perhaps justifiable not to include the rotational degrees of freedom of the neutral and anion for a molecule such as SF_6, since formation of SF_6^{-*} involves s-wave electron capture with no angular momentum into a totally symmetric A_{1g} orbital. The spherical top symmetry is therefore not disturbed, and extensive rotational coupling is not expected. However, it must be noted that electron capture typically promotes significant geometry change, and therefore change in the rotational density of states for the anion relative to the neutral. This aspect may also be related to changes in molecular symmetry upon electron attachment. Since electron capture by some molecules promotes change in molecular symmetry, C_6F_6 for example, goes from from D_{6h} to C_{2v} and all of the molecular moments of inertia change, it is not clear that the same argument can be made for neglecting the rotational contribution to the sum and densities of states. Treatment of the rotational degrees of freedom would be essential for a description of diatomic systems, since this is the only "pool" of available motions to redistribute energy into besides the active coordinate of the single vibrational mode.

4.6 Determination of Energies

One of the basic assumptions of QET is that energy in the anion is shared equally by the various internal degrees of freedom, i.e. IVR is complete upon electron attachment, and thus the anion density of states is calculated according to the total internal energy in the anion. This total internal energy of the anion, E^* is determined by the adiabatic electron affinity, EA , the electron impact energy, $E_{e_{in}}$, and the initial internal energy of the neutral molecule before electron attachment, $E_{initial}(T)$.

$$E^* = EA + E_{e_{in}} + E_{initial}(T) \tag{4.19}$$

In comparison to equation (4.1), it should be noted that while the sum of the initial internal energy of the neutral and the impact electron energy must equal the sum of the internal energy left in the neutral and the outgoing electron energy, the individual terms are not necessarily equal.

$$E_{int} + E_e = E_p = E_{initial}(T) + E_{e_{in}}$$

but

$$E_{int} \neq E_{initial}(T)$$

and

$$E_e \neq E_{e_{in}}.$$

The result is a distribution of the autodetachment lifetimes that depends upon the partitioning of the energy between the product neutral and autodetaching free electron. The observed lifetime for a given anion energy E^* is comprised of a distribution of values weighted by the probability of an autodetaching electron with each possible value of E_e. This energy distribution of autodetaching electrons has not been thoroughly experimentally characterized, but in analogy to thermionic emission, the distribution of these energies is expected to lie in the the range of meV for most autoionizing electrons [31]. The autodetachment lifetime can be calculated for any possible partitioning of energy between E_{int} and E_e, but for a representative value of the autodetachment lifetime a autodetaching electron energy of 1 meV is used. This choice not only affects the density of states of the free electron and the sum of states of the product neutral, but also the choice of $\sigma(v_e)$.

4.6.1 Determination of Adiabatic Electron Affinity, EA

Accurate determination of E^* requires a reliable zero-point-energy-corrected adiabatic electron affinity value, EA, which is experimentally available for some molecules, and is also available by electronic structure computations involving geometry optimization and harmonic frequency calculations. Highly accurate experimental determinations of electron affinities are often difficult to attain experimentally, and thus the use of computational results provides a useful check on the experimental value, and in some cases is the only available value. For a computational determination of the electron affinity, it is not sufficient to compare the minimum energies of the neutral and anion. The zero-point-energy correction makes a non-negligible contribution to the EA due to the effect the changed chemical bonding in the anion has in producing often very different force constants from the neutral, and hence different vibrational frequencies.

4.6.2 Determination of Electron Impact Energy, $E_{e_{in}}$

The electron impact energy, $E_{e_{in}}$, is straightforward for free-electron attachment experiments, as this parameter is determined by direct experimental measurement. For

favorable cases, such as SF_6, detailed measurements of electron energy-dependent cross-sections are available that allow for an exact QET prediction of an electron-energy dependent lifetime. For molecules lacking this detailed information, where only thermal attachment rates are available, a typical thermal electron energy on the order of meV is appropriate. Rydberg Electron Transfer, or RET, formation of anions is typically done from atoms with electrons promoted to very loosely bound states, with low kinetic energies. For example, in recent experiments [23] the SF_6^{-*} and $C_6F_6^{-*}$ anions were formed by RET from excited Potassium atoms in the process

$$K(np) + M \longrightarrow M^{-*} + K^{+}. \tag{4.20}$$

The electrons of the Potassium atom were excited up to $n = 45$, which amounts to an electron kinetic energy of approximately 1.3 meV [23]. It is clear that in comparison with typical electron affinities and the internal vibrational energies of polyatomic molecules, the contribution of $E_{e_{in}}$ to the total energy E^* is almost negligible.

4.6.3 Determination of $E_{initial}(T)$

Assuming an initial equilibrium between the vibrational degrees of freedom and the translational, the initial internal energy of the neutral, $E_{initial}(T)$, is a function of temperature and the vibrational frequencies of the neutral. The amount of initial internal energy in the neutral for a given temperature can be determined by weighting the energy in excited vibrational states by the Boltzmann probabilities of those states. In the harmonic approximation, for a molecule with vibrational modes each of frequency ν_i the energy of the v^{th} excited vibrational state of mode i is given by

$$E_i(v) = h\nu_i(v + \frac{1}{2}). \tag{4.21}$$

However, we are specifically interested in the vibrational energy of the molecule *above* the zero-point energy. For a molecule with a total of s vibrational modes ($s = 3N - 5$ if the molecule is linear and $s = 3N - 6$ if not, where N is the number of atoms) the zero-point energy is defined as

$$\sum_{i=1}^{s} \frac{h\nu_i}{2}. \tag{4.22}$$

Thus to calculate the *excess* vibrational energy, instead of defining the energy as in equation (4.21) above, we define the energy as relative to the zero-point-energy,

$$E_i(v) = vh\nu_i. \tag{4.23}$$

The un-normalized probability in excited state v of mode i is given by the Boltzmann distribution,

$$p_i(v, T) = \frac{e^{-E_i(v)kT}}{Q_i} \tag{4.24}$$

where

$$Q_i = \sum_{v=0}^{v_{max}} e^{-E_i(v)kT}. \tag{4.25}$$

The normalized population of excited vibrational states is

$$P_i(v,T) = \frac{p_i(v,T)}{\sum_{v=0}^{v_{max}} p_i(v,T)}. \tag{4.26}$$

With the probability of excitation for each quantum state within in a given mode established, we can calculate the amount of energy stored in each excited state by multiplying the excitation energy by the fractional population. The summation of these energies over all the possible excitations within a given mode gives the amount of energy within that mode for a certain temperature.

$$E_i(T) = \sum_{v=0}^{v_{max}} P_i(v,T) E_i(v) \tag{4.27}$$

Since the vibrational modes are independent degrees of freedom, the probability of excitations in each mode i is represented by equation (4.26). Thus the total amount of internal vibrational energy within the molecule is given by the sum of the energy stored in each mode, as given by equation (4.27) above, so that for a molecule

$$E_{initial}(T) = \sum_{i=1}^{s} E_i(T). \tag{4.28}$$

Finally, by combining equations (4.23) through (4.27), we have an expression in equation (4.28) for the initial internal vibrational energy of the molecule given as a function of the vibrational frequencies and the temperature. This requires us to therefore define the temperature for each predicted autodetachment lifetime, but allows for a method for investigation of the temperature dependence of the autoionization lifetime. Often, as in the case of SF_6, the total electron capture cross section is relatively constant with temperature, and thus, the primary influence of the temperature on the autodetachment lifetime is through this parameter, the initial internal energy of the neutral that increases the total energy within the metastable anion.

4.7 Summary of Parameters Required for QET Calculation

The required parameters for QET prediction of the autodetchment rate of a molecule include the electron attachment rate, ($\sigma(v_e)v_e$ or k_a), attaching electron energy, $E_{e_{in}}$, the detaching electron energy, E_e, the vibrational frequencies of the neutral and anion, the zero-point-energy-corrected adiabatic electron affinity, EA, and the temperature-dependent initial internal vibrational energy of the neutral, $E_{initial}$. All but the first two parameters are amenable to calculation by molecular orbital computations for the case of unavailable experimental data. The first parameter must be experimentally determined. The second parameter requires an assumption about the unknown energy distribution of autoionizing electrons, and thus the QET calculated lifetimes within this work are given as a representative values for "typical" autodetaching electrons of 1meV in energy. The effect of this assumption, as well as the effect of all of the parameters on the calculated lifetimes are assessed in detail for a variety of molecules. A major advantage of the

current formulation is that the temperature dependence of the autoionization rate is accounted for, and the QET model reproduces the experimental trends.

Chapter 5

Application of QET to Temperature-Dependent Autodetachment Lifetimes: Selected Molecules With Zero-Energy Electron Capture Resonances

5.1 Measurement of Anion Lifetimes

Historically, the experimental methods for the anion autodetachment rate determinations centered on free electron attachment and subsequent time-of-flight mass spectrometry (TOF-MS) techniques, but in recent decades experiments have been done in ion storage systems and also utilizing atoms in high Rydberg states for the electron transfer process. There is a wide variety of examples of anion autodetachment lifetimes determined by these techniques. A small selection of the many molecular anions studied is presented in Table 5.1, excluding the SF_6^- ion which is discussed in detail separately in Table 5.2. All of the ions listed show a electron capture resonance at zero electron energies, and positive electron affinities.

Lifetime measurements from RET experiments often corroborate the TOF-MS results, as in the case of $C_6F_6^-$ and $C_2Cl_4^-$, and somewhat less so for $C_{10}F_8^-$ and $C_7F_{14}^-$. The SF_6^- anion, however provides a very notable exception, as shown in table 5.2. The case of SF_6^- is interesting due to the severity and reproducibility of the discrepancies between the experimental methods.

Table 5.1: Autodetachment lifetime measurements using Time-of-Flight Mass Spectroscopy (TOF-MS) and Rydberg Electron Transfer (RET) techniques for various long-lived metastable anions.

Molecule	Reference	Lifetime (in μs)	Comment
SF_4^-	[21]	$16.3 \pm .03$	TOF-MS
$C_2Cl_4^-$	[42]	14 ± 3	TOF-MS
	[43]	$3 - 30$	RET
$(1,1,2)C_2Cl_3F_3^-$	[44]	0.001	RET
$C_4F_8^-$	[1]	12	TOF-MS
$C_6H_5NO_2^-$	[36]	40	TOF-MS
	[21]	47.3 ± 1	TOF-MS
	[45]	49	TOF-MS
	[37]	17.5	TOF-MS
	[46]	1600	RET
$C_6D_5NO_2^-$	[37]	22	TOF-MS
$C_6H_5CN^-$	[37]	5	TOF-MS
$C_6F_5CN^-$	[37]	17	TOF-MS
$C_6F_6^-$	[1]	12	TOF-MS
	[45]	13.3	TOF-MS
	[47]	10	RET
	[23]	12	RET
$C_6F_5Cl^-$	[37]	17.6	TOF-MS
$C_6F_{12}^-$	[1]	450	TOF-MS
$C_7F_{14}^-$	[1]	793	TOF-MS
	[47]	2100	RET
$C_{10}F_8^-$	[37]	123	TOF-MS
	[47]	350	RET
$C_{12}H_4N_4^-$ (TCNQ)	[48]	2000	TOF-MS 0eV
	[48]	100	TOF-MS 4eV

5.2 The Interesting Case of SF_6^{-*} Autodetachment

5.2.1 Experimental Background

The autodetachment lifetime for SF_6^{-*} ions formed by the unimolecular attachment of low energy electrons to the SF_6 molecule, i.e.

$$e^- + SF_6 \longrightarrow SF_6^{-*}$$

was first observed by Edelson *et al.* [39] in a time-of flight mass spectrometer. Their method consisted of attaching "low energy" electrons to gaseous SF_6 and measuring the ratio of $SF_6{}^o$ neutrals resulting from autodetachment compared to the surviving SF_6^- ions arriving at the detector after a predetermined flight time down the flight-tube of a time-of-flight mass spectrometer. Four years later, Compton *et al.* [36] determined this ratio as a function of the TOF by varying the ion velocity down the flight-tube in order to obtain an exponential decay law lifetime measurement. Five years after this study, Harland and Thynne [21] again measured the autodetachment lifetime using a TOF-MS for three different ion energies. Seven years later, Applehans and Delmore [49] also used the TOF method to determine the autodetachment lifetime by measuring the $SF_6{}^o$ neutrals resulting from autodetachment of SF_6^{-*} ions as a function of the distance along the flight path. These authors also found that the "effective lifetime" increased from 15 to 20 μs as the temperature of the SF_6 was reduced from 475 to 375 K. All of these studies employed a wide and somewhat ill-defined electron energy distribution using thermionic emission from a filament for the electron source. Thirteen years later, Le Garrec *et al.* [50] measured the autodetachment lifetime of SF_6^{-*} as a function of the incident electron energy for SF_6 cooled in a free-jet expansion, again using the TOF technique. They employed a laser photodetachment source of high resolution electrons and reported no change in the autodetachment lifetime in the range from 0 to 100 meV. Autodetachment lifetime studies of SF_6^{-*} using the TOF-MS technique over the past 40 years have reported lifetimes varying from $\sim$ 10 to 60μs, as summarized in Table 5.2.

In parallel with the TOF-MS studies, a series of SF_6^{-*} lifetime measurements were undertaken using ion cyclotron resonance (ICR) methods beginning in the nineteen seventies. In the first of these Henis and Mabie [51] obtained a lifetime of $\sim 300\mu s$ for SF_6^{-*} ions formed by slow electron attachment. Subsequently, Odom, Smith and Futrell [52] used an ICR technique and found that the "apparent" autodetachment lifetime of SF_6^{-*} varied as a function of the observation time (non single exponential decay) from 50μs to 10ms. These authors argued that those ions living longer than 10 ms may be undergoing radiative stabilization. Foster and Beauchamp [53] also reported relatively stable SF_6^- in an ICR mass spectrometer and also attributed this observation to radiative stabilization. Recent measurements by Liu et al. [54] following free electron attachment in a Penning ion trap point to non-exponential decay and formation of SF_6^{-*} ions with a range of lifetimes of $\sim$ 1 to $> 10ms$.

SF_6^{-*} lifetimes measured using high-n Rydberg atoms and electron transfer reactions of the type

$$K_{(np)} + SF_6 \rightarrow K^+ + SF_6^{-*}$$

assume an essentially-free-electron model of Rydberg atom collisions. This asserts that

Table 5.2: SF_6^{-*} Lifetime Measurements using Time-of-Flight Mass Spectroscopy (TOF), Ion Cyclotron Resonance (ICR), and Ion Trap methods.

Reference	Lifetime	Description
[39]	$\sim 10\mu s$	TOF, single energy meas.
[36]	$25\mu s$	TOF, exponential decay meas.
[21]	$68 \pm 2\mu s$	TOF, three ion energies
[49]	$15\mu s$	TOF, many energies, 475 K
[49]	$20\mu s$	TOF, many energies, 375 K
[57]	$\sim 2, 12-17, 22-27\mu s$	TOF, temp. dependence
[50]	$19.1 \pm 2.7\mu s$	TOF, ind. of electron energy
[51]	$\sim 300ms$	ICR
[52]	$50\mu s$ to $10ms$	ICR, non single exp. decay
[47]	$\sim 10ms$	Penning Ion Trap, RET
[54]	$\sim 1ms$ to $> 10ms$	Penning Ion Trap, free electron attach.
[23]	$\sim 1ms$	Ion Trap, RET, 300K
[23]	$\sim 10\mu s$	Ion Trap, RET, 600K

highly excited weakly-bond electrons with sufficiently large values of principal quantum number n behave as free electrons. This assumption has been debated as to it's applicability in all systems, as certain electron transfer processes in SF_6 have been demonstrated to be influenced by the Rydberg ion core [55]. However, the subsequent studies of RET to SF_6 involve highly excited Rydberg states, so it is not clear if there is, in fact, significant interaction between the molecule and the Rydberg core. Initial TOF studies by Foltz *et al.* [56] revealed no evidence of significant decay of SF_6^{-*} ions formed in high-n collisions on timescales of $\sim$ 10-20 μs pointing to a long $SF_6{}^{-*}$ lifetime. This was confirmed in subsequent work by Liu *et al.* [47] in which the product SF_6^{-*} ions were injected into a Penning ion trap. Ion decay in the trap was characterized by a non-single exponential, pointing to creation of ions with a range of lifetimes extending from $\sim$ 1 to $>$ 10 ms. These results and the correlate TOF results are summarized in Table 5.2.

It is clear that the free-electron attachment anions detected by time-of-flight mass spectrometry show a very different result than the ion trap and RET-formed anions. Many of the RET and ICR experiments show a non-single exponential decay, leading some to suggest the possibility of multiple anion states, some of which decay more quickly [23, 47, 54]. Another possible mechanism to consider is the cyclotron motion of an electron in a strong magnetic field, because some autodetaching electrons will be bent back towards the molecule and recaptured. However, estimations of this cyclotron radius for the electron suggests this mechanism is not important [23]. The discrepancies between the lifetimes determined using time-of-flight techniques and ion-cyclotron and Rydberg atom methods have been the subject of considerable debate, and remains unresolved. Development of a theoretical model of anion autodetachment lifetimes provides a means for analysis of the relevance of the important parameters and may provide insight into the possible sources of the discrepancies.

Table 5.3: SF_6 experimentally determined fundamental vibrational frequencies and mode symmetries, from reference [20].

Mode	ν_1	ν_2	ν_3	ν_4	ν_5	ν_6
Symmetry	A_{1g}	E_g	T_{1u}	T_{1u}	T_{2g}	T_{2u}
Energy (in cm^{-1})	774	642	948	615	523	346

5.2.2 QET Calculation Parameters

A full account of each of the relevant parameters for the QET lifetime calculation is given below. These parameters are unique for each molecular anion, however, as stated earlier, some common assumptions are made for all molecules to simplify the discussion. Unless otherwise stated, the incoming electron energy is set at a near-zero energy, 1 meV. The energy of the outgoing electron is set at the same energy, 1 meV, although this is only one energy in a distribution. As stated before, this is justified by the fact that the autoionizing electron energy distribution is expected to peak at zero [31]. The result of this assumption is to basically postulate little change in the vibrational "temperature" of the molecule from the initial to the final state. The effect of these assumptions about the electron energies upon the value of the calculated autodetachment lifetime is assessed in each case.

Attachment Rate

SF_6 has one of the largest free-electron attachment cross-sections known, approaching the theoretical maximum for s-wave capture [36]. The well-characterized value [2,36] has been confirmed by a recent study of Braun, *et al.* [25] to provide highly accurate energy-dependent cross-sections. This electron capture cross-section shows a $1/v_e$ dependence, with a value of 2 x $10^{-17} m^2$ at 1meV. The energy-dependent data from Braun, *et al.* [25] is shown with a 1/v fit function in Figure 5.1.

The extremely effective electron capture to SF_6 is a primary reason for it's industrial and scientific use, however, the underlying physical reason for this efficiency remains to be determined. Nonetheless, this molecule essentially provides the standard to which other molecular electron-capture cross-sections are compared.

Neutral Vibrational Frequencies and Zero-Point Energy

Since the SF_6 molecule is of O_h symmetry, the Raman- and IR-active vibrational modes are mutually exclusive. In addition, there are "dark-modes" that involve no change in the dipole moment or polarizability of the molecule in time, and thus the fundamentals are not observed in IR or Raman spectroscopy. However, the vibrational frequencies of SF_6 have all been experimentally determined, including assignment of the dark modes by using combination bands [20,58]. The neutral frequencies used are taken from McDowell, *et al.* [20], are are given in Table 5.3.

The harmonic approximation is used throughout this treatment, so the zero-point energy is calculated according to equation (4.22). Using the neutral vibrational frequen-

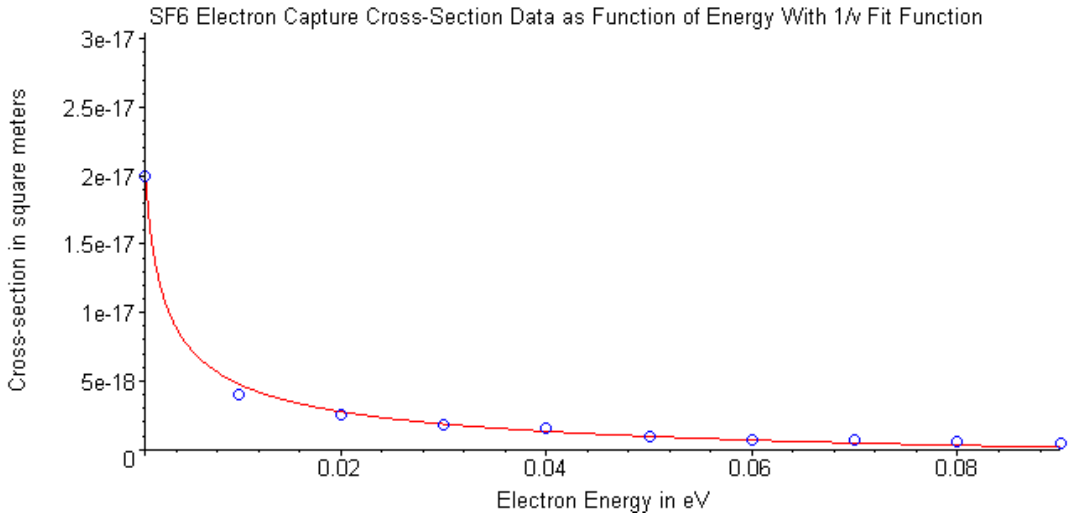

Figure 5.1: The SF_6^- electron attachment cross-section data from Braun, *et al.* [25]

Table 5.4: The calculated Boltzmann population in each of the vibrational modes of SF_6 for the first five quantum states at 300K.

Mode	v=0	v=1	v=2	v=3	v=4
ν_6	0.810	0.154	0.293x10−1	0.558x10−2	0.106x10−2
ν_5	0.919	0.748x10−1	0.609x10−2	0.496x10−3	0.403x10−4
ν_4	0.948	0.496x10−1	0.260x10−2	0.136x10−3	0.713x10−5
ν_2	0.954	0.439x10−1	0.202x10−2	0.929x10−4	0.427x10−5
ν_1	0.976	0.238x10−1	0.582x10−3	0.142x10−4	0.347x10−6
ν_3	0.989	0.105x10−1	0.111x10−3	0.118x10−5	0.125x10−7

cies of Table 5.3, this gives a value of 4677.0 cm^{-1} , or 0.58 eV for the SF_6 zero-point energy.

Anion Vibrational Frequencies and Zero-Point Energy

The vibrational frequencies of the SF_6^- anion are discussed in detail in Chapter 2 of this work. Using equation (4.22) for the freqencies results in a zero-point energy of the anion of $\sim$ 2800 cm^{-1} or $\sim$ 0.35 eV, the exact result depending upon which calculation method is employed. The Witten and Rabinovitch [41] formulation of the anion density of states involves two different functions, equations (4.5 and 4.6), depending upon whether the ratio of the total energy, E^*, to the anion zero-point energy is greater or less than unity. The zero-point energy of the anion is thus required to determine what function is used, and to calculate the parameter E' used in equations (4.5, 4.6 and 4.7).

Adiabatic Electron Affinity, EA

The adiabatic electron affinity of SF_6 is discussed in detail in Chapter 2. The experimental value of 1.05 eV from Grimsrud, Chowdhury, and Kebarle [7] is used for the current treatment, and the effect of this value upon the lifetime prediction is assessed.

Initial Internal Energy, $E_{initial}(T)$, and Total Anion Energy, E^*

Equation (4.28) is used to determine the amount of internal vibrational energy present in the neutral at a given temperature. This equation requires the normalized probability of excitation in a given vibrational quantum state for each mode, as given by equation (4.26). An example of these calculated probabilities for SF_6 at 300K are given in table 5.4.

Multiplying these probabilities times the energies of the vibrational excited states and summing over frequencies (including degeneracies) results in a value of $E_{internal}(300K)$=596.7 cm^{-1} for SF_6. The results for temperatures ranging from 300 to 600 K are given in Table 5.5 and Figure 5.2.

The internal energy of the neutral is added to the electron energy and electron affinity according to equation (4.19) to give the total energy in the metastable anion, E^*. For SF_6^{-*} at 300K, $E^* = 1.125$ eV, and at 600K $E^* = 1.125$ eV.

Table 5.5: The excess vibrational energy present in the SF_6 molecule at typical experimental temperatures. For comparison, the zero-point energy of SF_6 is 0.58 eV.

Temperature (K)	300	400	500	600
$E_{internal}(cm^{-1})$	596.7	1218.7	1967.2	2794.6
$E_{internal}(eV)$	0.074	0.151	0.244	0.346

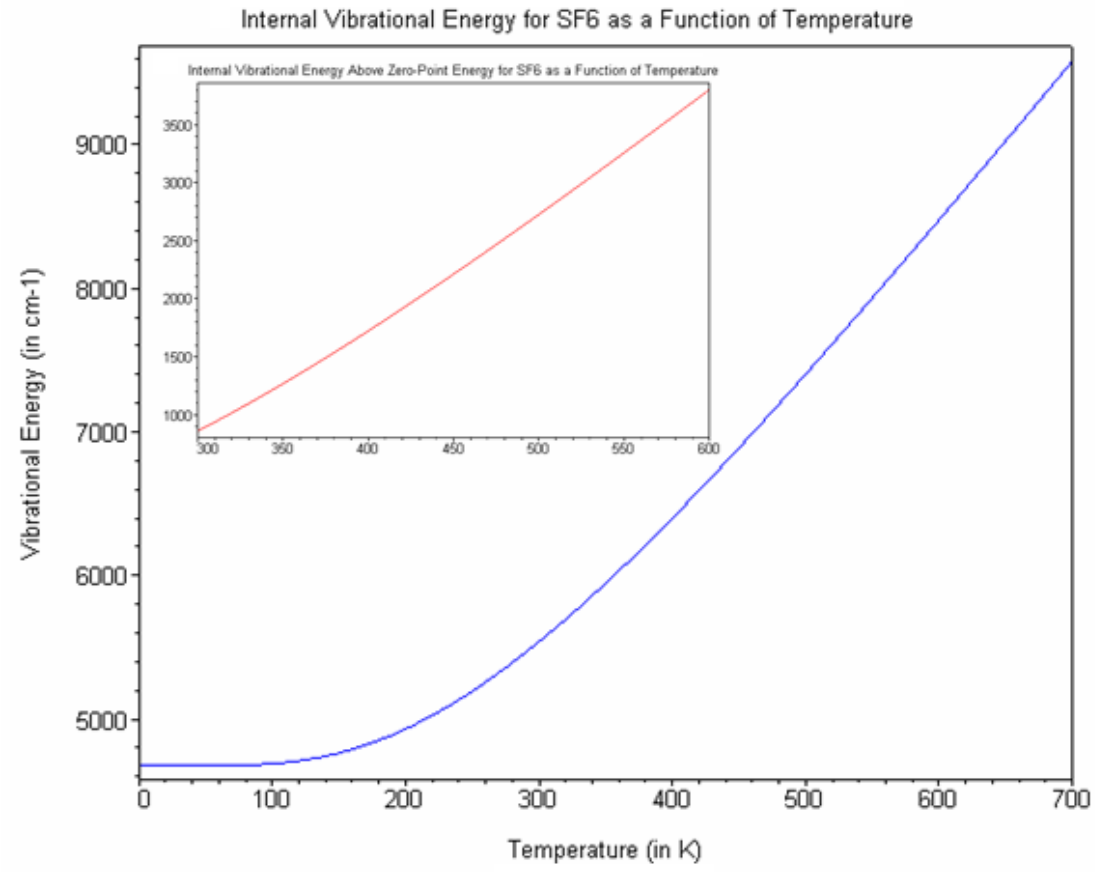

Figure 5.2: The SF_6 internal energy as a function of temperature, using the harmonic approximation and frequencies from [20].

Product Density of States: Electron Sum and Density of States and Neutral Sum and Density of of States

Recalling the relationship of equation (4.13), the product of the electron density of states and the neutral sum of states is compared to the product of the electron sum of states and the neutral density of states. This comparison provides the justification for equation (4.15). A numerical calculation of the relevant quantities for this system demonstrates the extremely large difference in magnitude between the terms.

The sum and density of states for a free electron, as given by equations (4.11) and (4.12), respectively, are functions of the outgoing electron energy. An electron with a kinetic energy of 1 meV has a velocity of 18755 m/s and sum and density of states of 1.084 x 10^{-8} m^{-3} and 1.344 x 10^{45} $J^{-1}m^{-3}$, respectively.

The sum and density of states for the SF_6 neutral product is calculated according to equation (4.4) and (4.7), respectively, using the initial internal energy of the neutral, $E_{internal}(T)$. This energy is less than the zero-point energy of the neutral for the temperature range in consideration, so in the Witten and Rabinovitch [41] formulation of the sum and density of states, equation (4.5) is used. The sum of states for SF_6 in the experimental temperature range is shown in Figure 5.3. The results range from $\sim$ 7 excited vibrational states available with the internal energy at 300 K to $\sim$ 8000 at a temperature of 600K.

The calculated density of states for SF_6 ranges from $\sim$2 x 10^{21} J^{-1} at 300K to $\sim$1 x 10^{24} J^{-1}. Now that all of the necessary quantities have been calculated, the relationship of equation (4.13) can be assessed. It is clear that term involving the electron density of states and the neutral sum of states (10^{45} $J^{-1}m^{-3}$ $\times$ 10^{3} = 10^{48} $J^{-1}m^{-3}$) is much larger than the term involving the electron sum of states and neutral density of states (10^{-8} m^{-3} $\times$ 10^{24} J^{-1} = 10^{16} $J^{-1}m^{-3}$). This example numerical analysis of the relevant quantities holds for all of the molecules considered in this work and at all temperature ranges considered. This rigorous treatment of the product system density of states provides a justification for the approximations and inclusion of product "degeneracy" states by previous authors [36], [33], [42].

Anion Density of States

The energy in the anion, E^*, is greater than the zero-point energy of the anion at all temperatures, so the density of states for the anion is calculated with equation (4.6) in equation (4.7). This quantity varies greatly with the temperature, and is also somewhat sensitive to the choice of vibrational frequency calculation used. In particular, the differences in calculated values for the low frequency vibrational modes play a significant role in these differences. Computations using DFT and CCD methods form one loose cluster, and the MP2 calculations form another. The reason for this is in the large difference these methods have in the value of the lowest vibrational frequency for SF_6^-, as shown in Table 2.5. The values range from $\sim$ 2 x 10^{30} to $\sim$ 2 x 10^{32} at 300K for the different frequency methods, and are presented in Figure 5.4.

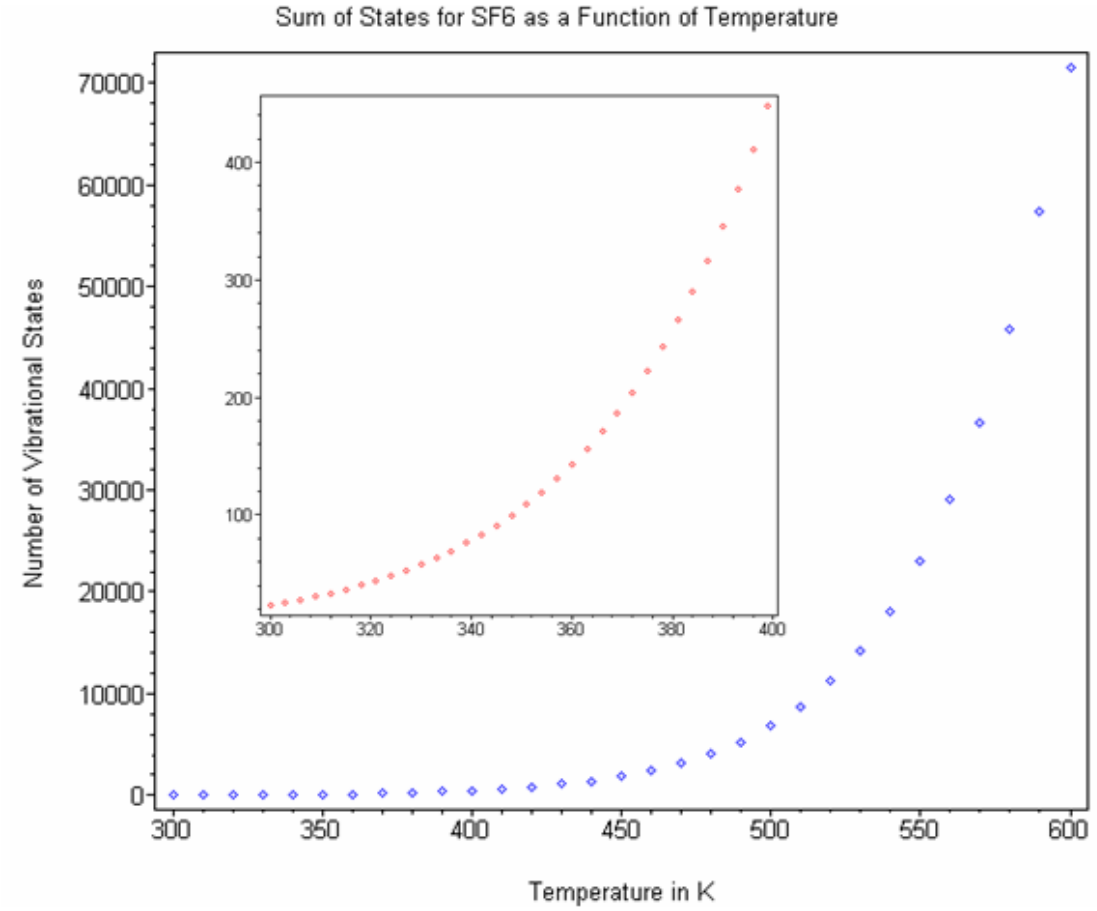

Figure 5.3: The SF_6 vibrational sum of states as a function of temperature.

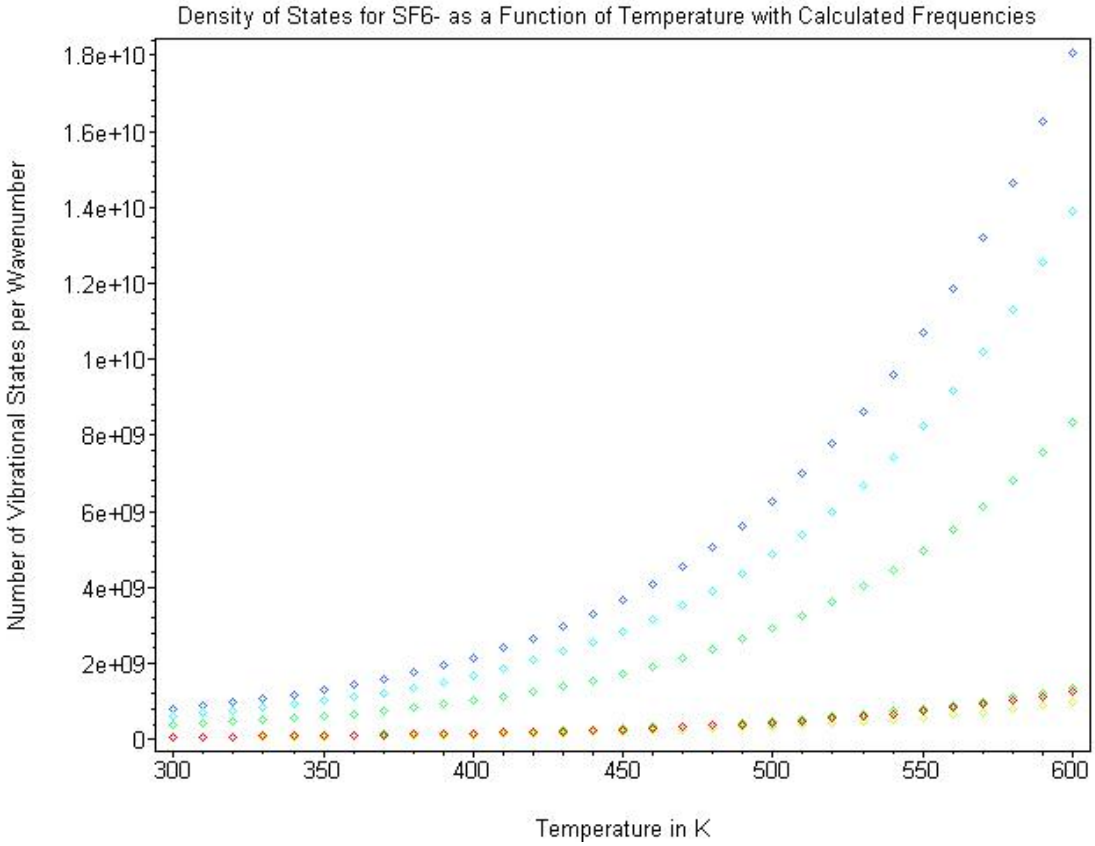

Figure 5.4: The SF_6^- density of states as a function of temperature for various vibrational frequency calculation methods. The DFT results are in blue, CCD results in green, and MP2 results are shown in warm colors.

5.2.3 QET Lifetimes

With all of the required parameters of equation (4.17) determined, the temperature dependent lifetime of the SF_6^{-*} anion can be calculated. The temperature-dependent QET-predicted lifetimes for a selected group of anion vibrational frequency calculations are shown in Figure 5.5. The calculated lifetimes are on the order of milliseconds, and show the same clustering and dependence on anion vibrational frequency calculation method as the anion density of states. Results using MP2 calculations from Gutsev and Bartlett, [8] and DFT calculations from Brinkmann and Schaefer [9] have been compared to selected MP2 and CCD calculations of the current work.

The temperature dependence of the autodetachment lifetime is opposite that of the anion density of states, however, and is seen to decrease rapidly. This result reproduces the experimental trend. The primary effect of increasing temperature is to increase the amount of internal energy in the target SF_6 molecule. The resulting increase in anion density of states with temperature (through the increasing parameter $E_{internal}$) is offset by a more rapid increase in the neutral sum of states (through the same parameter.) This relationship is shown in Figure 5.6.

Inclusion of the initial internal energy of the neutral in the QET model successfully reproduces the experimental trends observed for the temperature dependence of the autodetachment rate. Recent measurements [23] of the $SF_6{-}^*$ autodetachment lifetime as a function of target temperature over the range $\sim$ 300 to 600 K were made for $SF_6{-}^*$ formed by Rydberg charge exchange, RET, from Potassium atoms. As is consistent with the RET experiments, only the formation of long-lived SF_6^{-}* ions with lifetimes $\tau \geq 1$ ms was seen at 300 K. This is consistent with the result the QET method predicts. As the temperature was increased the lifetime of these long-lived ions was reduced, as low as $\sim$ 0.4 ms. The appearance of a short-lived, $\tau \leq 10$ μs, SF_6^{-*} signal was also observed. This is also in line with what is predicted by QET, as shown in Figure 5.5. However, while these experimental results corroborate the QET predictions, the question remains as to why these results disagree with the great many free-electron attachment TOF-MS results which give a lifetime on the order of microseconds, shown in Table 5.2.

The lifetime varies linearly with the electron attachment cross-section, and that is a very well-characterized experimental result, so no further consideration is given to this parameter. The vibrational frequencies of the neutral are also well-characterized, but the harmonic approximation is employed to determine the internal energy, $E_{internal}$. The incoming electron energy is also assumed to be 1meV, but thermal electrons employed for the experimental studies may be as high as 30meV or more. These energies affect the E^* term in the anion density of states. However, comparison of the magnitudes of $E_{e_{in}}$ and $E_{internal}$ to the electron affinity term show the major contribution to E^* is through EA. Thus, the effect of the assumed value of $EA = 1.05$eV is examined in Figure 5.7.

The value of the lifetime is quite sensitive to the electron affinity, but this sensitivity is not sufficient to account for the TOF-MS lifetimes on the order of milliseconds unless the electron affinity of SF_6 is lower then 0.8 eV, which is unlikely considering the experimental and computational corroboration for a value just over 1.0 eV. Thus, there is an interesting question as to why the QET calculations corroborate the RET results, and why free-electron MS-TOF methods give a different value. To address this issue, we examine

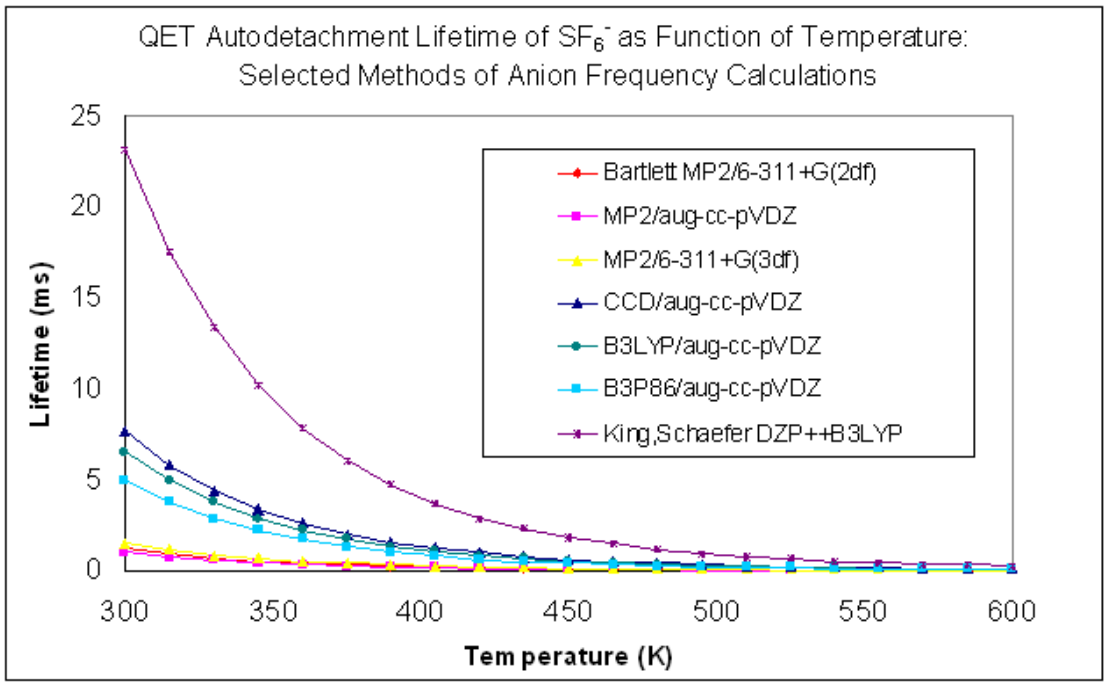

Figure 5.5: QET SF_6^{-*} autodetachment lifetimes for various anion frequency calculations.

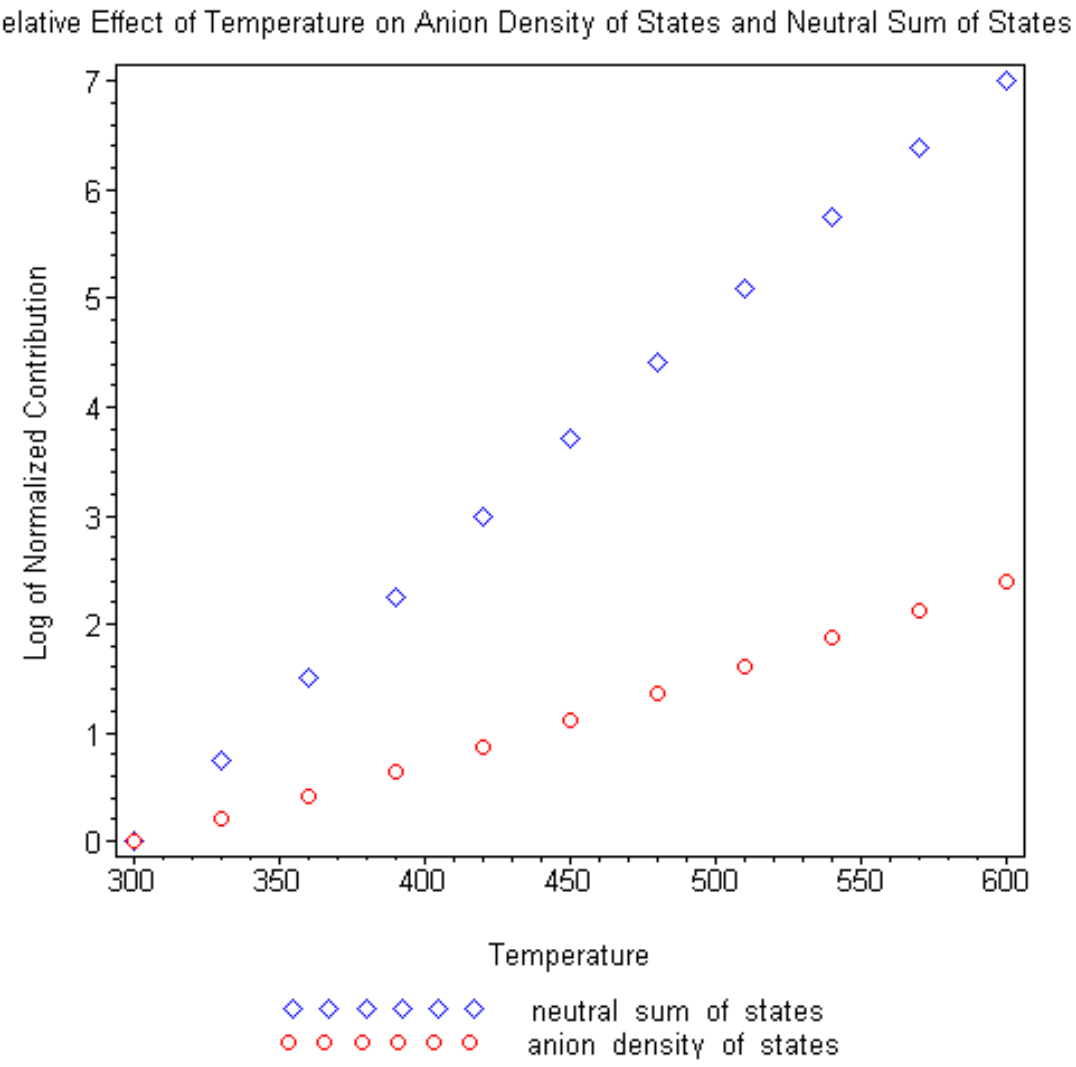

Figure 5.6: A comparison of the relative increase of the SF_6^- density of states and the SF_6 sum of states demonstrates why the lifetime decreases with temperature.

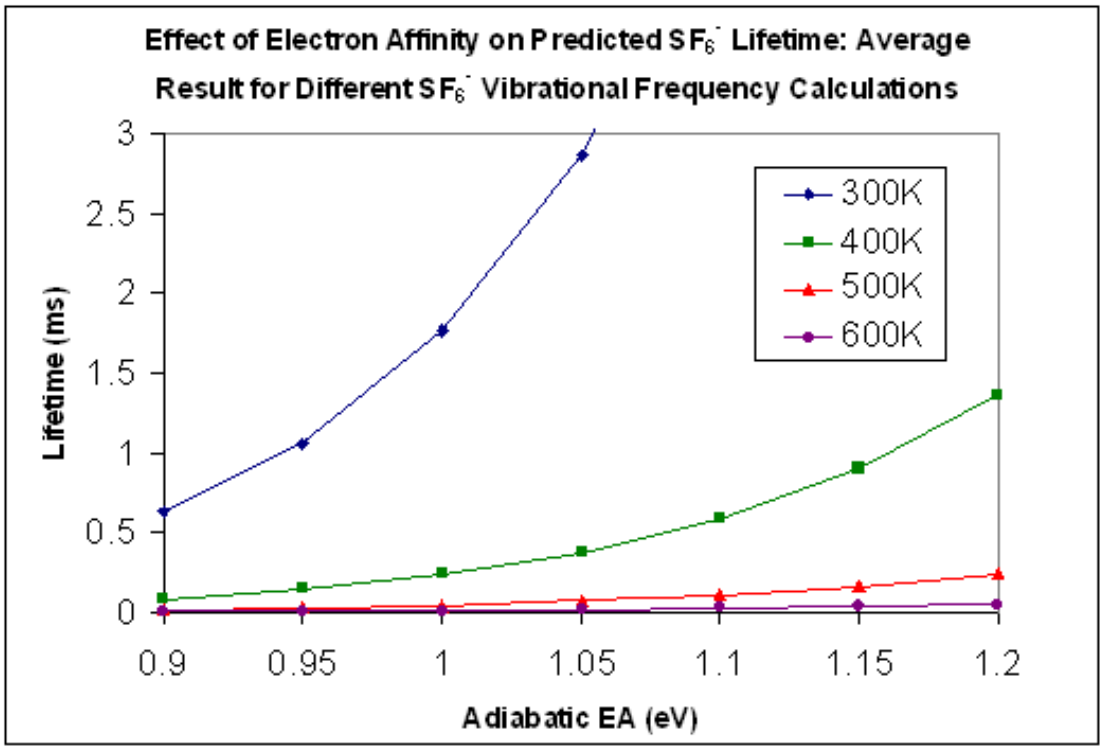

Figure 5.7: Effect of the assumed electron affinity on the calculated QET SF_6^{-*} lifetime.

the role of symmetry and geometry changes upon electron attachment and IVR in the metastable anion in the following chapter.

5.3 $C_6F_6^{-*}$

5.3.1 Experimental Background

The recent temperature-dependent lifetime study of SF_6 by Cannon *et al.* [23] was extended to C_6F_6, providing an opportunity for testing the QET autodetachment model. The experimentally observed autodetachment lifetimes for $C_6F_6{-}^*$ are summarized in Table 5.1. The autodetachment lifetime for $C_6F_6^{-*}$ ions formed through slow-electron attachment has been measured using TOF techniques by Naff *et al.* [1] and Harland *et al.* [45] yielding lifetimes of 12 s and 13 s, respectively. A similar value was obtained by Suess *et al.* [47] in earlier Rydberg electron transfer measurements. Unlike $SF_6{-}^*$, $C_6F_6{-}^*$ does not seem to show preference for experimental apparatus. In recent experiments [23] Rydberg electron attachment at room temperature again led predominantly to the production of short-lived ($\tau \leq$10 μs) $C_6F_6^{-*}$ ions but a small signal from longer-lived ($\tau \sim$ 50–100 μs) ions was also seen. As the target temperature was increased the longer-lived signal disappeared and the lifetime of the shorter-lived ions decreased dramatically. Like SF_6, the temperature dependence of the short-lived ions is in good agreement with the QET predictions, and there is good numerical agreement between the predicted and measured lifetimes.

5.3.2 QET Calculation Parameters

Attachment Rate

C_6F_6 was measured to have an absolute free-electron attachment cross-section of 1.23 $^{-18}$ m^2 at 30 meV [59]. This rate constant times the electron velocity gives the attachment rate (at this specific energy) of 12 x 10^{-8} cm^3/s. There is also an experimental result representing an energy integrated attachment cross section available. Miller *et al.* [60] determined a thermal electron attachment rate constant of 8.6 x 10^{-8} cm^3 s^{-1}. The energy specific value agrees well with the energy-integrated value, and thus the thermal attachment rate is the value that will be used in equation (4.18.

Neutral Molecule Vibrational Frequencies

Vibrational frequencies for the neutral are available from Steele and Whiffen [61]. The calculated frequencies are in good agreement with the experimental. Using these frequencies, the harmonic zero-point energy of the neutral is 1.386 eV.

Anion Vibrational Frequencies

The anion vibrational frequencies were calculated according to MP2 and DFT methods and these results are shown in Table 5.6. Again, the MP2 results differ significantly from those of DFT calculations.

Table 5.6: Calulated vibrational frequencies of the $C_6F_6^-$ anion. The results of the ab-initio calculations are scaled by 0.95, the DFT calculations by 0.98. The zero-point energies are given in units of eV in the final row.

MP2	**B3LYP**	**B3LYP)**	**B3LYP)**	**B3LYP**	**B3LYP**
6-311+G*	**6-311+G***	**6-311+G(2d)**	**6-311+G(2df)**	**aug-cc-pVDZ**	**aug-cc-pVTZ**
116	58	58	59	60	60
119	96	99	100	97	102
169	118	119	119	117	118
223	174	174	176	171	174
245	248	246	248	243	249
247	250	248	251	245	251
254	261	260	262	258	262
285	282	282	285	280	285
307	289	289	291	287	291
381	350	354	357	348	355
398	407	408	409	402	409
401	411	412	414	404	412
413	413	415	416	406	415
496	501	504	508	496	506
593	517	521	527	508	524
604	522	534	534	511	526
636	584	594	596	582	590
725	597	647	645	594	636
764	733	736	739	723	737
873	829	832	846	824	842
943	861	863	876	857	873
995	928	933	947	923	941
1102	957	961	975	952	970
1129	1097	1107	1117	1059	1112
1260	1248	1247	1258	1250	1252
1353	1322	1324	1330	1325	1328
1520	1331	1328	1333	1338	1331
1554	1444	1438	1443	1456	1440
1597	1510	1509	1508	1514	1508
2591	1613	1610	1611	1620	1609
1.381	**1.237**	**1.244**	**1.250**	**1.230**	**1.247**

Using these frequencies gives a zero-point energy of ~ 1.25 eV, depending upon the method used, as shown in Table 5.6.

Adiabatic Electron Affinity, EA

Based on the work of Miller *et al.* [60] an electron affinity of 0.53 eV is used. Each pair of neutral and anion vibrational frequency calculations of the same method gives a computational prediction of the zero-point energy corrected adiabatic electron affinity. These agree with the experimental result.

Initial Internal Energy, $E_{initial}(T)$

The internal energy in the neutral is shown as a function of temperature in Figure 5.8 about 0.2 eV at room temperature and as high as 0.7 eV above 600K.

5.3.3 $C_6F_6-^*$ QET Lifetimes

The detailed calculations of the anion density of states and the neutral sum of states are similar to the case of SF_6. Calculated $C_6F_6^{-*}$ lifetimes are shown in Fig 5.9.

The lifetimes are predicted to decrease from ~ 10 μs to ~ 1 μs as the target temperature increases from ~ 300 to ~ 600 K. This gives good agreement with the experimetal result of 12 μs [1, 45] and the temperature dependence of the RET studies of Cannon *et al.* [23] is reproduced.

The success with these two molecules suggests this method may be applicable to a wide selection of these types of anions. The temperature dependence shown in the experiments of Cannon *et al.* [23] is reproduced by the QET model very well. This is due to the improved account of the neutral state. The order-of-magnitude agreement for the room-temperature results is surprisingly good. This is subject to concern though, for many reasons, especially considering the experimental discrepancies among SF_6-^* results. The question remains as to why the agreement of QET predictions is with RET experiments and not with free-electron attachment MS-TOF experiments. In addition, a sample of two molecules is perhaps too small to be a measure of the quality of a general theoretical approach, so application of the methods described herein to a subset of the metastable anions in Table 5.1 seems to be a prerequisite for drawing any conclusions about the SF_6-^* results. The concluding section of the chapter integrates all of the methods described previously into a general approach towards calculation of anion autodetachment anions.

5.4 General Application of a QET Model for Autodetachment Lifetimes

The QET model developed for SF_6^{-*} and $C_6F_6^{-*}$ experiments may be applied to a wide variety of molecular anions discussed in Table 5.1. It's application as currently formulated is limited to molecules that have zero-energy electron capture resonances. In the cases where a thermal rate constant or absolute cross-section for electron attachment is

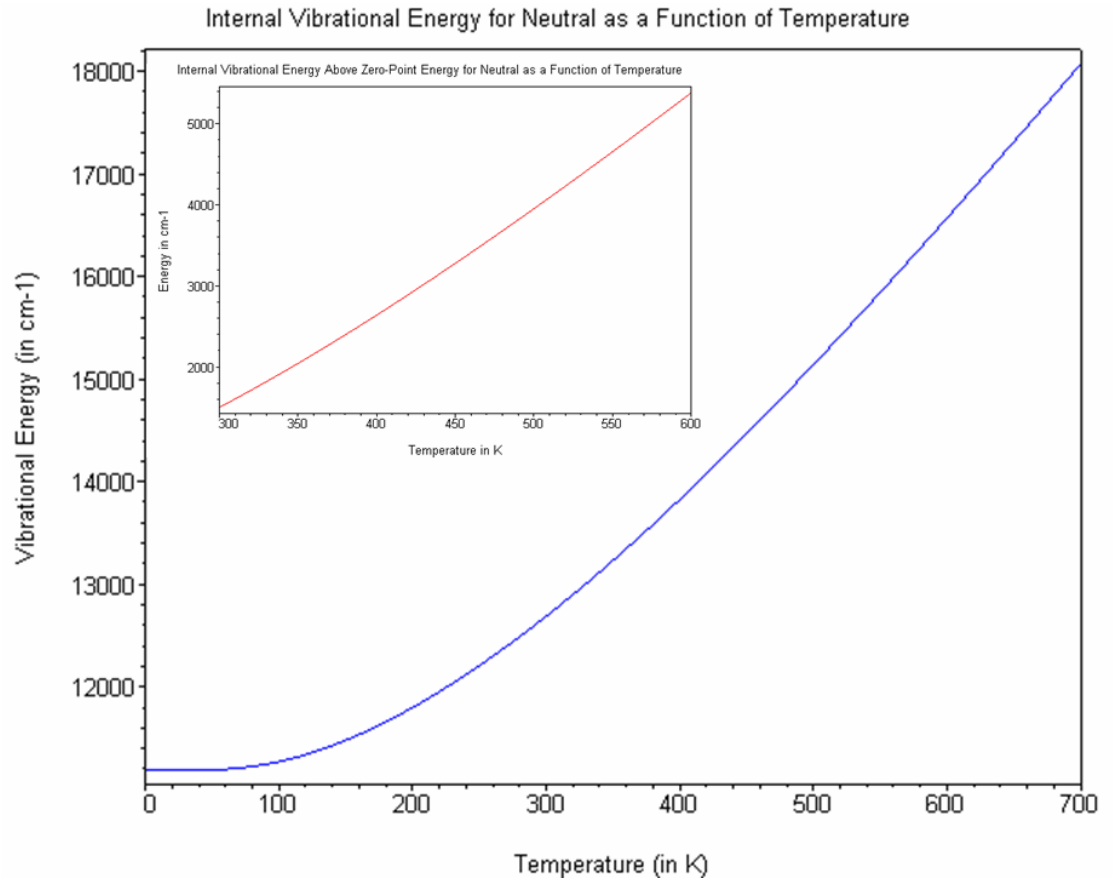

Figure 5.8: The internal vibrational energy of the C_6F_6 molecule.

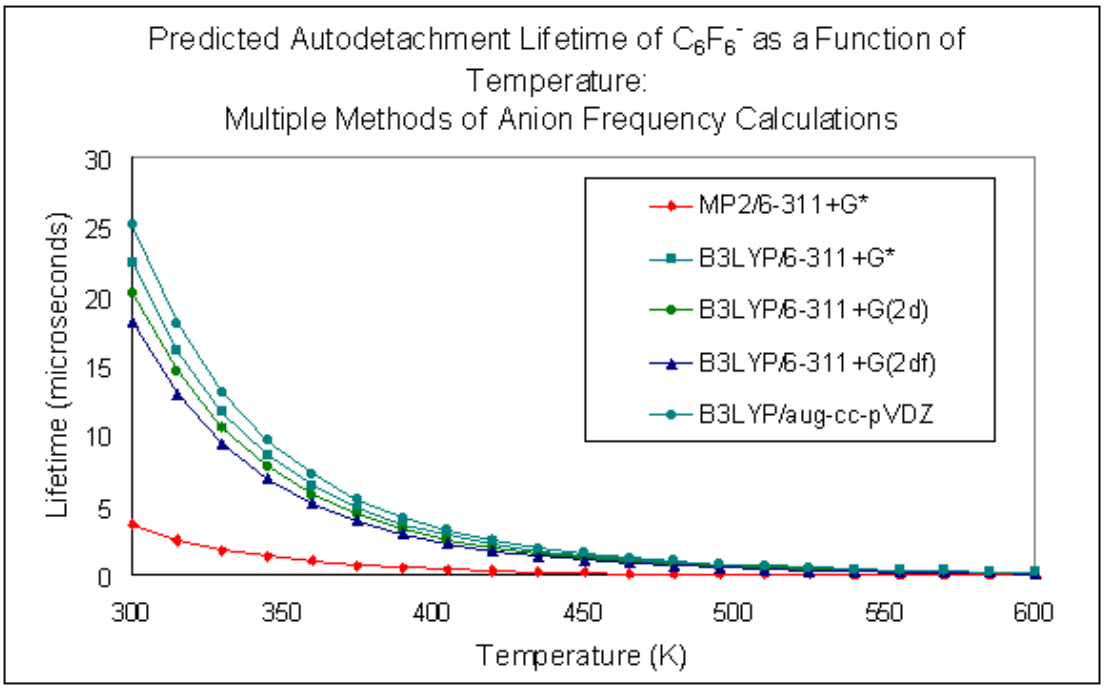

Figure 5.9: The QET predicted autodetachment lifetimes of $C_6F_6^{-*}$. For comparison, the experimental references are in Table 5.1.

not known, it is reasonable to use the value for SF_6 to provide a standard and a lower limit on the lifetime. For instance, the zero-energy electron capture cross section for SF_4 is approximately 100 times smaller than that for SF_6 [21], C_6F_6 about 25 times smaller [60], C_4F_8 about 40 times smaller [62]. This gives a reasonable range for estimation when necessary. Experimental electron affinities are used when available, and calculated as well. This approach is facilitated by the ability to calculate the vibrational frequencies of the neutral molecule and the molecular anion, as well as the electron affinity. When possible, higher-order CCD methods are used, but for larger molecules, B3LYP, the faster DFT method is used. A basis set size of at least aug-cc-pVDZ was used when possible. The experimental results are summarized in Table 5.1.

5.4.1 $C_4F_8^{-*}$

The autodetachment lifetime of $C_4F_8^{-*}$ was measured by TOF-MS methods [1] to be 12 μs. The work of Miller *et al.* [62] is used for the electron affinity value of 0.63 eV and for the thermal attachment rate. The vibrational frequencies of the neutral molecule and anion are calculated with the B3LYP/aug-cc-pVDZ method. These calculations give a zero-point energy of 1.24 eV and 1.07 eV for the neutral and anion respectively. The internal energy, $E_{initial}(T)$, at 300K is equal to 0.2 eV, so the total energy in the ion is 0.83 eV. The QET calculated autodetachment lifetime at 300K is 320 μs, greater than an order of magnitude off the experimental value, but within the proper range.

5.4.2 $C_2Cl_4^{-*}$

The autodetachment lifetime of $C_2Cl_4^{-*}$ was measured by TOF-MS methods [42] to be $\sim$14 μs, and RET methods [43] to be in the range of 3 to 30 μs. The work of Chen *et al.* [63] is used for the electron affinity value of 0.64 eV. The experimental free-electron attachment cross-section for C_2Cl_4 is not available, so a value 50 times smaller than SF_6 is used that is commensurate with other halocarbon attachment rates. The vibrational frequencies of the neutral molecule and anion are calculated with the CCD/aug-cc-pVDZ method. These calculations give a zero-point energy of 0.41 eV and 0.38 eV for the neutral and anion respectively. The internal energy, $E_{initial}(T)$, at 300K is equal to 0.1 eV, so the total energy in the ion is 0.75 eV. The QET calculated autodetachment lifetime at 300K is 6.2 μs, in good agreement with the experimental result.

5.4.3 SF_4^{-*}

The autodetachment lifetime of SF_4^{-*} was measured by TOF-MS methods [21] to be $\sim$16 μs. The work of Miller *et al.* [22] is used for the electron affinity value of 1.5 eV. The attachment cross-section of Harland and Thynne [21] is used. The vibrational frequencies of the neutral molecule and anion are calculated with the CCD/aug-cc-pVDZ method, as shown in Table 2.9. These calculations give a zero-point energy of 0.3 eV and 0.2 eV for the neutral and anion respectively. The internal energy, $E_{initial}(T)$, at 300K is equal to 0.06 eV, so the total energy in the ion is 1.56 eV. The QET calculated autodetachment lifetime at 300 K is 2000 μs, in poor agreement with the experimental result, with more than two orders of magnitude difference.

5.4.4 $C_6F_5Cl^{-*}$

The autodetachment lifetime of $C_6F_5Cl^{-*}$ was measured by TOF-MS methods [37] to be 17.6 μs. The experimental value of 0.82 eV from Dillow *et al.* [64] is used for the electron affinity. The attachment cross-section is estimated to be about 50 times smaller than SF_6. The vibrational frequencies of the neutral molecule and anion are calculated with the B3LYP/aug-cc-pVDZ method. These calculations give a zero-point energy of 1.33 eV and 1.24 eV for the neutral and anion respectively. The internal energy, $E_{initial}(T)$, at 300K is equal to 0.2 eV, so the total energy in the ion is 1.02 eV. The QET calculated autodetachment lifetime at 300 K is 21 μs, in excellent agreement with the experimental result.

5.4.5 nitrobenzene^{-*} and d$-$nitrobenzene^{-*}

The autodetachment lifetimes of $C_6H_5NO_2^{-*}$ and $C_6D_5NO_2^{-*}$ were measured by TOF-MS methods [37] to be 17.5 μs and 22μs respectively. However, as is the case with SF_6^{-*}, a RET experiment determined a much longer lifetime of 1600 μs [46]. The electron affinity is 1.3 eV, as calculated by the B3LYP/aug-cc-pVDZ method, and 1.000 from the experimental studies of Desfrancois *et al.* [65]. The experimental value is well-established, so this is the value that is used. The attachment cross-section of Compton *et al.* [36] is used, approximately 50 times smaller. The vibrational frequencies of the neutral molecules and anions are calculated with the B3LYP/aug-cc-pVDZ method. These calculations give a zero-point energy of 2.74 eV and 2.66 eV for the non-deuterated neutral and anion respectively, and 2.30 eV and 2.23 eV for the deuterated neutral and anion respectively. The internal energy, $E_{initial}(T)$, at 300K is equal to 0.11 eV, for $C_6H_5NO_2$ and 0.13 eV for $C_6D_5NO_2$. The total energy in the ion is 1.11 eV for $C_6H_5NO_2^{-*}$ and 1.13 eV for $C_6D_5NO_2^{-*}$. The QET calculated autodetachment lifetime at 300 K for $C_6H_5NO_2$ is 6000 μs, and 12000 μs $C_6D_5NO_2$. This reproduces the qualitative ordering between the two observed by free-electron capture studies of Compton *et al.* [37], but not the magnitudes. This result is very similar to that for SF_6^{-*} in that it reproduces the RET lifetime result instead of the free-electron result. Possible reasons for this are discussed in the concluding chapter.

Chapter 6

Conclusions

6.1 General Approach of QET Method

A general derivation of the QET formulation for autodetachment lifetimes was presented. The usefulness of computations for determination of parameters necessary for formulation of the anion autodetachment rate was demonstrated. Vibrational spectroscopy of the SF_6^- and SF_5^- anions is useful for validation of the computational methods. Overall, the agreement of the QET model predictions of autodetachment rates is reasonable. The results are summarized in Table 6.1. It is assumed for sake of comparison that all experiments above were done at 300K.

The overall suitability of the QET method has been demonstrated, but there are unresolved issues that remain. A few molecules show large deviations from the experiential result, and reasons for this are discussed. These include temperature effects,

Table 6.1: Autodetachment lifetime measurements using Time-of-Flight Mass Spectroscopy (TOF-MS) and Rydberg Electron Transfer (RET) techniques compared to predictions from QET model at 300K.

Molecule	Measured Lifetime(μs)	Comment	QET Lifetime (μs)
SF_6^-	20	TOF-MS	
	2000	RET	2000
$C_6F_6^-$	12	TOF-MS	
	12	RET	12
SF_4^-	$16.3 \pm .03$	TOF-MS	2000
$C_2Cl_4^-$	14 ± 3	TOF-MS	
	$3 - 30$	RET	6
$C_4F_8^-$	12	TOF-MS	320
$C_6H_5NO_2^-$	17.5	TOF-MS	
	1600	RET	6000
$C_6D_5NO_2^-$	22	TOF-MS	12000
$C_6F_5Cl^-$	17.6	TOF-MS	21

incorrect electron affinity values, and the possible role of symmetry and intra-vibrational relaxation, IVR, in the stabilization process. The most outstanding trend is that in cases where RET-determined lifetimes are available, the QET results corroborate them. When lifetimes from anions formed from free-electron attachment are available, the QET predictions sometimes greatly overestimate these. Reasons for this may be related to the degree of vibrational coupling.

6.2 Symmetry and IVR Upon Electron Attachment

Since the condition of complete IVR is required for application of the QET model, if the vibrational energy in the metastable anion is not randomized the lifetime will be overestimated because there is statistically more sampling of the reaction coordinate. An analysis of the geometry change upon electron attachment may provide insight into the initial degree of IVR occurring. The anharmonic coupling between modes plays the major role in how IVR proceeds over the period of microseconds, but the initial impetus of vibrational excitation will be primarily into modes perturbed by the geometry change. This method of analyzing the geometry change upon electron attachment was investigated in Figure 2.10. The same method can be applied to the molecules studied with the QET approach.

Each of the metastable anions is analyzed to determine the initial vibrational excitation, and the mode projections from anions that showed poor agreement to QET are compared to those that showed good agreement to see if a discernable pattern appears. Poor agreement for these purposes is defined by a calculated lifetime that is more than an order of magnitude off the experimental. These ions are SF_6^{-*}, SF_4^{-*} and $C_4F_8^{-*}$. The mode projections for these molecules are shown in Figures 6.1, 6.3 and 6.2. It is expected that anions retaining high symmetry will perturb fewer modes, and this is apparent in the SF_6 projection, and somewhat less so with C_4F_8 and SF_4.

The QET lifetime calculations of $C_6F_6^{-*}$, $C_2Cl_4^{-*}$ and $C_6F_5Cl^{-*}$ give satisfactory agreement with experiment. The mode projections for these molecules are shown in Figures 6.4, 6.5, 6.6 and 6.7. Examination of these mode projections as a group show much less symmetry is retained in the anion upon formation. The clear feature is the multiplicity of modes perturbed by the geometry change upon electron attachment. This is in contrast to molecules such as SF_6 that have a limited amount of initial distribution of vibrational excitation throughout the molecule upon electron attachment. If coupling within modes is not strong, is is possible that energy would stay directed along the perturbed modes, and the QET method would overestimate the lifetime of the incompletely coupled anion. For the case of SF_6^-, this may be particularly severe.

This treatment gives a qualitative argument for the possible role of symmetry in the autodetachment lifetimes, but it is not completely convincing because of the poor agreement of $C_6H_5NO_2^{-*}$ and SF_4^{-*} predictions despite the obvious perturbation of multiple modes. A close look at the SF_4^- anion modes excited show they are only of two symmetries, B_2 and A_1, so the mode coupling may indeed be weak. There may be other explanations for the result but the electron affinity is reasonably well established as is the electron capture cross section. Thus the poor result for the SF_4^{-*} anion is a puzzle that suggests directions for further investigation. The MP-IRD spectroscopy of SF_4^- would be

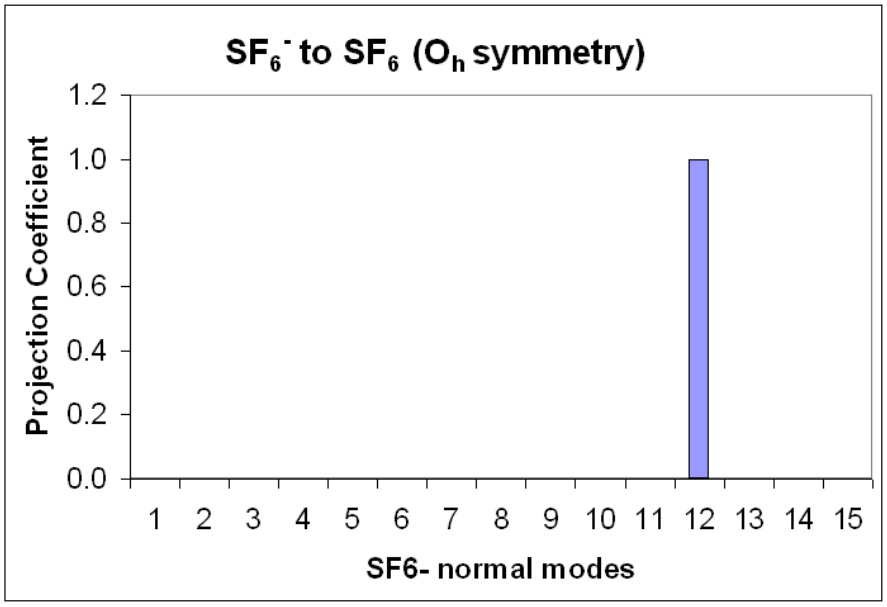

Figure 6.1: Projection of geometry change of SF_6 upon electron attachment on the normal modes of the anion.

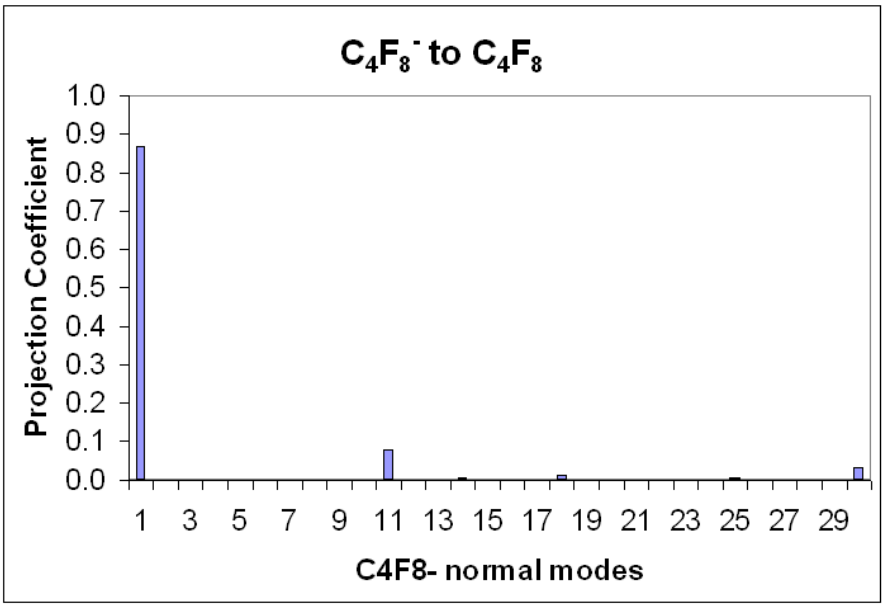

Figure 6.2: Projection of geometry change of C_4F_8 upon electron attachment on the normal modes of the anion.

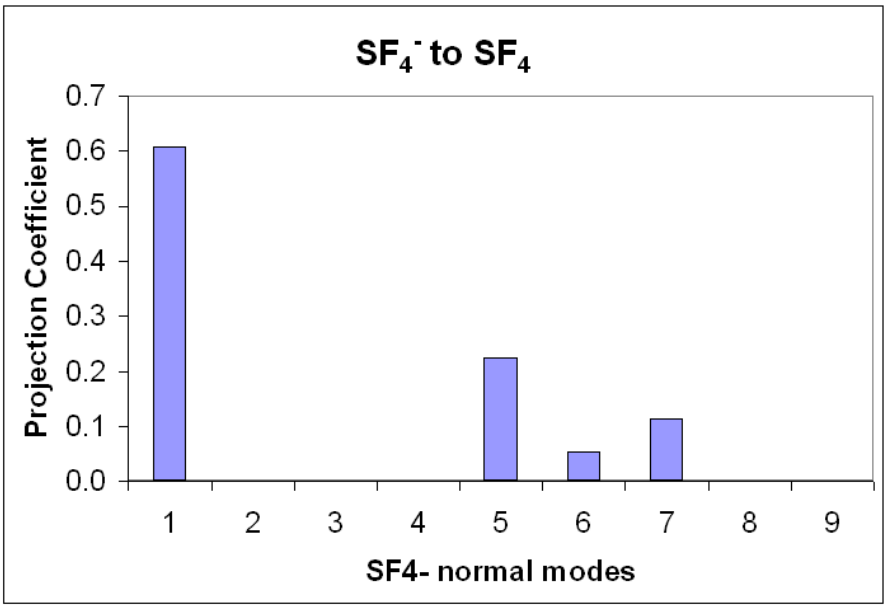

Figure 6.3: Projection of geometry change of SF_4 upon electron attachment on the normal modes of the anion.

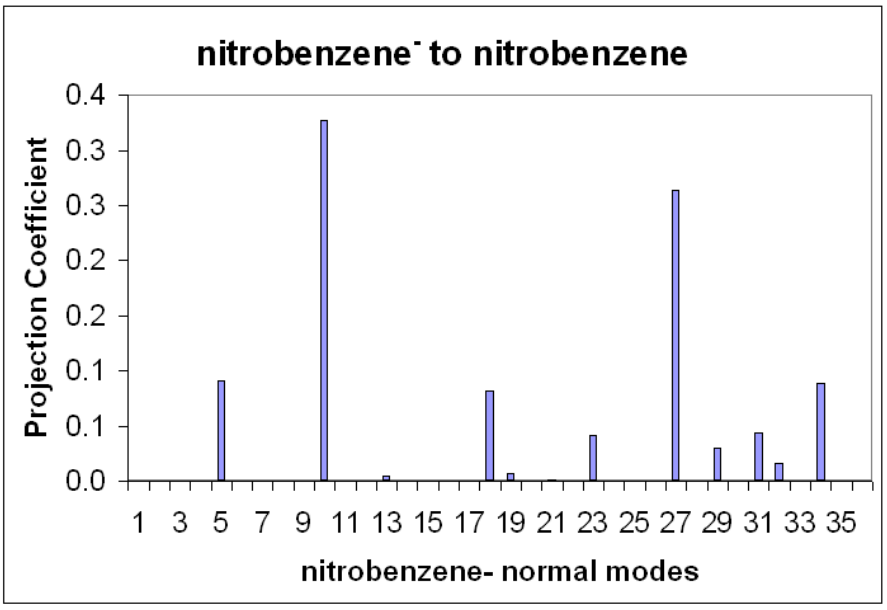

Figure 6.4: Projection of geometry change of nitrobenzene upon electron attachment on the normal modes of the anion.

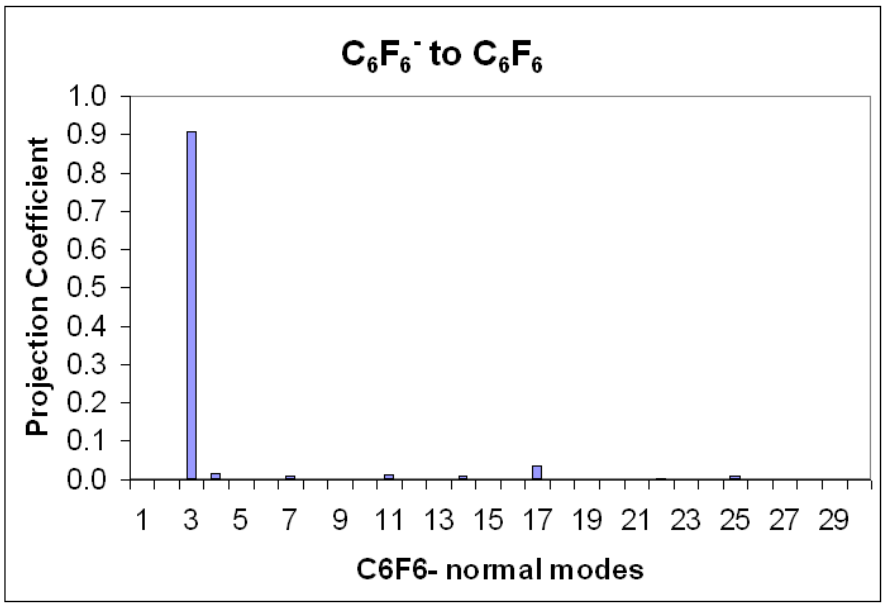

Figure 6.5: Projection of geometry change of C_6F_6 upon electron attachment on the normal modes of the anion.

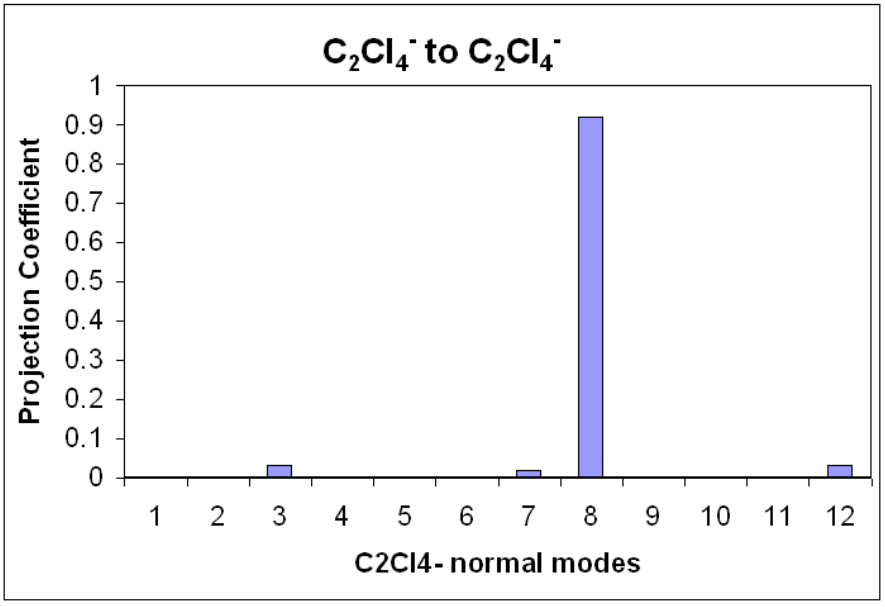

Figure 6.6: Projection of geometry change of C_2Cl_4 upon electron attachment on the normal modes of the anion.

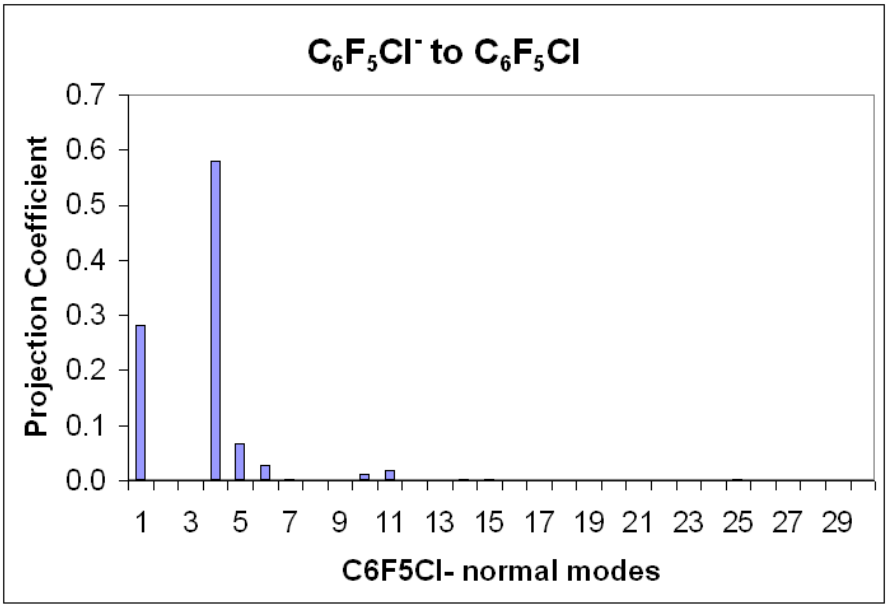

Figure 6.7: Projection of geometry change of C_6F_5Cl upon electron attachment on the normal modes of the anion.

very useful for verification of calculated anion vibrational frequencies. Potential energy surface calculations of the SF_4^- anion can determine the degree of anharmonic coupling between modes of the same and different symmetries. In addition, RET experiments of SF_4^{-*} lifetimes would be very useful to see if, like SF_6^{-*} and nitrobenzene, RET results agree with the QET predictions.

6.3 SF_6 RET vs. Free-Electron Capture

The analysis of the possible role of IVR in the autodetachment process may provide an explanation for the historical discrepancies between RET and free-electron attachment methods. For the case of SF_6^{-*}, RET results are reproduced by the QET model, suggesting the RET experiments may produce anions in a vibrationally randomized state. It is possible that the degree of randomization for the RET process is greater than the free-electron capture process, and that this is the determining factor in the different results of the two methods.

The free-electron attachment data of Braun, *et al.* [25] shows clear cusps in the attachment cross-section for strong coupling between certain modes of SF_6 and the electron capture process. These modes include ν_1, ν_3, ν_2, and ν_5. If the subset of these modes is used as the *active* vibrational degrees of freedom, the autodetachment lifetime drops from the 10 milliseconds to the MS-TOF experimental range of 20 μs. This suggests that the Rydberg ion core may be playing a role in facilitating the IVR process that extends the autodetachment lifetime. For molecules such as C_6F_6, the geometry change is more asymmetric, and thus IVR upon free-electron attachment may be much quicker, thus there would be no difference expected between RET and free-electron attachment results. The best possible experimental validation of this hypothesis is to do RET lifetime experiments for the SF_4 and C_4F_8 molecules to see if the QET results that disagree with the TOF-MS experiments would agree with the RET results.

6.4 Extension of QET to MP-IR Dissociation and Detachment

Multiple photon infrared dissociation spectroscopy was used to validate the calculated vibrational frequencies of the SF_6^- and SF_5^- negative ions. These frequencies were applied to the autodetachment of metastable anions, but it was noted that the MP-IRD process itself shows strong similarities to the autodetachment problem. The interesting competition between the SF_5^- photodissociation and photodetachment processes observed in the IR-MPD spectra demonstrates there is a need for a theoretical exploration of the basis of this competition. Extension of the QET method to dissociation processes may provide this foundation. The application of this method to the IR-MPD process holds promise for a deeper understanding of the underlying physics, as well as insight into manipulations of practical benefit. For example, one possible new experimental scheme involves indirectly detecting the IR photodetachment of negative ions with the SF_6 electron scavenger technique. Small ions previously unable to be studied with dissociation processes may become open to analysis by detachment, since electron affinities are often

much smaller than bond energies. Gas-phase infrared spectroscopy of small negative ions such as CN^-, C_nH^-, and NO_3^- will serve as a starting point for identification of these species in atmospheric and interstellar systems.

Bibliography

Bibliography

[1] W. T. Naff, C. D. Cooper, and R. N. Compton. Transient negative-ion states in alicyclic and aromatic fluorocarbon molecules. *J. Chem. Phys.*, 49(6):2784, 1968.

[2] J. A. D. Stockdale, R. N. Compton, and H. C. Schweinler. Negative ion formation in selected hexafluoride molecules. *J. Chem. Phys.*, 53(4):1502, 1970.

[3] R. A. Morris, T. M. Miller, A. A. Viggiano, J. F. Paulson, S. Solomon, and G. Reid. Effects of electron and ion reactions on atmospheric lifetimes of fully fluorinated compounds. *J. Geophys. Res. [Atmospheres]*, 100(D1):1287, 1995.

[4] A. Szabo and N. S. Ostlund. *Modern Quantum Chemistry.* Dover, 1996.

[5] J. Simons and K. Jordan. Ab initio electronic structure of anions. *Chem. Rev*, 87:535, 1987.

[6] G. E. Streit. Negative ion chemistry and the electron affinity of SF_6. *J. Chem. Phys.*, 77(2):826, 1982.

[7] E. P. Grimsrud, S. Chowdhury, and P. Kebarle. Electron affinity of SF_6 and perfluoromethylcyclohexane. *J. Chem. Phys.*, 83(3):1059, 1985.

[8] G. L. Gutsev and R. J. Bartlett. Adiabatic electron affinities of PF_5 and SF_6: a coupled-cluster study. *Molecular Physics*, 94(1):121, 1998.

[9] N. R. Brinkman and H. F. Schaefer. The SF_6^- enigma for density functional theory. *J. Chem. Phys.*, 381:123, 2003.

[10] R. A King, J. M. Galbraith, and H. F. Schaefer. Negative ion thermochemistry: The sulfur fluorides SF_n/SF_n^- (n = 1-7). *J. Phys. Chem.*, 100:6061, 1996.

[11] GAUSSIAN03 Revision C.02. Gaussian, Inc., Wallingford CT, 2004.

[12] T. M. Miller, S. T. Arnold, and A. A. Viggiano. G3 and G2 thermochemistry of sulfur fluoride neutrals and anions. *Int. J. Mass Spec.*, 227:413, 2003.

[13] NWChem, A Computational Chemistry Package for Parallel Computers, Version 5.0. Pacific Northwest National Laboratory, Richland, Washington 99352-0999, USA, 2006.

[14] C. Blondel, P. Cacciani, C. Delsart, and R. Trainham. High resolution determination of the electron affinity of Flourine and Bromine using crossed ion and laser beams. *Phys. Rev. A*, 40:3698, 1989.

[15] H. Hotop and W. C. Lineberger. Binding energies in atomic negative ions. II. *J. Phys. Chem. Ref. Data*, 14:731, 1985.

[16] D. R. Linde. *Handbook of Chemistry and Physics*. CRC Press, 1992.

[17] M. A. Polak, M. K. Gilles, and W. C. Lineberger. Photelectron spectroscopy of SF^-. *J. Chem. Phys*, 96(9):7191, 1992.

[18] J. C. Bopp, J. R. Roscioli, M. A. Johnson, T. M. Miller, A. A. Viggiano, S. M. Villano, S. W. Wren, and W. C. Lineberger. Spectroscopic charachterization of the isolated SF_6^- and $C_4F_8^-$ anions. *J. Phys. Chem. A*, 111:1214, 2007.

[19] P. M. Morse. Diatomic molecules according to the wave mechanics II. Vibrational levels. *Physical Review*, 34:57, 1929.

[20] R. S. McDowell, J. P. Aldridge, and R. F. Holland. Vibrational constants and force feild of sulfur hexafluoride. *J. Phys. Chem.*, 80(11):1203, 1976.

[21] P. W. Harland and J. C. J. Thynne. Autodetachment lifetimes, attachment cross sections, and negative ions formed by sulfur hexafluoride and sulfur tetrafluoride. *J.Phys. Chem.*, 75(23):3517, 1971.

[22] A. E. S. Miller, T. M. Miller, A. A. Viggiano, R. A. Morris, J. M. Van Doren, S. T. Arnold, and J. F. Paulson. Negative ion chemistry of SF_4. *J. Chem. Phys*, 102(22):8865, 1995.

[23] M. Cannon, L. Seuss, F. B. Dunning, J. D. Steill, and R. N. Compton. Temperature dependence of negative ion lifetimes. 2007. (Currently under review).

[24] C. L. Lugez, M. E. Jacox, R. A. King, and H. F. Schaefer. Experimental and *ab initio* study of the infrared spectra of ionic species derived from SF_6 and SF_4 and trapped in solid Neon. *J. Chem. Phys*, 108(23):9639, 1998.

[25] M. Braun, S. Barsotti, S. Marienfeld, E. Leber, J. M. Weber, M. W. Ruf, and H. Hotop. *Eur. Phys. J. D*, 35:177, 2005.

[26] K. O. Christe, E. C. Curtis, C. J. Schack, and D. Pilipovich. Vibrational spectra and force constants of the square-pyrimidal anions SF_5^-, SeF_5^- and TeF_5^-. *Inorganic Chemistry*, 11(7):1679, 1972.

[27] D. T. Moore, J. Oomens, L. van der Meer, G. von Helden, G. Meijer, A. G. Marshall, and J. R. Eyler. *Chem. Phys. Chem.*, 5:740, 2004.

[28] D. Oepts, A. F. G. van der Meer, and P. W. van Amersfoort. *Infrared Physics and Technology*, 36:297, 1995.

[29] D. C. Harris and M. B. Bertolucci. *Symmetry and Spectroscopy*. Dover, 1989.

[30] V. N. Bagratashvili, V. S. Letokhov, A. A. Makarov, and E. A. Ryabov. *Multiple Photon Infrared Laser Photphysics and Photchemistry.* Harwood,Chur, 1985.

[31] D. Ding, R. N. Compton, R. E. Haufler, and C. E. Klots. Multiphoton ionization of C_{60}. *J. Phys. Chem. A*, 97:2500, 1993.

[32] P. S. Drzaic and J. I. Brauman. Infrared multiphoton induced electron detachmnet from SF_6. *Chem. Phys. Lett.*, 83(3):508, 1981.

[33] C. E. Klots. Statistical aspects of autoionization lifetimes. *J. Chem. Phys.*, 46(3):1197, 1967.

[34] C. E. Klots. Reformulation of the quasiequilibrium theory of ionic fragmentation. *J. Phys. Chem.*, 75(10):1526, 1971.

[35] C. E. Klots. Rate constants for unimolecular decomposition at threshold. *Chemical Physics Letters*, 38(1):61, 1976.

[36] R. N. Compton, L. G. Christophorou, G. S. Hurst, and P. W. Reinhardt. Nondissociative electron capture in complex molecules and negative ion lifetimes. *J. Chem. Phys.*, 45(12):4634, 1966.

[37] W. T. Naff, R. N. Compton, and C. D. Cooper. Attachment of electrons to substituted benzenes. *J. Chem. Phys.*, 54(1):212, 1971.

[38] L. G. Christophorou, A. Hadjiantoniou, and J. G. Carter. Long-lived parent negative ions formed via nuclear-excited feshbach resonances: Part 3. *J.C.S. Faraday Trans. 2*, 69(11):1713, 1973.

[39] D. Edelson, J. E. Griffiths, and K. B. McAfee. *J. Chem. Phys.*, 37:917, 1962.

[40] R. A. Marcus and O. K. Rice. The kinetics of the recombination of methyl radical and iodine atoms. *J. Phys. and Colloid Chem.*, 55:894, 1951.

[41] G. Z. Whitten and B. S. Rabinovitch. Accurate and facile approximation for vibrational energy sums. *J. Chem. Phys.*, 38(10):2466, 1963.

[42] J. P. Johnson, L. G. Christophorou, , and J. G. Carter. Fragmentation of aliphatic chlorocarbons under low energy ($\leq$ 10 eV) electron impact. *J Chem. Phys.*, 67(5):2196, 1977.

[43] L. Seuss, R. Parthasarathy, and F. B. Dunning. Nondissociative low energy electron attachment to C_2Cl_4: $C_2Cl_4^-$ ion lifetime. *J. Chem. Phys.*, 118(14):6205, 2003.

[44] C. D. Finch, R. Parthasarathy, H. C. Akpati, P. Nordlander, and F. B. Dunning. Low-energy dissociative electron attachment to $CFCl_3$, CF_2Br_2, and 1,1,1- and 1,1,2-$C_2Cl_3F_3$: Intermediate lifetimes and decay energies. *J. Chem. Phys.*, 118(14):6205, 2003.

[45] P. W. Harland and J. C. Thynne. The effect of substituents upon the autodetachment lifetimes of the perfluorobenzene and nitrobenzene anions. *J.C.S. Chem. Comm*, 8:476, 1972.

[46] L. Seuss, Y. Liu, R. Parthasarathy, and F. B. Dunning. Rydberg electron transfer to $C_6H_5NO_2$: Lifetimes and charachteristics of the product $C_6H_5NO_2^-$ ions. *J. Chem. Phys.*, 122:124315, 2005.

[47] L. Seuss, R. Parthasarathy, and F. B. Dunning. Nondissociative low energy electron attachment to SF_6, C_6F_6, $C_{10}F_8$, and c-C_7F_{14},: Negative ion lifetimes. *J. Chem. Phys.*, 117(24):11222, 2002.

[48] R. N. Compton and C. D. Cooper. Negative ion properties of tetracyanoquinodimethane: Electron affinity and compund states. *J. Chem Phys.*, 66:4325, 1977.

[49] J. E. Delmore and A. D. Applehans. *J. Chem. Phys.*, 84:6238, 1986.

[50] J. L. Le Garrec, D. A. Steinhurst, and M. A. Smith. Measurement of the autodetachment lifetime of SF_6^{-*} as a function of electron energy in a free-jet expansion. *J. Chem. Phys.*, 114(20):8831, 2001.

[51] J. M. S. Henis and C. A Mabie. *J. Chem. Phys.*, 53:2999, 1970.

[52] R. W. Odom, D. L. Smith, and J. H. Futrell. *J. Phys. B: Atom. Molec. Phys.*, 8:1349, 1975.

[53] M. S. Foster and J. L. Beauchamp. *Chem. Phys. Lett.*, 31:482, 1975.

[54] Y. Liu, L. Seuss, and F. B. Dunning. Rydberg electron transfer to SF_6: Product ion lifetimes. *J. Chem. Phys.*, 122:214313, 2005.

[55] A. Pesnelle, M. Perdix, and G. Watel. Dependence on collisional energy of negative ion formation in collisions of He(14 ^{1}P) Rydberg atoms with SF_6. *J. Chem. Phys.*, 96(6):4303, 1991.

[56] G. W. Foltz, C. J. Latimer, G. F. Hildebrandt, F. G. Kellert, K. A. Smith, W. P. West, F. B. Dunning, and R. F. Stebbings. *J. Chem Phys.*, 67:1352, 1977.

[57] A. D. Applehans and J. E. Delmore. Refinement of the autoneutralization lifetimes of short lived states of SF_6^-. *J. Chem. Phys.*, 88(9):5561, 1988.

[58] C. W. F. T. Pistorius. Potential field and force constants of octahedral molecules. *J. Chem. Phys.*, 29(6):1328, 1958.

[59] K. S. Gant and L. G. Christophorou. Attachment of slow electrons to hexafluorobenzene. *J. Chem. Phys.*, 65(8):2977, 1976.

[60] T. M Miller, J. M. Van Doren, and A. A. Viggiano. Electron attachment and detachment : C_6F_6. *International Journal of Mass Spectrometry*, 233:67, 2004.

[61] D. Steele and D. H. Whiffen. The vibrational frequencies of hexafluorobenzene. *Trans. Faraday Soc.*, 55:369, 1959.

[62] T. M Miller, J. F. Friedman, and A. A. Viggiano. Electron attachment and detachment and the electron affinity of cyclo-C_6F_6. *J. Chem. Phys*, 120(15):7024, 2004.

[63] E.C.M. Chen, J. R. Wiley, C. F. Batten, and W. E. Wentworth. Determination of the electron affinities of molecules using negative ion mass spectrometry. *J. Phys. Chem.*, 98:88, 1994.

[64] G. W. Dillow and P. Kebarle. Substituent effcet on the electron affinities of C_6F_5X. *J. Am. Chem. Soc.*, 111:5592, 1989.

[65] C. Desfrancois, V. Periquet, S. A. Lyapustina, T. P. Lippa, D. W. Robinson, K. H. Bowen, H. Nonaka, and R.N Compton. Electron binding to valence and multipole states of molecules: Nitrobenzene, para- and meta-dinitrobenzenes. *J. Chem. Phys.*, 111:4569, 1999.

Vita

Jeffrey Daniel Steill was born in Lafayette, Indiana, on September 28, 1974, the son of Barbara and Daniel Steill. After graduating in 1992 from Firestone High School in Akron, Ohio, he attended The Ohio State University in Columbus, Ohio. After a transfer to The University of Tennessee, Knoxville, he received a Bachelor of Science degree with a major in Chemistry in 2002. During his undergraduate studies, he worked at the Oak Ridge National Laboratory in Oak Ridge, Tennessee. In 2002, he began the doctoral program of The University of Tennessee in Chemical Physics, and completed his Doctor of Philosophy degree in 2007. Future plans include employment starting in 2007 as a post-doctoral research scientist with the Molecular Dynamics group at the FOM Institute, Rijnhuizen, in the Netherlands.